Multi-purpose Electromagnetic Energy Harvesting System

by

James Ugwuogo

A thesis
presented to the University of Waterloo
in fulfillment of the
thesis requirement for the degree of
Doctor of Philosophy
in
Electrical and Computer Engineering

Waterloo, Ontario, Canada, 2019

Examining Committee Membership

The following served on the Examining Committee for this thesis. The decision of the Examining Committee is by majority vote.

External Examiner	Nady Boules President NB Motors, LLC
Supervisor(s)	Saffieddin Safavi-Naeini Professor of Electrical and Computer Engineering
Internal Examiner	Slim Boumaiza Professor of Electrical and Computer Engineering
Internal Examiner	David Nairn Professor of Electrical and Computer Engineering
Internal External	Behrad Khamesee Professor of Mechanical & Mechatronics Engineering
Internal External	Eihab Abdel-Rahman Professor of Systems Design Engineering

.

Author's Declaration

I hereby declare that I am the sole author of this thesis. This is a true copy of the thesis, including any required final revisions, as accepted by my examiners.

I understand that my thesis may be made electronically available to the public.

Abstract

This thesis proposes a multi-purpose electromagnetic energy harvesting system that harnesses mechanical energy from diverse types of mechanical motion sources and converts it into low power electrical energy. The harvested electrical energy is either used to supply power to low-power electronic devices or stored in an internal storage battery for later use. The proposed energy harvester can be i) mounted on a human's knee, elbow, or hip, ii) hand-cranked, as well as iii) installed on any enclosure with fixed and movable parts (e.g., doors and/or windows). When mounted on a knee or hip, the device is actuated only during the so-called negative energy cycle of the motion and does not disturb the motion in the forward direction.

The key building blocks of the proposed multi-purpose electromagnetic energy harvesting system is a new brushless AC electromagnetic generator, an adaptive motion translation mechanism and a smart power management system. The brushless AC generator consists of a new structure with a detachable rotor arrangement comprising mainly Neodymium rare-earth magnets mounted on an adjustable height rotor shaft and a stator made up of top and bottom flanges and a single continuous coil arrangement on a non-magnetic spool worn on a center magnetic stator core. The stator and rotor arrangement is carefully designed to allow for variable air gap so that the initial amount of torque required to move the rotor is adjustable and the amount of the generated output voltage can be controlled.

Finite-element modeling magnetics (FEMM) simulation tool was used for the optimization of the new brushless generator, selecting the different generator materials, and determining the placement of the key components to achieve an efficient and truly adjustable system to the variation of frequencies and torque conditions. Furthermore, a gearbox was used as a mechanical up conversion mechanism to multiply the relatively low human motion to up to 5000 RPM at a walk pace of about one step per second. For this purpose, a three-stage spur gear system was designed using a roller-clutch at the front end to only allow motion during the negative cycle. The gearbox, when assembled together with the generator, works together with the adjustable height rotor to create the desired effect – adaptive, multi-purpose energy harvesting system.

The power management design was optimized to maximum energy harvesting at rated RPM. When an external load is detected, the harvested power is routed to the external load, else, the power is routed to the internal storage battery for later use.

The completed system generates between 2.5 watts and 7.5 watts of electrical power at an overall system efficiency of up to 84%.

Acknowledgements

First and foremost, I thank the Lord God almighty for the gift of life and for the grace given me to combine both work and school. It has only been by His grace. Father, I thank You.

Secondly, I want to express my unreserved appreciation and thanks to my supervisor, Professor Safieddin Safavi-Naeini for his support, inspiration and guidance. There were times things seemed a bit tough for me, but your encouragements were like 'winds beneath my wings'. A big **thank you** to you, sir.

I also want to thank my PhD committee members – Professor David Nairn, Professor Slim Boumaiza, Professor Eihab Abdel-Rahman, and Professor Behrad Khamesee and my External Examiner, Dr. Nady Boules. I say a very big thank you to you all.

I owe a great debt of gratitude to my family starting with my mom, Madam Alice Ugwuogo who encouraged me as a child to seek excellence. Her words about pushing oneself and being inspired by successful peers kept ringing in my ears all these years. And to my late father, James D. Ugwuogo Snr. I am grateful for having him as my father. I remember his last few words to me on my first day at the secondary school – 'namesake', he said, 'I know you will not join bad groups'; to which I responded, 'yes sir'. Somebody please, help me and tell my father that am doing well.

To my step-mom of blessed memory, Mrs. Monica Ugwuogo with whom I lived from childhood until I obtained my bachelor's degree, thank you for the values of dedication and persistence you instilled in me.

To my siblings – Chiesonu, Uchechukwu, Chinyere-Grace, Chibuzo, Chinekwu, John, Christopher, Dom, David and many more…what you might not know was how much you inspired me to be all I could ever be. I say a very big thank you to you all. And to my very special brother, Engr. Calistus Mba who was behind my journey to Canada, I owe you a ton of thanks. May God greatly bless you.

To my lovely wife. The love of my life. Sunshine – Chiazor Chinwe Ugwuogo; thank you for the many times you stood by me. The many nudges to keep going when I was lacking in inspiration - thank you. Thank you for practically running the home while I go out to hunt for the 'spoils'. For taking care of our lovely children and being there for us all. I just want you to know that this would not be possible without you.

And to my lovely generation – Chimmeremnma Delight Ugwuogo and Nnasokam Marvelous Ugwuogo. Thank you for the additional joy you brought into my life. Sometimes when I don't feel like getting up and going, my desire to provide the best in life for both of you than I ever had, drives me to keep going. Thank you for understanding with me the many weekdays and weekends that I had to stay away from home for work. And to Ugomsinachim Splendor Ugwuogo, we are all so excited in anticipation of your soon arrival, this is for you also.

And finally, to my faith family – Pastor Marshall Eizenga and Apostle Aloy C. Diugwu. The two men I approached with all forms of burdens as I went through this journey. Thank you for standing with me in prayers. The completion of this program is a testimony to answered prayers.

Dedication

Dedicated to ‘my squad’ - Sunshine, Delight, Marvelous and Splendor

Table of Contents

List of Figures

List of Tables

List of Abbreviations

Abbreviations	Meaning
AC	Alternating Current
CIGS	Copper Indium Gallium Selenide
CMOS	Complementary Metallic Oxide Semiconductor
DC	Direct Current
FET	Field Effect Transistor
GHz	Giga Hertz
Hz	Hertz
Inc.	Incorporated
ISM	Industrial Scientific and Medical
KHz	Kilo Hertz
Km	Kilometre
MEMS	Microelectromechanical System
MHz	Mega Hertz
MIT	Massachusetts Institute of Technology
mm^2	Millimetre Square
MPPT	Maximum Power Point Tracking
mT	MilliTesla
mW/cm^2	MilliWatt per centimetre square
Pb	Lead
P-I-N	Personal Identification Number
PZT	Piezoelectric Transducer
RF	Radio Frequency
RFID	Radio Frequency Identification
T	Tesla
TEGs	Thermoelectric Generators
Ti	Texas instrument
V	Voltage
Vs	Versus

W/cm^2	Watt per Centimetre square
w.r.t	With respect to
μW	Micro Watt
G	Generator
$\mathbf{V_G}$	Generator open-circuit voltage
$\mathbf{R_G}$	Generator internal resistance
$\mathbf{V_L}$	Generator on-load voltage
$\mathbf{R_L}$	Load resistance
$\mathbf{X_L}$	Reactive Impedance

Chapter 1

Introduction

1.1 Energy Harvesting

Energy harvesting is a growing and an attractive concept that has continued to inspire huge research interests. This has been made especially possible due to the breakthroughs in semiconductor electronics which paved the way for ultra-miniaturized systems that depend completely on energy harvesting technologies for their complete power solutions/requirements.

Energy harvesting is a process where energy is recycled or converted from one form into other forms, usually from ambient sources that would otherwise have been wasted. It is a way of converting and reusing energy that would have otherwise been dissipated.

Energy harvesting technologies might be developed as a standalone system or integrated with other human interfacing devices. Each approach could bring about some unique features. The standalone approach can be installed on rigid structures like doors and windows while the ones with human interface could be both rigid and flexible and could be installed on rigid as well as flexible surfaces.

Whatever the approach adopted, there are corresponding adaptations, methods and technologies that is adopted for that particular need. The energy harvesting technology on focus in this research work is a human wearable system.

Several parts of the human body are potential sources for energy harvesting activities, these include – a top-down list – the shoulder, the elbow, the wrist, the hip, the knee, the ankle, and the heel as well as the center of mass method.

However, due to the level of movement involving the lower limbs of the human anatomy during regular movement - namely, the hip, the knee, the ankle and the heel –, many energy harvesting research has been focused on these areas [1]. Some of the key research focus has been on the center of mass, the heel strike and the knee motion-based methods.

For instance, by using the center of mass method, [2] demonstrated a system that generated electrical energy while carrying a backpack with some special adaptations. The system designed based on this method generated up to 7.4 Watts carrying a 38 kg load while walking at approximately 6.5 km/h.

[3] described various systems that used the heel strike method to generate electrical energy from the relative motion of the foot and the ground from regular gait. They described electromagnetic, piezo electric and electrostatic generators employing this heel strike method to generate various levels of electrical energy. Each of these energy harvesting technologies was inserted in the heels/soles of shoes and used to convert the heel strike action into electrical energy.

While [4] described a system using the knee motion method to generate watt level of electrical energy. This method involves harvesting the energy that helps in deceleration or in maintaining stability, called negative energy. This energy would have been dissipated as heat by the knee [5].

Each of the above methods applied varying energy harvesting technologies to achieve the desired result of converting energy from one form to another. Usually from a form that would have been wasted to heat to an electrical energy. The efficiency of the conversion process depends on the principles and technology involved.

1.2 Motivation and related previous works

The electromagnetic energy harvesters have been demonstrated to have the highest energy conversion efficiency compared to all other forms of energy harvesters [6]. It was further observed that the lower limbs – particularly the knee-joints possess the highest energy harvesting potential [3]. In [7] the authors suggested that revisions to their work to improve the **fit**, **weight**, and **efficiency** will not only reduce the cost of the energy harvesting device but will also increase the amount of generated electricity.

They further suggested that a generator designed specifically for an energy harvesting application could have lower internal losses and require a smaller, lighter gear train [7].

Taking the foregoing into consideration, the motivation for this research endeavor was to design a novel light-weight, adjustable power, and highly efficient electromagnetic energy harvester that satisfies some of the above conditions.

Based on an extensive literature review, it was concluded that by utilizing just a fraction of the ‘so-called’ negative work, as cited by these research references [1], [8] a significant amount of power could be harvested. Research resources were then dedicated toward converting the so-called negative work during normal gait to useful electrical power – using custom-made electromagnetic generators built using the Neodymium rare-earth magnets.

This type of generator will overcome some of the inherent limitations (high volume and high weight as well as low magnetic flux density) of the traditional DC motor-based generators referred to in [7].

In [1] the authors showed that the percentage of negative work in the knee for the elderly and younger adult subjects is between 85 and 91 percent. The authors further predicted an energy harvesting system that is selectively engaged to harvest energy only during the cycle that

correspond with the negative energy cycle. This method will allow part of the previously unused 90% of the negative energy to be harvested into electrical energy at a little or no additional metabolic cost and without adversely impacting the gait of the subject [9], [10].

The above agrees closely with the work in [8] in which the authors stated that there is a net negative work done by the knee during level walking; which further supports the decision to explore energy harvesting techniques based on human body motions.

Before going any further, the concept of 'negative work' will be fully defined. Negative work is the work done by the muscles during the swing phase in a normal gait to slow the leg down. It assists in braking and stability. It is the form of energy that does not help the subject in moving forward rather used to help in braking and in maintaining stability and is usually dissipated as heat [5]. An energy harvesting device could then be used in harvesting kinetic energy during deceleration, thereby helping the knee muscles reduce the energy they need to spend during deceleration [1].

A prior work in this area of study used a DC brushless motor as a generator but the generator was not optimized for energy harvesting in terms of weight and power generation [11]. Another similar concept used the piezoelectric harvester which, although could generate higher voltages, the current was low resulting in an overall output power a single digit milli-watt [12].

The idea and approach pursued in this thesis is the design of a new type of multi-purpose electromagnetic energy harvester with adjustable power outputs. The subjects will have the ability to adjust the energy harvesting potential as needed. The energy harvester will harvest electrical power at various levels for the device of the subject but could also be used in places with hinged openings – like doors and windows. With a human-wearable system in mind, the energy harvesting system shall be lighter and custom-made with specific power considerations tailored for a range of human subjects.

Now, the ratio of negative muscular work to positive muscular work was deemed to be 3:1 [5], which reinforces the concept of harvesting energy only during the negative work cycle (see Fig. 1.1). The proposed new design, much like the one proposed by other researchers in [7], uses a one-directional roller clutch and harvests energy only during the swing phase but unlike their work which uses an algorithm to engage the energy harvester while the gearbox is constantly in motion, the design of the new motion translation gear-box controls the entire harvesting cycle but only engaging towards the end of the swing phase thus simplifying the design concept and making it more efficient.

There is no complex circuitry controlling the harvesting phase, unlike in the previous work. A roller clutch is mounted at the 'front end' of a multi-stage motion translation gear-box/system which allows the secondary and tertiary stages of the gear system to continue their motion uninterruptedly after an initial input motion from the input shaft.

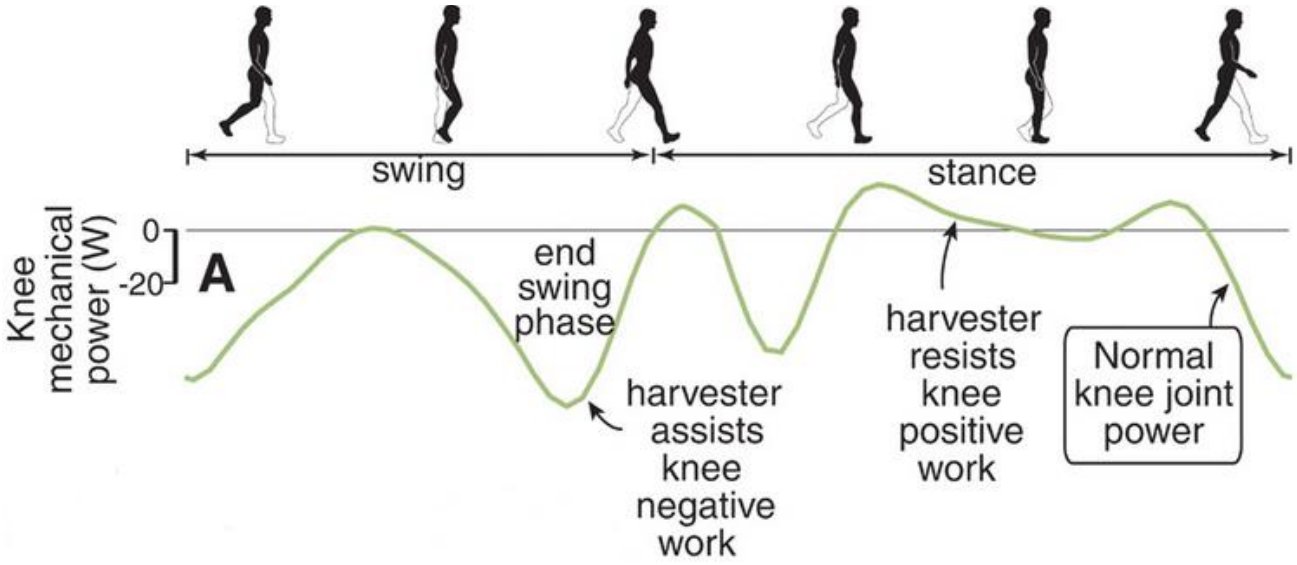

Fig. 1.1 - Phases of the knee motion during walking [11]

The motion translator was designed with a mechanical advantage of five (5) which ensures that the generator continuously moves in only one direction for 5 complete revolutions from just the initial (first) swing. At the same time the roller clutch does not permit the interruption of the motion by the shaft during the stance phase. The next input comes during the next swing phase.

This method creates a continuous one-directional motion with constant energy harvesting without the use of any complex circuitry to monitor the knee angle as described in [7] and to control the energy harvesting phases.

1.3 Fundamental Research Problem / Problem Statement

How do we solve power supply problems for connected-mobile systems?

As our lives become more and more intertwined with electronic gadgets, the demand for a closer integration between connectivity and mobility has never been more apparent. However, to realistically maintain a true sense of 'connected-mobility', the integration should be seamless and must have the least amount of interference with regular use or with human movement.

- **Short term solution – Single-use Batteries?**

For mobile electronic gadgets to be useful to us in any way, they must be powered. Now, most of the power comes from single-use electrochemical cells which, unfortunately, have not kept up

pace with the rate of electronic advancements. These single-use electrochemical cells are bulky, unreliable, and sometimes, outright expensive. When we factor in the potential environmental hazards posed by their disposal into refuse dumps and landfills [13], we get an urgent sense for (an) alternative solution(s).

- **Intermediate solution - Multi-Use Rechargeable Batteries?**

This solution is the rechargeable 'multi-use' batteries. While they tend to minimize the number of batteries in potential landfills, they still require charging from time to time and hence some downtime. True 'connected-mobility' requires a user to be connected and mobile all the time through most of the day with little or no downtimes. Advancements in multi-use battery technologies have some promising solutions with long lasting useful battery life between charges, however, in places where electricity is not readily available for recharging batteries, this is not a viable option. Other places that are less developed where traditional electricity supply is considered a luxury or areas that require constant mobility leaves little or no rooms for downtime to recharge batteries – for example, soldiers in war-zones or relief workers in disaster hit areas - these places need alternate reliable solution(s).

- **Permanent Solution - Energy Harvesting?**

The alternative solution to carrying bulky large-capacity batteries or relying on downtimes to recharge multi-use rechargeable batteries is the energy harvesting technology. Energy harvesting is the ability to convert energy from other energy forms to electrical energy which will then be used to provide power to connected devices. Since connected-mobility is in view, as well as the ability for harvesting large amounts of electrical energy, this thesis is focusing on harvesting energy from regular human motions targeting the lower extremities [1] into useful electrical energy form to supply power to user electrical gadgets. This will eliminate the need to carry bulky batteries [14] and also minimize any need for downtimes for battery maintenance - to recharge or replace dead batteries [12].

1.4 Gaps to be addressed

Although there are many solutions in the space of energy harvesting technology, some gaps still exist. This thesis research will be attempting to address some of them. It is intended that at the end, at least some or most of these identified gaps would have been addressed to some degree. In the following, a list of the gaps is highlighted:

1. Lack of Adjustable Power Electromagnetic Generators

In practice, the devices that are currently powered by energy harvesting technologies require different power levels. Previous energy harvesting devices are usually designed to produce a preset power level. The then means that there must be a different energy harvester for each target device, if the power requirement of the said target device is higher than that of the current harvester.

To address this problem, this research will focus on designing an electromagnetic energy generator capable of generating adjustable output power levels to meet various device requirements.

The harvested power should be adjustable to suit various energy harvesting conditions and needs. When compared to other energy harvesting sources, the electromagnetic energy harvested was described as having the highest conversion rate [15], and would be a better solution when compared to say piezo electric or elastomer.

Being adjustable will make the harvester customizable and adaptable to various hosts and to specific needs. This approach will be seeking to overcome some of the problems encountered by other researchers in terms of weight, size and function [16]. When used as a wearable energy harvesting system, the subjects will be able to dial in the expected level of harvested power – Low, Medium, or High – based on the respective desire or walk pattern.

The adjustable nature comes from the unique design of the generator rotor which has an adjustable height over the stator core designed to concentrate changing magnetic fluxes within a compact area where the generator coil is placed [17].

2. Inefficient Motion Translation Gear-Box

Current energy harvesting systems which rely on Motion translation gear-boxes end up expending some of the available harvestable energy in driving the gear trains while energy was not being harvested. This method reduces the efficiency of the complete system (mechanical to electrical energy conversion efficiency).

This research is seeking to extend an existing solution which uses a gear box that allows continuous driving of the gear box with every step while using an algorithm to track and engage the energy harvester [18].

Here, a light-weight motion translation gear-box which engages a set of gear trains only during specific walk cycles (referred to as ‘toward the end of the swing phase’, during which the so called ‘negative energy’) is used to drive the generator’s prime mover.

The design presented in this thesis will be using a roller-clutch in the motion translator front end to prevent wasting of energy in the gear system. The gear-box provides a high mechanical advantage (motion multiplication) for the generator.

3. **Limited options for a Light-Weight Hip/Knee Harnesses**

There are several harnesses in existence in some journals and publications today in which the authors used full-fledge knee braces as interface harnesses for their energy harvesting systems. This leads to a bulky system adding to the weight, increasing the cost of harvesting (COH) and reducing the value of the figure of merit.

> In this research, a light-weight Hip/Knee harness will be designed and used to integrate the energy harvester to the hip or the leg of the human subject who wears the harvester. This approach eliminates the use of full-fledged knee-braces as presented in [18] and helps in reducing the weight of the overall product. This research further extends this existing concept by designing a universal harness that not only integrates on the human subject but also on other possible interfaces like doors and windows.

4. **Limited scope for Power Management Systems**

While the concept of a power management system is not new to energy harvesting technology, many current power management circuits require the input power source(s) to be stable, clean and somewhat predictable for voltage conditioning and storage, but energy harvesting sources are not [19]. They have high and low values throughout their active usage period putting the burden on the power management system(s) to effectively regulate and manage the output power.

> The multi-purpose energy harvesting system presented in this thesis will to managing both the 'highs' and 'lows' of the received input power from the energy harvester – it will receive, process and store every received power – whether pulsed or continuous – and will also automatically detect the presence of an external load when connected to route power/charging to such device(s).

1.4.1 Proposed Solution

Design of an Electromagnetic Energy Harvesting System

Although many potential alternative solutions to the 'problem statement' exist in literatures and in practice, one solution stands out among the pack based on power and efficiency. This generator/harvester is the electromagnetic energy harvester. This thesis explored this solution and presents a novel design that can be custom-made to suit various use cases. Some of the advantages of the novel design over other forms of energy harvesters that make it a suitable candidate as the solution for the problem statement include:

1. **Power Generation** – Electromagnetic energy generators have the highest amount of power generation per kilogram [15].

2. **Impedance matching** – As the proposed generator is to be designed from ground up, it could be impedance-matched to the power management circuitry to improve maximum power transfer. To achieve this, the coil size and number of turns will be taken into consideration to ensure the right amount of coil DC impedance while the complex inductive impedance portion of the coil is matched with a conjugate value of capacitive impedance.
3. **Adjustable Power** – The amount of harvested power could be adjusted by the end user post fabrication. Since the amount of negative energy vary between young adults and the elderly [1], the tolerance of each might also differ between individuals. This harvester allows the human subject to adjust the energy harvesting potential as required.
4. **Cost effectiveness** – If the harvested voltage is high, the interface electronics would be low cost. Off-the-shelf components with no special adaptions could be used for the rectifier and power storage systems. The power management system in the proof of concept was designed entirely from off-the-shelf components (and proven satisfactory).
5. **Highly customizable** – The proposed solution can be customized for various scenarios. It will find multi-purpose functions in various energy harvesting applications, namely, human wearable and rigid surface installations. The design could also vary in size as dictated by the need or demand and the output power could range from microwatt to watt level.
6. **Variable Frequency operation** – The design can harvest electrical energy from less than 1 Hz (impact) to several KHz (continuous rotation). Unlike the Piezoelectric energy harvesters, which, could be used in much the same way as the electromagnetic energy harvesters [12] but which must operate at resonance [20] to enable efficient and reasonable energy harvesting, the efficiency of the electromagnetic energy harvesters is not resonant-frequency dependent.

1.5 Organization of the Thesis

Chapter 1 section 1.1 discussed the concept of energy harvesting in a more generalized way. Section 1.2 presented the motivation and related works. In section 1.3 fundamental research problem was presented. In section 1.4, a list of some of the gaps in the existing solutions in this research area was presented with some of the key contributions this research is seeking to make to address some of them. Section 1.4.1 discussed the proposed solution of a multi-purpose electromagnetic energy harvesting system. The theoretical framework for this research work was presented in chapter 3. Section 3.2 discusses the principle of operation of the electromagnetic energy harvesting system, while section 3.3 focuses on the architecture and the configuration of the proposed design. Section 3.4 dealt with the initial proof of concept. In section 3.5 a presentation of the generator structure was made followed by the Generator simulation in section 3.6.

The design of a motion translation gear box is presented in section 3.7, while section 3.8 discussed the fabrication and testing, as well as test setups for the initial concept.

Chapter 4 presents advancements and progress over initial concept while section 4.6 presents the system integration, experimental results and conclusions.

Finally, the summary of this thesis research work is presented in Chapter 5. Drawing a conclusion on the thesis and discussing opportunities for future works.

Chapter 2

Literature Review

2.1 Review of the state of art methods

Energy harvesting from the lower extremities of the human anatomy during regular walking pattern [1] offers some potential for generating significant amounts of electrical energy to supply power to electronics devices like personal digital assistants and prosthetic limb [3]. Several research reports exist in this area and will be reviewed in this section.

2.1.1 Center of mass motion method

By using the method of center of mass, it is possible to generate significant amount of electrical energy while walking to power small electronic devices. For example, when carrying a backpack, the body applies forces on the backpack or any other mass which changes the direction of its motion. This method was demonstrated in [2] with a spring-loaded backpack that utilizes vertical oscillations to harvest energy. The paper presented a system that generated about 7.4 W from a load weighing 38 kg with the subject walking at a relatively fast pace (at approximately 6.5 km/h).

When walking with the backpack, it makes a 3-D like motion, that is an Up-Down, Right-Left motion resulting in a relative displacement of approximately 50 mm. The linear motion was converted into rotary motion and was used to drive an alternating current (AC) generator (at 25:1 geared motor). Energy was generated with small amount of extra metabolic cost (19 W which is equivalent to 3.2% more than carrying a load in regular backpack mode, that is, with no relative motion).

Another backpack concept was demonstrated in [21] where the energy harvester generated a power of 50 mW from a piezoelectric material mounted to the shoulder strap of a 44-kg backpack.

In [9], a linear electrical generator was built that was based on the oscillations of a floating magnet during motion. The generator produced power output in the range of 90-780 mW depending on the walking conditions. The electrical circuits and linear generator design were optimized to produce the highest power output from the walking motion.

2.1.2 Heel Strike Method

The heel strike method is another approach in the state of the art of energy harvesting around which several devices were built. Some of the devices built using this method harvest the energy from the relative motion between the foot and the ground during regular gait [22]. Others used the energy from the bending of the shoe sole as the heel lifts from the ground [23]. What is common in both cases is that the energy harvesters attempt to reuse the energy that would have otherwise been wasted or dissipated in the heel deformation.

One realization of this concept is a hydraulic reservoir with an integrated Electromagnetic generator. It uses the difference in pressure distribution on the shoe sole to generate a flow during the gait cycle. The prototype produced between 250 to 700 mW while the subject was walking (depending on the weight and pace of the subject). One major drawback of this approach is its weight and bulkiness.

[22] described a generator which was built based on heel strike and the toe off motions which harvested up to 10 mW during a gait cycle from piezo-electric shoe inserts. The paper also described a magnetic rotary generator applying the same method. The average power generated over three consecutive steps for this magnetic generator was then calculated and found to be approximately 58.1 mW, with the peak power reaching approximately up to 1.61 Watts.

In [24] electrostatic generators were developed based on the electroactive polymers (EAPs) which generate electricity as a function of mechanical strain. The technology described provided energy densities for practical devices of 0.2 J/g. The design incorporated an elastomer into the heel of a boot which achieved a 0.8 J/step harvested during a compression of 3 mm of the heel of the boot.

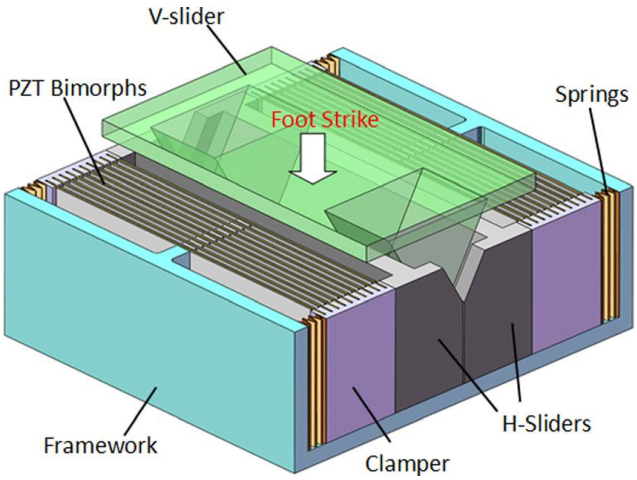

Fig. 2. 1 Piezoelectric energy harvester model, which includes an amplification mechanism (V slider, H-sliders, and clamper), PZT bimorphs and a framework. When the foot strikes the V-slider, the amplification mechanism transfers the impact force to the clamper, which then deforms the PZT bimorphs to generate electricity [25].

An advantage of this type of design is that it can easily be incorporated into the heels of an existing shoe with no need for any special modification. On the other hand, the power output is relatively low and not suitable for any watt level application.

[25] described a piezoelectric energy harvesting system (Fig. 2. 1) based on the heel strike method and generated between 18.6 mW and 27.5 mW with the subject walking at 1.0 Hz and 1.5 Hz, respectively. The system used a motion amplification method to increase energy harvesting efficiency by modifying the mode in which the piezoelectric bimorph was deformed.

2.1.3 Knee Motion method

In [9] and [10], some devices were proposed that would take advantage of the negative energy by the knee during gait to generate electricity. This concept was subsequently developed and presented in [11] and [26]. The device comprised of an orthopedic knee brace in a fashion that allows the knee motion to drive a gear train through a unidirectional clutch, transmitting only knee extension motion to a DC brushless motor that served as the generator. This method generated 2.5 W per knee at a walking speed of approximately 1.5 m/s. A similar concept was also reported in [18] and the is shown in Fig. 2. *2*.

Fig. 2. 2 - The biomechanical energy harvester comprises an aluminum chassis and generator (cylindrical component at the top of the chassis) mounted on a customized knee brace (black) [18].

The additional metabolic cost of generating energy (not including the cost of carrying the device) was 4.8 W, i.e., 12.5% of the metabolic cost required by conventional human power generation. The drawback associated with this device is that it used only a small part of the motion of the knee (end of the swing phase - (swing phase is defined as the period between safe toe clearance and a gentle foot landing [1], [11])) to generate energy.

Now, the muscle net work in the knee joint during a gait is mostly negative work. As stated in [1] and [3], about 90% of the work done by the knee is deemed to be negative work, which

translates to approximately 34 W of available energy but the device harvested energy only at the end of swing phase with a 65% efficiency.

The difference between the power harvested by the current device and an ideal device (device that can convert most of the negative work into harvestable energy) is given by the following expression:

The available power $= [total\ power - \frac{current\ power}{efficiency}] x\ device\ efficiency$

Based on available data, and applying the above formula, the authors of [3] demonstrated through calculations that the amount of available power from the knee for harvesting is:

$$= \left[33.5 - \frac{5}{0.65}\right] x\ 0.65 = \ 16.8\ \text{W}.$$

This expression shows that there is still a lot of power available for harvesting compared to what was actually harvested. However, the main obstacle here is that the resistance to motion during gait increases with harvested energy.

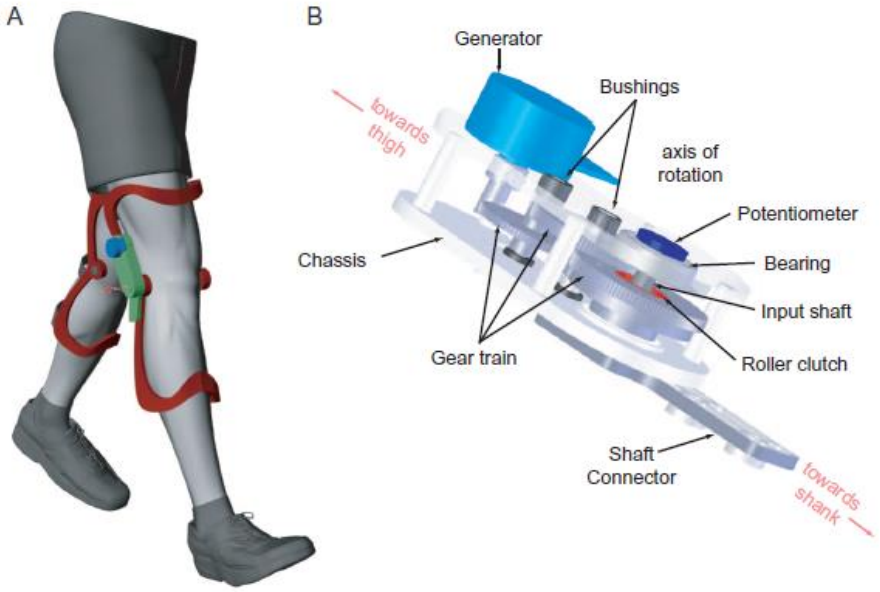

Fig. 2. 3 - Biomechanical energy harvester. (A) harvesters are worn on both legs. (B) mechanical design [27].

A similar concept is shown in Fig. 2. 3 for a similar concept described in [27] as a system whose gear train are driven during the swing phase but whose load is only connected towards the end of the swing phase. The concept described generated up to 5 V and a minimum of 0.1 A current. The system was used as a USB charger for electronic devices. However, this type of design requires almost the same level of effort to drive the gear train whenever they are worn – excepting the effect of the load on the rotor torque when a load is connected.

Moreover, this design is using an off-the-shelf generator that was not optimized for this type of wearable energy harvester, however, there are significant energy harvesting potentials at the knee that with the right techniques and optimizations they would offer a more efficient solution.

Another concept of the knee-motion based energy harvesting system utilizing the concept of negative energy that employed a piezoelectric energy harvester is shown in as described in [12].

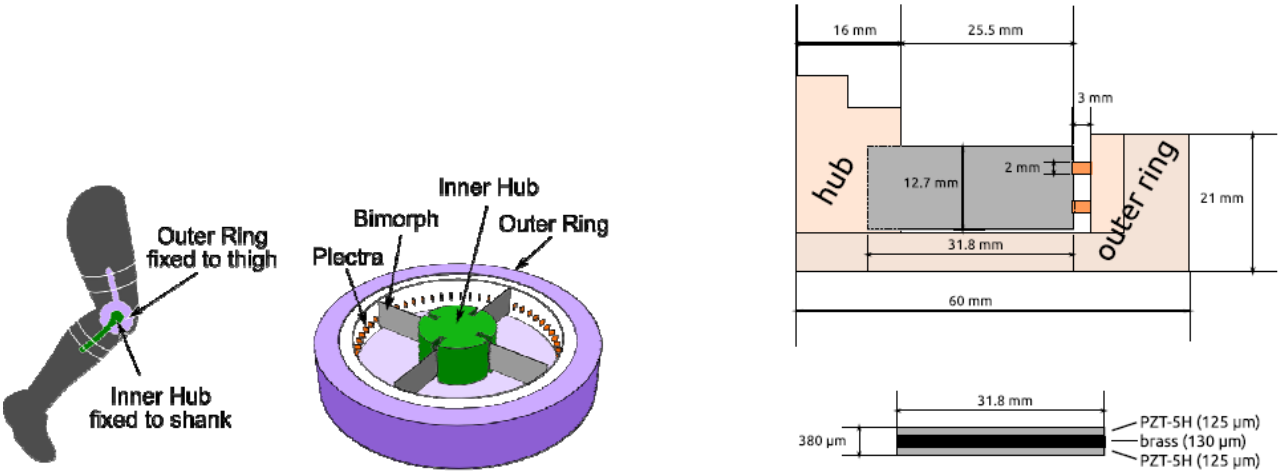

Fig. 2. 4 - Knee-joint piezoelectric harvester. It is worn on the external side of the knee and fixed by braces. Inside, a hub carries number of bimorphs which are plucked by the ring-mounted plectra as the joint rotates during walking. b. geometrical details of the harvester showing side view (above) and top view of mounted bimorph (below) [12].

2.1.4 Ankle Method

According to [10], the ankle was listed as having the highest amount of energy harvesting potential, the knee and the hip being the next two, respectively (Table 2. *1*). However, there is the challenge of designing an energy harvesting system that connects solely to the ankle.

Table 2. 1- Energetic motions for biomechanical electric power [10]

Joint/Motion	Work [J/Step]	Power [W]	Max Moment [Nm]	Negative work [%]
Heel Strike	1(1-5)	2(2-20)		
Ankle	34.9(33.4)	69.8(66.8)	~140	42(28.3)
Knee	24.7 (18.2)	49.5(36.4)	~40	85.2(92)
Hip	19.6(18.96)	39.2(38)	~40	11.5(19)
Elbow	1.07	2.1	1-2	37
Shoulder	1.1	2.2	1-2	61
Center of Mass	0.5	1		

A simulation describing the design of an energy efficient transfemoral prosthesis using lockable parallel springs and electrical energy transfer was discussed in [28]. It concluded by proposing a form of energy transfer mechanism from the knee to the ankle. While there is theoretical energy harvesting opportunity at the ankle, the implementation still poses a considerable challenge.

2.1.5 Competing Technologies – Challenges and Limitations

The fundamental research question was one that seeks to address power supply problems for connected mobile devices. As stated in [19], "we have systems that are wireless except for power." Some technologies have been adopted by many researchers in an attempt to address this power problem. For this reason, a review of many of the existing energy technologies was done and presented in this section. This was done in an effort to formulate a clear target and research focus – if there are better alternative solutions to the problem statement in terms of relative availability, relative low cost of harvesting, and amount of harvested power, it should be adopted.

Table 2. 2 shows a comparison of the competing technologies which include temperature, solar, piezoelectric, radio frequency and Electromagnetic energy.

Table 2. 2 - Comparison of the power output of most of the known energy harvesting sources

Energy Source Power	Density & Performance	Source of Information
Acoustic Noise	0.003 μW/cm3 @ 75Db 0.96 μW/cm3 @ 100Db	(Rabaey, Ammer, Da Silva Jr, Patel, & Roundy, 2000)
Temperature variation	10 μW/cm3	(Roundy, Steingart, Fréchette, Wright, Rabaey, 2004)
Ambient Radio Frequency	1 μW/cm2	(Yeatman, 2004)
Ambient Light	100 mW/cm2 (direct sun) 100 μW/cm2 (illuminated office)	Available
Thermoelectric	60 μW/cm2	(Stevens, 1999)
Vibration (micro generator)	4 μW/cm3 (human motion—Hz) 800 μW/cm3 (machines—kHz)	(Mitcheson, Green, Yeatman & Holmes, 2004)
Vibration (Piezoelectric)	200 μW/cm3	(Roundy, Wright, & Pister, 2002)
Airflow	1 μW/cm2	(Holmes, 2004)
Push Buttons	50 μJ/N	(Paradiso & Feldmeier, 2001)
Shoe Inserts	330 μW/cm2	(Shenck & Paradiso, 2001)
Hand generators	30 W/kg	(Starner & Paradiso, 2004)
Heel strike	7 W/cm2	(Yaglioglu, 2002) (Shenck & Paradiso, 2001)
**Knee (Negative Energy from knee motion)	5 W (Empirical result)	Donelan JM, Li Q, Naing V, Hoffer JA, Weber DJ, Kuo AD

A snapshot of the comparison of the energy harvesting potentials of various energy harvesting sources [15] is presented in the above table. Although the figure of merit was not based on the same units, probably due to the nature of the energy harvesting technology represented, the density and performance column shows flattery figures for hand generators. However, hand generators require some unnatural hand motion for operation as well as the extra metabolic costs associated with using them in such a way.

Heel strike and knee-joint generators are the next two, respectively and could offer useful harvested energy at very little extra metabolic costs – while maintaining their natural uses.

Here below are some of the contending energy harvesting technology solutions – potentials and limitations.

2.1.5.1 Solar Energy Harvesting

Solar cells take advantage of the photovoltaic effects to convert light energy into electrical energy. These cells are mainly made of silicon doped with some impurities. When exposed to light energy, the electrons in their structures break free from the silicon and flow through the silicon surface to create direct current (DC) electricity. This process is referred to as the photovoltaic effect.

Solar energy is one of the most abundant sources of energy for harvesting. The irradiance ranges from 100 $\mu W/cm^2$ in brightly lit indoor environment to 100 mW/ cm^2 in bright sunlight [29]. The efficiency of solar energy harvesting is a measure of the ratio of the actual energy harvested to the available solar energy.

Solar converters commonly used in calculators, with conventional single crystal and polycrystalline structures, have efficiencies between 10 and 20 percent in direct sunlight [29]. Their efficiency, however, degrades rapidly with decrease in luminous intensity of the available sunlight.

For ubiquitous energy harvesting solar panels, they are sometimes attached to non-rigid surfaces. However, most existing solar panels are inflexible and difficult to attach to non-rigid surfaces. The authors of [30] demonstrated an organic based semi-conductor solar panel that solves this problem. This type of solar cell operates with constant efficiency over different brightness levels, the downside is the low overall efficiency level, usually around 1 to 1.5 percent. Another disadvantage of flexible organic solar cells is that they are reactive to water and oxygen. Researchers have devised a means of overcoming this shortfall. One approach followed was encapsulation against environmental degradation [29].

Recent advancements in photonic materials trade more area for less money or less area for better efficiency [31]. Organic and Copper Indium Gallium Selenide (CIGS) systems have demonstrated flexibility and durability innate to their design with an at best efficiency range of 5 to 20. Fig. 2. 5 shows the image of an organic semi-conductor based small molecular solar cell.

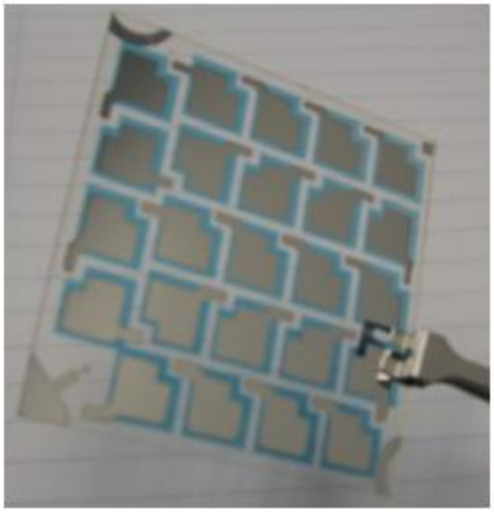

Fig. 2. 5 - An organic semiconductor-based small-molecule solar cell [29].

2.1.5.2 Acoustic Energy Harvesters

Acoustic energy harvesters convert sound energy into electrical energy. The technology behind this is the Helmholtz resonator which consists of an orifice, a cavity, and a piezoelectric diaphragm.

When air is forced into a cavity, air pressure inside the cavity will increase in proportion to the force of the outside air; however, when the external force pushing the air into the cavity is removed, the higher-pressure air inside will flow out. But this surge of air flowing out will tend to over-compensate, due to the inertia of the air in the neck, and the cavity will be left at a pressure slightly lower than the outside, causing air to be drawn back in. This process repeats, creating acoustic energy whose magnitude changes, decreasing each time until its effect is no longer felt.

The acoustic energy so generated is then converted into mechanical energy as the sound wave incident on the orifice generates an oscillatory pressure in the cavity, which in turn causes the vibration of the diaphragm. Piezoelectric transduction converts this acoustic energy into electrical energy.

The form of energy generated by acoustic harvesters is in the form of alternating current (AC) [32] which is then conditioned to supply direct current (DC) voltages. Acoustic power generation have been proven to generate power with an overall power density of 70 W/cm^2 and 25 W/cm^3 using a pre-stressed stacked PZT ceramics operating at 16 KHz with an efficiency of 84% [32].

Acoustic converters take input signals with frequencies ranging from as low as less than 1 Hz to 10’s of KHz. The input signals could come from various sources including but not limited to machines, humans or nature.

Fig. 2. 6 shows an illustration of the acoustic energy harvesting concept. The incident wave/signal present at the plane wave tube input is converted by the energy harvester circled in

red below which is conditioned by the energy harvesting circuitry otherwise known as power management circuit before it is used to charge a super-cap or battery where the energy is stored until it is needed.

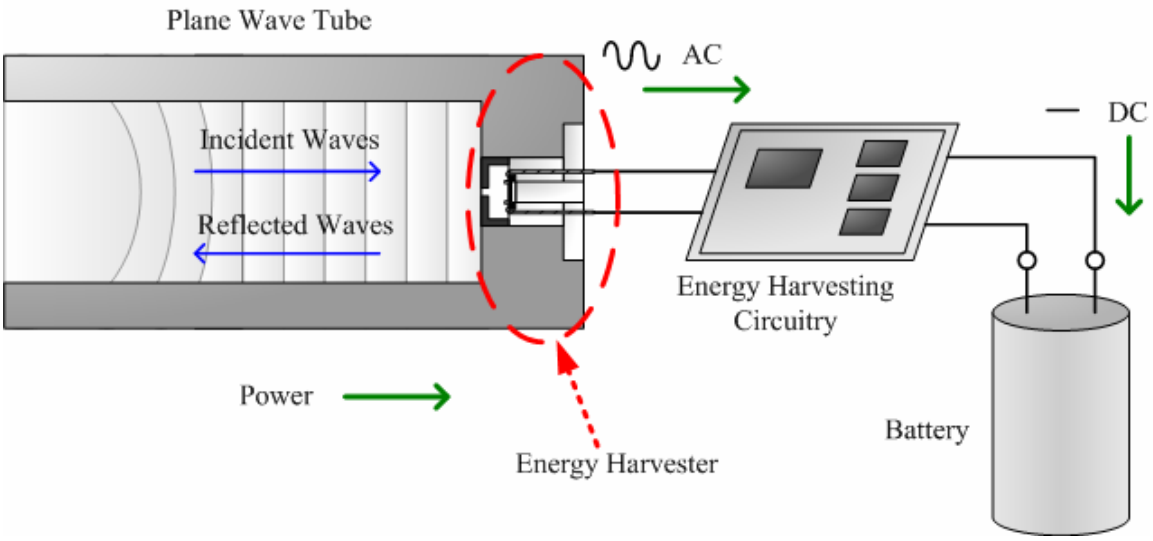

Fig. 2. 6 – Schematic of overall energy harvesting concept

A major competing technology to piezoelectric harvesting technology is the solar cell [33] discussed in the section above. Now, for piezoelectric generators to remain relevant in the solar harvesting technology world, they must have a large acoustic power density in the structure such that the generated power exceeds that of the photovoltaic cells, operate in an enclosed region such as buildings, tunnels or automobiles and moving structures such as a rotating system. Their special installation and handling makes them unsuitable as a wearable technology solution.

2.1.5.3 Thermal Energy Harvesters

Thermal harvesters make use of temperature differences in materials to generate electricity. At the Core of the thermoelectric effect is heat flow which arises due to a temperature gradient in conducting materials; this phenomenon gives rise to a process known as diffusion of charge carriers [34]. The resulting flow of charge carriers between two dissimilar temperature regions brings about a voltage difference.

Based on this technology, a German based company, Micropelt, fabricated an efficient thermoelectric energy harvesting device with up to 50 thermocouples per mm^2. Thus, the voltage per mm^2 is 200 to 400 times higher than that of legacy thermoelectric generators (TEGs), giving an ideal starting point for efficient conversion to useful battery-like operating voltages [35]. Micropelt developed a built-in chip thermo-generator which takes a few degrees of temperature differential and harvests thermal energy to operate a wireless sensor node, enabling unlimited battery-free operation.

Although the numbers are impressive for this technology, the overall power generated is less than 100 milli-watt output power making the generated power limited for many of the applications envisioned by this thesis research.

2.1.5.4 Mechanical/Piezo Energy Harvesters

Piezoelectricity is the form of electrical energy that is generated when a mechanical stress is applied to a piezo material.

Authors of [36] postulated different piezoelectric generators based on diverse applications. They reported that harvesting power from human body motion for implantable and wearable electronics have been studied. Drawing from the understanding that human motion is capable of large-amplitudes and low frequencies, and that smaller objects possess higher resonant frequency, they argued that it will be difficult if not impossible, with known technologies, to design a miniature resonant energy scavenger that works on humans. Thus, "for most piezoelectric generators in human applications, the piezoelectric patch is coupled either through direct straining or by impacting the kinetic driving source" [36]. The implication of this is that there is still a technical limitation on implementing energy harvesting technology with the piezo electric devices, with current technologies, as a human wearable system.

Now, the form of electrical energy generated by piezoelectric generators is AC in nature and would normally require some form of AC to DC conversion (Fig. 2. 7).

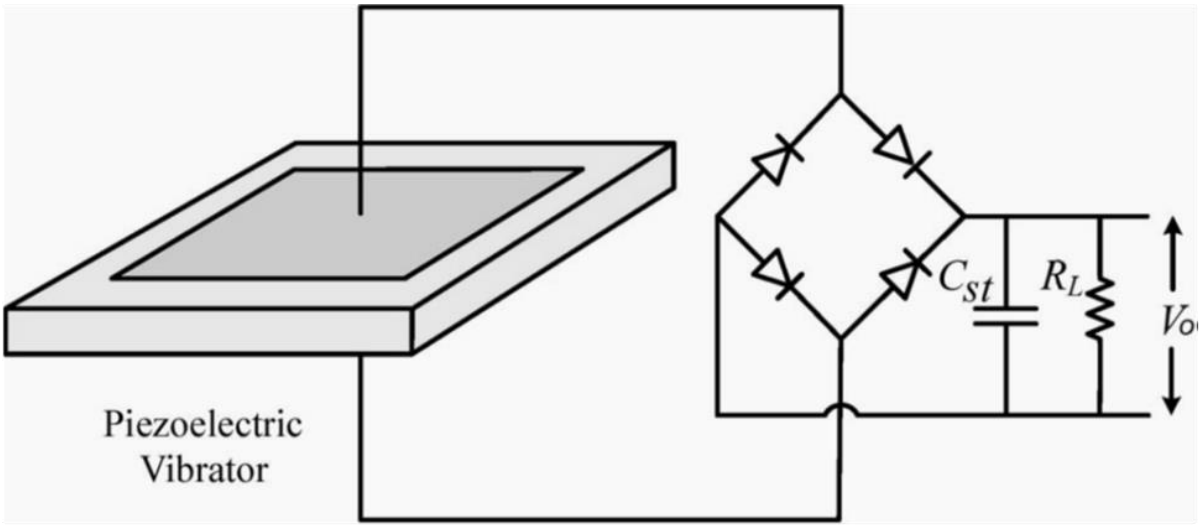

Fig. 2. 7 - Standard ac–dc harvesting circuit with piezoelectric generator [36].

Again, while the generated voltages could be very high, the generated currents are usually low in the order of micro amps or less, because they possess high input impedances, making the overall harvested power correspondingly low.

2.1.5.5 Radio Frequency (RF) Energy Harvesters

Energy from radio frequency waves can be harvested using RF harvesters. These energy sources are normally from high electromagnetic fields such as TV signals, Wireless Radio networks and cell phone towers.

When an electromagnetic wave is intercepted by an electrical conductor, there is an induced electrical energy. This induced energy is usually very weak and in the order of microwatts or less and would require some form of amplification of the received signal for regular radio communication to take place. Now, because energy scavenged by RF harvesters are usually very weak, voltage amplifications are needed to boost the received signals.

Fig. 2. 8 is a typical example of a voltage doubler circuit that could be used to improve the harvested DC voltage. This circuit configuration doubles the harvested voltage but the current will be reduced to half its original value. This behavior satisfies the rule of conservation of power which states that, in a lossless system, the power generated is equal to power delivered.

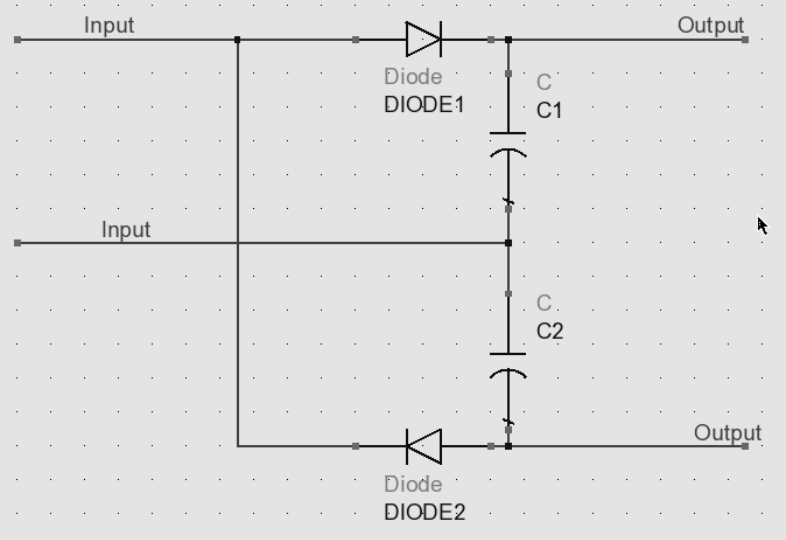

Fig. 2. 8 – Voltage-Doubler Circuit Diagram [34]

RF harvesters make use of RF antennas to receive these emitted signals and then convert them to DC voltage which is then stored in capacitors or other forms of energy storage devices. Fig. 2. 9 shows a generic block diagram of an RF harvesting system. This type of harvester has a great advantage over solar, acoustic and mechanical vibration harvesters.

This is because RF energy is constantly available and therefore more reliable than those other sources, however, the amount of power available for harvesting are not as much. It could be confirmed from table 2.1 that the amount of **power harvestable from RF sources are relatively low** although they might be suitable for other energy harvesting needs especially for sensor nodes that run on ultra-low power.

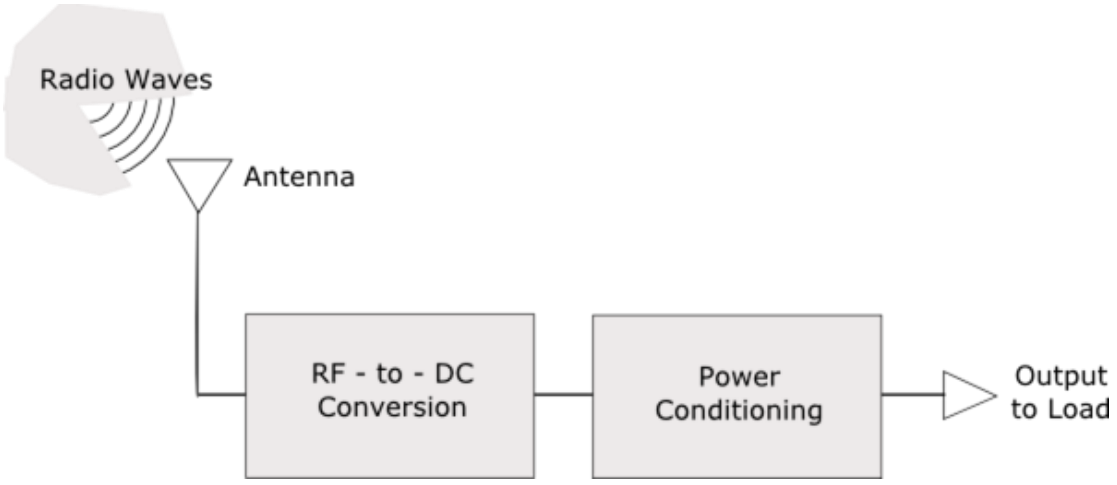

Fig. 2. 9 – Generic block diagram of an RF energy harvesting system showing the Core basic blocks [34]

Authors of [37] discussed a capacitive radio frequency micro-electromechanical switch (RF MEMS) which is a co-planar waveguide (CPW) shunt switch (see Fig. 2. 10). They demonstrated that the switch operates as a digitally tunable capacitor with two states. "When the membrane is in the up position (switch-off), the signal line sees a small value of parasitic capacitance, while when the membrane is pulled down by actuated voltage (switch-on), the signal line sees a high value capacitor shunted to ground."

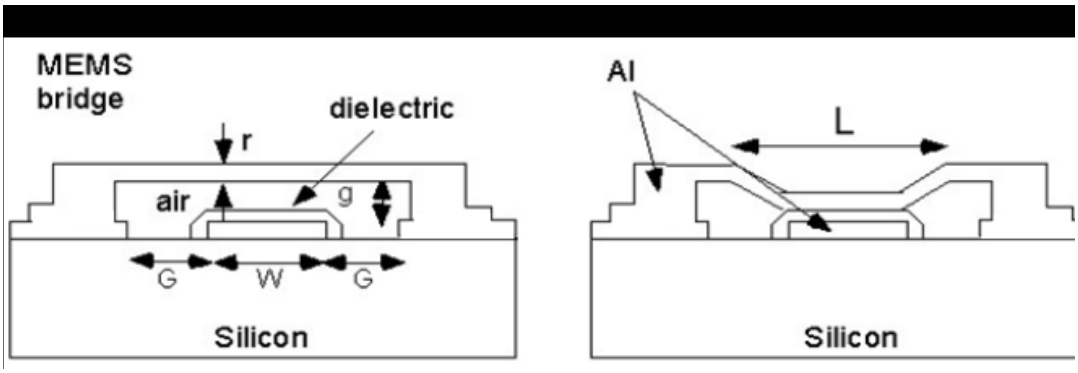

Fig. 2. 10 - Diagram showing the operation of an RF MEMS switch [37].

In [38], researchers demonstrated an RF harvester based on the principle of the crystal radio receiver. Their technology could harvest and convert energy from a TV station over 4 Km away

to up to 0.7 V of DC voltage, which was then used to power a wall-mounted household weather station.

Researchers from Georgia Tech School of Electrical and Computer Engineering demonstrated a unique system of RF energy harvesting with an antenna printed by ordinary inkjet using Nano-particle ink as shown in Fig. 2. 11. The substrate is either paper or a flexible polymer. The ink is described as 'a unique in-house recipe' containing silver Nano-particles and/or other Nano-particles in an emulsion [31]. This team's harvesting device could scavenge energy over a wide range of frequency bands spanning all known useful radio frequency bands from as low as 100 MHz up to and including 60 GHz.

Fig. 2. 11 - RF Energy Harvesting Sensor node printed on paper using inkjet technology [39]

In their work, they made the energy harvesting system 'environmentally friendly' - reducing the carbon foot print - by printing on biodegradable substrates. By combining the energy-scavenging technology with super-capacitors and cycled operation, they expect the harvested power to be sufficient for devices requiring around 50 mW of power.

Although this breakthrough has so many useful applications, the maximum energy harvesting potential is very low for any system that require more than a few milli-watts of power. There still, however, is a great potential and opportunity for radio frequency energy harvesters and research continue in the field of wireless power transmission and further advancements in electronic devices requiring lesser amount of power for normal operation.

2.1.5.6 Electromagnetic Energy Harvesters

Electromagnetic energy harvesters take advantage of the Faraday's law of Electromagnetic induction to generate electrical energy from mechanical motions. This involves a relative motion between an electrical conductor and a magnetic field. The voltage induced on the conductor is proportional to the rate of change of the magnetic flux linking the conductor.

Electromagnetic energy harvesters have been designed as an on-demand energy harvester [34] such that the amount of power they generated were targeted for specific applications. They could be designed as linear generators (example, push buttons) or rotary generators (example synchronous generators).

In [22] researchers demonstrated various systems with off-the-shelf DC brushless motors used as generators to generate 250 mW of power (with a peak of 1.61 W of output power).

A bottom up design approach to electromagnetic energy harvesting design has many advantages over off-the-shell generators. Their output impedances could be predetermined by the type and size of coils used in their windings. This is one of their unique features. This means that their adaptation to power management circuits could be seamless to optimize maximum power transfer. They also function efficiently over a wide frequency range making them suitable in both low frequency and high frequency applications.

They could be used in hand crank generators, shoe inserts, hip-mounted, knee-mounted, hinged-opening-mounted, push buttons and in vibrating environments. As shown in Table 2. 2, they have been shown to provide the highest amount of harvested power per kilogram.

Chapter 3

Electromagnetic Energy Generator

3.1 General overview

In view of the fundamental research question and the proposed solution in chapter 1 as well as the literature review of chapter 2, this chapter will be dedicated to the development of a proof of concept to actualize the proposed solution – electromagnetic energy generator.

The electromagnetic energy generator presented in this thesis, much like any other known electromagnetic generator, relies on the classical Faraday's law of electromagnetic induction [40]. This requires two parts that move relative to each other. To meet this condition, a conventional electromagnetic generator has a stationary part – called the stator and a moving part – called the rotor.

In these conventional generators, the rotor moves only in one dimension with respect to the stator, while in the proposed adjustable power electromagnetic energy generator, the rotor moves in two dimensions – rotary and vertical (see Fig. 3.1 below). In one dimension (rotary), it revolves around the stator axis while in the second dimension (vertical), it moves closer to or farther away from the stator to increase or decrease the magnetic flux concentration on the stator-core, respectively. This correspondingly increases or decreases the harvested power. Refer to section 4.1.2 for additional details on the Generator Structure.

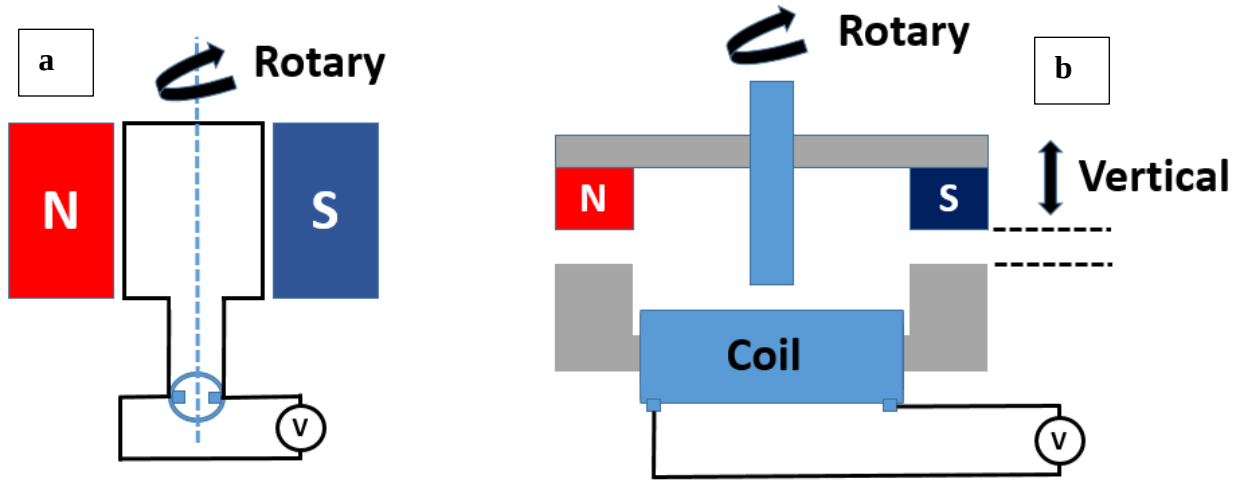

Fig. 3.1 – (a) Illustration of the conventional generator (left) vs (b) the adjustable generator (right)

3.1.1 Principle of Operation of the Electromagnetic Generator

When a magnetic flux crosses through a conductor or a conductor is brought into the path of a magnetic flux, see Fig. 3.3 below, there is an induction of electric energy called Electromotive force (EMF). This is the Faradays law of electromagnetic induction. This law states that 'the EMF around a closed path is proportional to the negative of the time rate of change of the magnetic flux enclosed by that path' [40]. This is the same principle of operation in electric generators, transformers, electric motors, and solenoids.

In mathematical form, the Maxwell – Faraday's law could be represented as [40]:

$$\nabla \text{ x } \mathrm{E} = -\frac{\partial B}{\partial t} \quad \text{.....Equation 1}$$

Here ∇ X is the curl operator and **E**(r, t) is the electric field strength while **B**(r, t) is the magnetic flux density. These fields can generally be functions of r and t representing position and time respectively. The units of the terms used above are the standard SI units.

The Maxwell–Faraday equation above is one of the four Maxwell's equations, and therefore plays a fundamental role in the theory of classical electromagnetism. It could also be expressed in an integral form by the Kelvin-Stokes theorem as:

$$\oint_{\partial \Sigma} \mathbf{E}.\, d\ell = -\int_{\Sigma} \frac{\partial \mathbf{B}}{\partial t}.\, d\mathbf{A} \quad \text{..... Equation 2}$$

Where, **Σ** is a surface bounded by the closed contour **∂Σ** (see fig. 3.2 below), **E** is the electric field strength, **B** is the magnetic flux density, d**ℓ** is an infinitesimal vector element of the contour **∂Σ**, d**A** is an infinitesimal vector element of surface **Σ**.

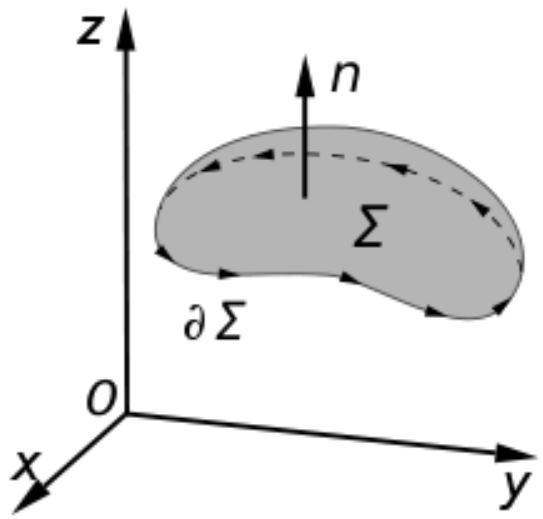

An illustration of Kelvin-Stokes theorem with surface Σ its boundary $\partial\Sigma$ and orientation n set by the right-hand rule.

Fig. 3.2 - Illustration of Kelvin-Stokes theorem [34]

The above equations represent an electromagnetic generator whose winding has a single turn. In a situation with N-turns tightly wound to each other, the equation is modified slightly such that the induced voltage is a multiple of N.

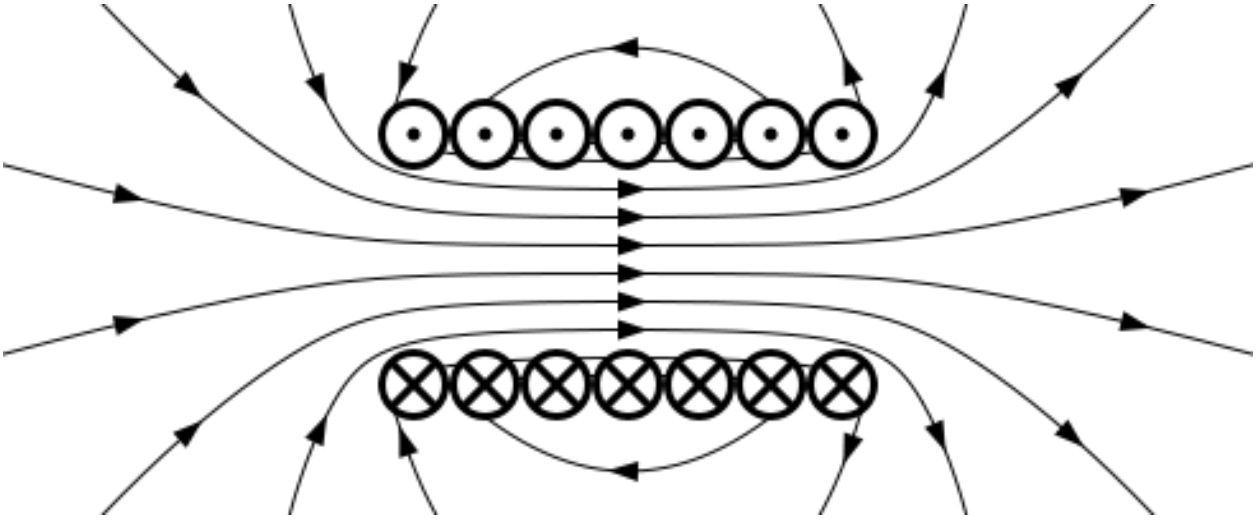

Fig. 3.3 – Magnetic field lines through a conductor [34]

From the foregoing, the following is deduced:

1. If the time rate of magnetic flux change is constant, the amount of flux variation experienced by the conductor/winding can be predicted. This implies that if the delta of the flux variation is known and the frequency of said variation is also known, then the

overall flux variation experienced in the conductor is a product of the 'delta' and frequency.

2. If the delta – amount of flux variation – in a given time can be determined, the magnitude of the generated voltage by using windings with 'N' turns that correspond with the expected output voltage can determined, and then using the right wire gauge for the expected DC impedance of the winding by applying the formula:

$$R = \rho\frac{l}{A} \quad \text{.....Equation 3}$$

Where R is the DC resistance of the winding, ρ is the resistivity of the winding conductor, l is the length of the conductor, and A is the cross-sectional area of the conductor.

3. By combining one and two above, a generator with specific output characteristics vis-à-vis output voltage, impedance and current could be built.

Fig. 3.4 shows a simplified version of the equivalent circuit of the proposed generator and load, where:

G = Generator
$\mathbf{V_G}$ = Generator open-circuit voltage
$\mathbf{R_S}$ = Generator internal resistance
$\mathbf{V_L}$ = Generator on-load voltage
$\mathbf{R_L}$ = Load resistance
$\mathbf{X_L}$ = Generator Coil Reactance

The impedance of the generator is made up of the series inductive reactance ($\mathbf{X_L}$) and the series coil resistance ($\mathbf{R_S}$). They are modeled in series as shown below.

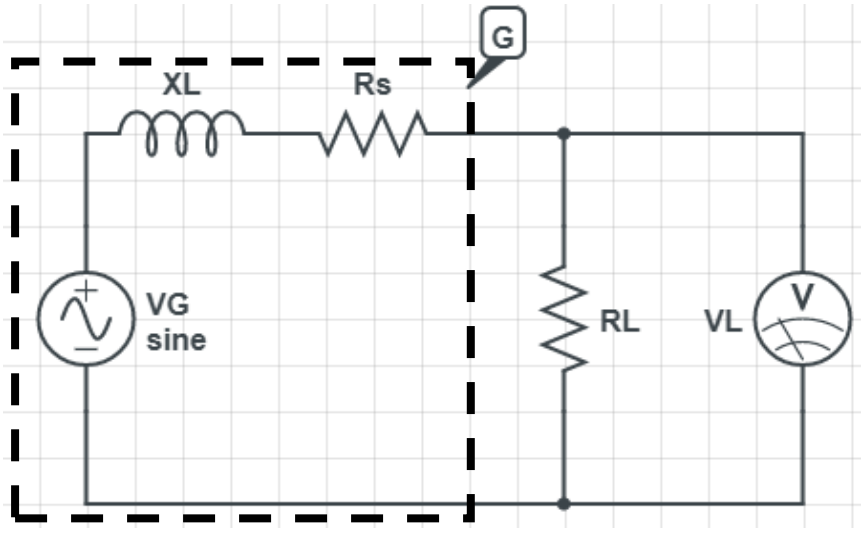

Fig. 3.4 - A simplified version of the Generator Equivalent Circuit.

This model represents a high-level simplistic model that does not include the effects of conductivities of all the solid parts, the leakage flux, and the real saturation in the various parts of the magnetic circuit.

3.1.2 Design Constraints

At the beginning of this research work, some agreements were reached with the sponsor on the material, design and geometry of the final product – henceforth referred to as constraints.

These constraints formed the overall guiding principles for the product that would later be developed and presented as a proof of concept. They are summarized below as follows:

Design constraints: Material, Design, and Geometry configuration.

- **Material constraints** – The design was constrained by the materials that are existent in the market today. It was not required to create or invent new materials for this research, rather to use existing materials in the proof on concepts.
- **Design Configuration Constraints** – The energy harvester shall be adjustable after final fabrication and packaging allowing the equipment to be used by different people and for various applications at selectable settings. The product should not hinder the, in a significant way, the regular functions of the motion source.
- **Geometry Constraints** – the design should be comparable in size to other equipment worn by military personnel. The size for the proof of concept was no more than (3” x 4” x 8”) based on the average size of a water canister. The size and the material have some guidelines around them, and the weight target should be under 500 grams or close to that.

The weight constraint is mainly because the intended target customer for this design is the military and they have strict requirement for weight. However, the dimension constraint was mainly to keep the design proportional to the legs and hands of a military personnel standing sentry such that the size is comparable to the water canisters or other equipment worn around the waist or knee by the said military personnel.

3.2 General Configuration of the New Generator Design

A changing high density magnetic field is essential to a corresponding high electromagnetic induction. This is made possible by using the Neodymium rare-earth magnets. They possess the highest known amounts of magnetic flux density per volume compared to other magnets [41].

Equation 4 predicts that more magnetic poles would favor higher electromagnetic induction. An optimistic approach might then be to use an unlimited number of poles, but it is impractical to have an infinite number of poles, the design constraints on the product size, notwithstanding.

As any of these increases - the number of poles, number of windings or size of magnet – there is the need to optimize, otherwise, there is the risk of building a product whose weight and size is

extremely high and will violate the design constraints on weight and size and in addition, cause an increase in the energy costs of carrying the device.

$\mathrm{EMF_{rms}} = 4.44\ \mathrm{k_c k_d} \phi f \mathrm{T_{ph}}$ ..... Equation 4 [42].

Where:

$\mathrm{k_c}$ = Coil Span Factor; $\mathrm{k_d}$ = Distribution factor; ϕ = Flux per pole; $f = frequency$ of induced EMF; $\mathrm{T_{ph}} = Number\ of\ turns\ per\ phase$; *and* $f = \frac{\mathrm{RPM\ x\ P}}{120}$

$here\ P = number\ of\ poles, while\ RPM\ is\ the\ revolutions\ per\ minute$

For a single coil design, as is the case presented in this thesis, $\mathrm{k_c} = 1$ and $\mathrm{k_d} = 1$.

$Therefore,\ \mathrm{EMF_{rms}} = 4.44\ x\ \phi\ x\ f\ x\ \mathrm{T_{ph}}$

Note also that from equation 1, the induced EMF is inversely proportional to the change in time 't'; where $\mathrm{t} = \frac{1}{f}$. Hence, the higher the value of 'f', the lower the value of 't' (and vice-versa), which invariably yields more EMF.

There are two major limitations to the number of feasible poles. The first being the relative size of the generator, as imposed by the design constraints, and the second being the proximity of the magnets to one another. The magnets should maintain a certain minimum clearance from one another to minimize flux leakage between the poles.

The idea is to have varying regions of very high and very low magnetic fluxes or alternating magnetic flux 'polarities'. This arrangement will ensure that as the rotor moves, the coil winding experiences changing magnetic fields from low to high or from north pole to south pole which as governed by the Faraday's law will lead to electromagnetic induction.

Having a continuous field of magnetic flux around the core of the stator and the windings without regions of low and high magnetic fluxes or alternating north and south poles distinct from each other will not work well with the configuration presented because the winding consists of a single continuous conductor on a single stator core (the stator arrangement is shown in Fig. 3.5).

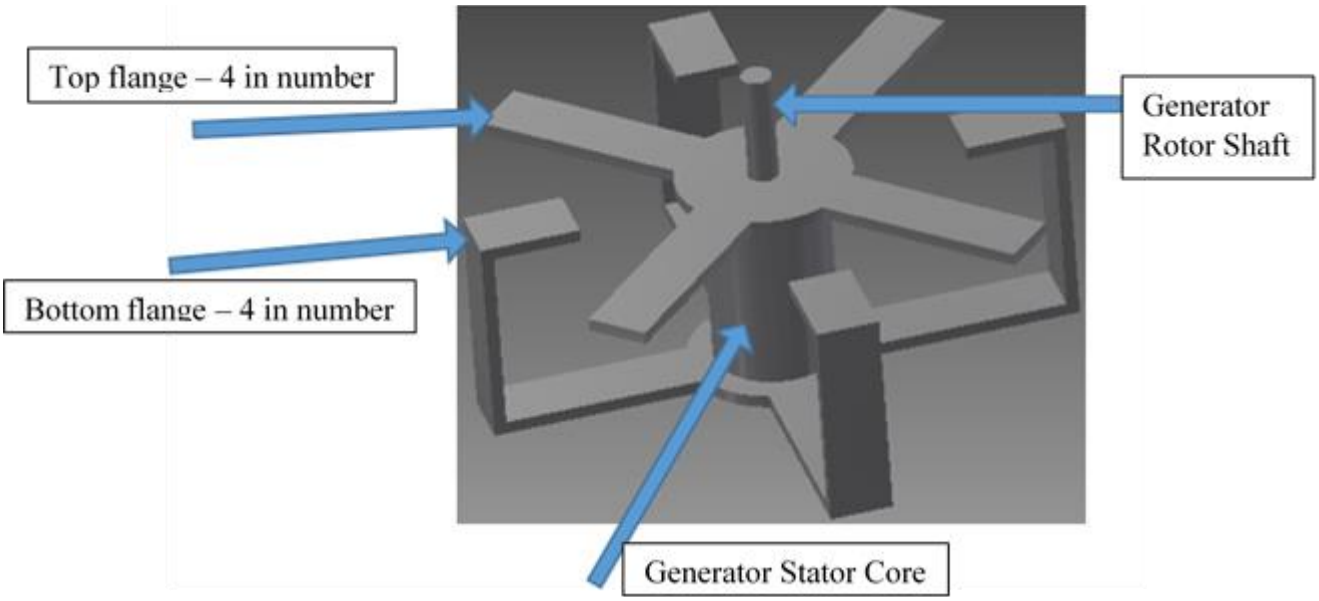

Fig. 3.5 - Stator of the generator showing the flanges and shaft for the adjustable height rotor

If opposite magnetic polarities are applied over a top and bottom flange pair, this will result in a magnetic polarity within the core. Now, as the magnet pair revolves and comes over next top-bottom flange pair, different magnet polarities are lined up against the top and bottom flange pair resulting is a reversal of the magnetic polarity within the core. More details are in section 4.1.2. As the revolution continues, the magnetic polarity of the core varies correspondingly.

Now, to determine the optimal separation distance between magnets in order to maintain a distinct magnetic flux 'polarity' within the stator core, a simulation of the field strength versus distance was run. The illustration of the setup for the measurement of the field strength variation with distance is shown in Fig. 3.6 while the result is shown in Fig. 3. 7.

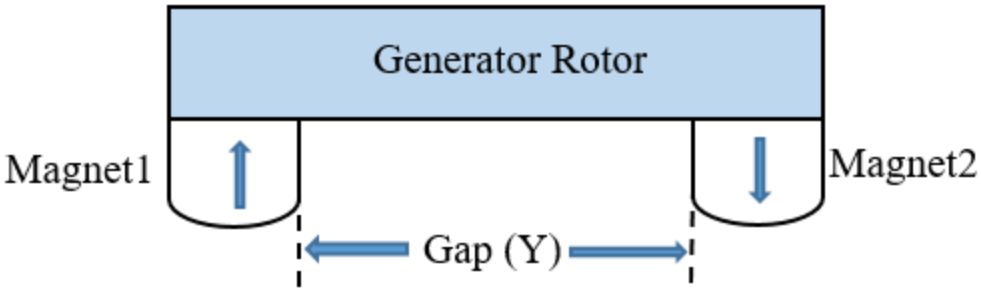

Fig. 3.6 – Illustration of the gap measurement to demonstrate the field strength with distance.

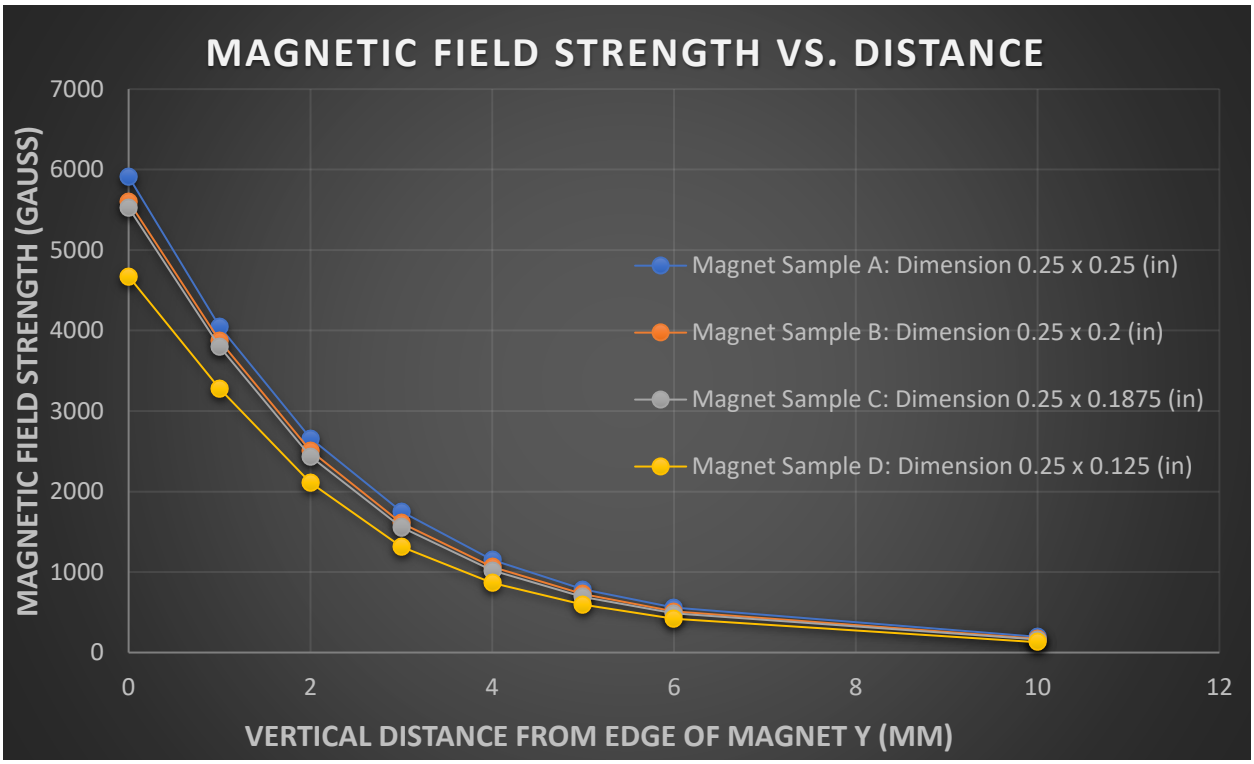

Fig. 3. 7 – Magnetic Field Strength vs. Distance.

Fig. 3.7 shows the values of the magnetic field strength at various distances from the magnet. It shows a result that decayed exponentially with distance. The magnets will be spaced equally apart to ensure symmetry in the flux distribution. For this reason, and to accommodate the dimension of the generator structure chosen to maintain the size constraint stated in chapter 2, the optimum distance was between 8 mm and 10 mm from the end of one magnet to the beginning of the next magnet.

At this distance, the magnetic field strength is significantly low compared to, being within 5 mm or less from the next magnet. This gap ensures that as the rotor revolves with the magnets, the magnetic transition clears one core flange from edge to edge completely before coming over the next flange's leading edge to create a clear alternating magnetic flux within the core of the generator.

The proposed stator core is designed with 4 top and 4 bottom flanges. The 4 top flanges are arranged such that they have the same magnetic polarities from the rotor magnets while the 4 bottom flanges are under the opposite set of magnetic polarities (see Fig. 3.5 above). This arrangement ensures that the generator core appears as a bar magnet at all times with one magnetic polarity on one end and the opposite magnetic polarity on the other end.

As the rotor revolves with the magnets, this stator core polarity alternates correspondingly with the polarity of the magnets directly over them from the rotor. The effect is that the coil winding on the stator core experiences changes in magnetic flux both in magnitude and direction. This change is responsible for the Electromagnetic induction. Fig. 3.8 shows the top view and three-

quarter views of the generator using arrows to indicate the change in the direction of the magnetic flux as the rotor revolves around its axis with the pair of magnets - one over each corresponding top and bottom flange pair – the big orange arrow at the center of each the three-quarter views in Fig. 3.8 represents the direction of the flux within the stator core.

The direction of the arrows indicate the flux direction from the north pole and returning through the south pole of the next magnet using any of the indicated magnetic pair pieces [labeled A, B, C, and D in the top view] as a reference. Note that the opposite sides of the magnets are closed in pairs (one north and one south pole) by another piece of magnetic material to complete the 'magnetic circuit'.

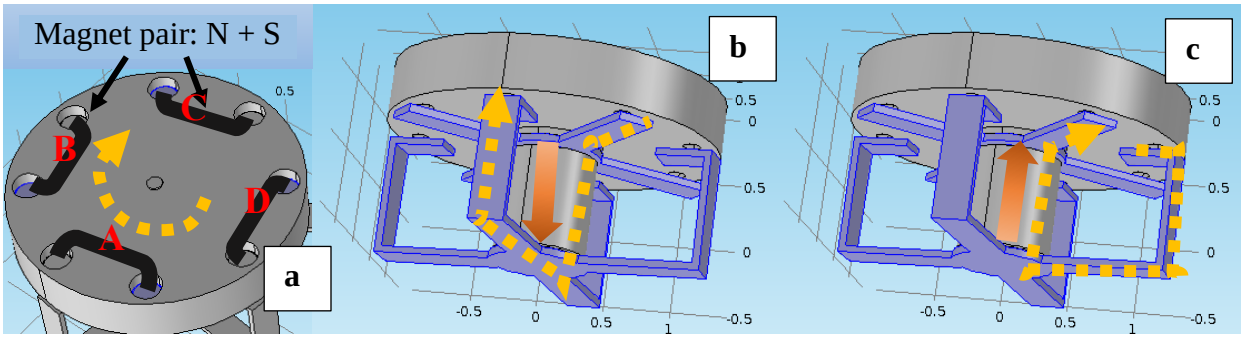

Fig. 3.8 – the direction of the magnetic flux within the generator core (a) top view (b) and (c) three-quarter views

This could be analogous to the way magnetic fluxes are linked in AC tranformers through the transformer core. The source of the magnetic flux in the transformer being the primary winding while in the case of the AC generator, the source of the magentic flux is the permanent magnets.

With the right core arrangement, high concentration of magnetic flux is possible which would lead to a more compact, light-weight and efficient (power-to-weight ratio) design.

3.3 Proof of concept

Having discussed the theoretical framework, principle of operation and the general configuration of the proposed design, the actual parts were fabricated, assembled and tested for the first time. Materials were selected for the prototype, then simulations ran to predict the expected behavior after fabrication.

3.3.1 Prototype, Design Fabrication and Testing

To design this new Electromagnetic generator, some key parameters were identified and optimized for weight and power requirements. Three main parameters were identified as fundamental to achieving an efficient design.

1. **Magnet material and size selection,**
2. **Stator core material selection** and the
3. **Generator Structure.**

3.3.2 Magnet Material and Size Selection

As previously stated, change in magnetic flux linkage with an electrical conductor is key to Electromagnetic energy induction [34]; fortunately, one of the natural sources of magnetic flux is the permanent magnet.

Now, among the permanent magnets, the neodymium rare-earth magnets have the highest known amounts of magnetic flux per unit volume or mass compared to all other magnet types. Their high-energy product is the reason they find application in compact and efficient designs and will also be adopted in this proof of concept.

Table 3.1 - Material Magnetic Properties showing different magnets and their respective magnetic properties [41]

	Maximum Energy Product *Bhmax(MGOe)*	Residual Flux Density *Br(G)*	Coercive Force *Hc(Koe)*	Working Temperature ^{o}C
Ceramic 5	3.4	3950	2400	400
Sintered Alnico 5	3.9	10900	620	540
Cast Alnico 8	5.3	8200	1650	540
Samarium Cobalt 20 (1,5)	20	9000	8000	260
Samarium Cobalt 28 (2, 17)	28	10500	9500	350
Neodymium N45	45	13500	10800	80
Neodymium 33uH	33	11500	10700	180

Table 3.1 above compares some known magnet grades with high magnetic flux densities. Since the amount of induced voltage is proportional to the change in magnetic flux density, the neodymium N45 was chosen for this design prototype, over the other magnets listed in Table 3.1. The reason for the choice was because of its high Br value of 13500 Gauss (equivalent to 1.35 Tesla). And apart from having the highest Br value, they also boast the highest BHmax value of 45 MGOe.

The BHmax is defined as the potential energy density in a magnetic material volume in KJ/m^3 or MGOe. 1 MGOe is equivalent to 1,000,000 Gauss Oersted.

After determining the best grade of magnet that could be used, the next design step was choosing the right magnet profile that fulfills the design requirement in terms of weight and performance. Several available profiles were considered as shown in the Fig. 3. 9 & Fig. 3.10 and Table 3.2 & Table 3. 3.

Four magnet sizes 0.25” by 0.25”; 0.25” by 0.20”; 0.25” by 0.1875”; and 0.25” by 0.125” were simulated using the FEMM and their respective magnet pull forces plotted in Table 3.2 and Fig. 3.9. The thickness of the steel plate used in the simulation was 5 mm and the magnet poles were placed perpendicular to the flat surface of the plate. The pull force simulation determined the force required to separate the magnet and the plate.

Table 3.2 – Magnet Pull Force

Magnet Size	**0.25 x 0.25 (in)**	**0.25 x 0.2 (in)**	**0.25 x 0.1875 (in)**	**0.25 x 0.125 (in)**
Distance (mm)	**Pull Force (lb)**	**Pull Force (lb)**	**Pull Force (lb)**	**Pull Force (lb)**
0	3.59	3.29	3.21	2.26
1	0.99	0.88	0.86	0.63
2	0.44	0.39	0.37	0.27
3	0.22	0.19	0.18	0.13
4	0.12	0.1	0.1	0.07
5	0.07	0.06	0.05	0.04
6	0.04	0.03	0.03	0.02
7	0.02	0.02	0.02	0.01
8	0.01	0.01	0.01	0.01
9	0.01	0.01	0.01	0
10	0.01	0	0	0
11	0	0	0	0

Table 3.2 – magnet Pull force table for the 4 magnets compared for use in the design

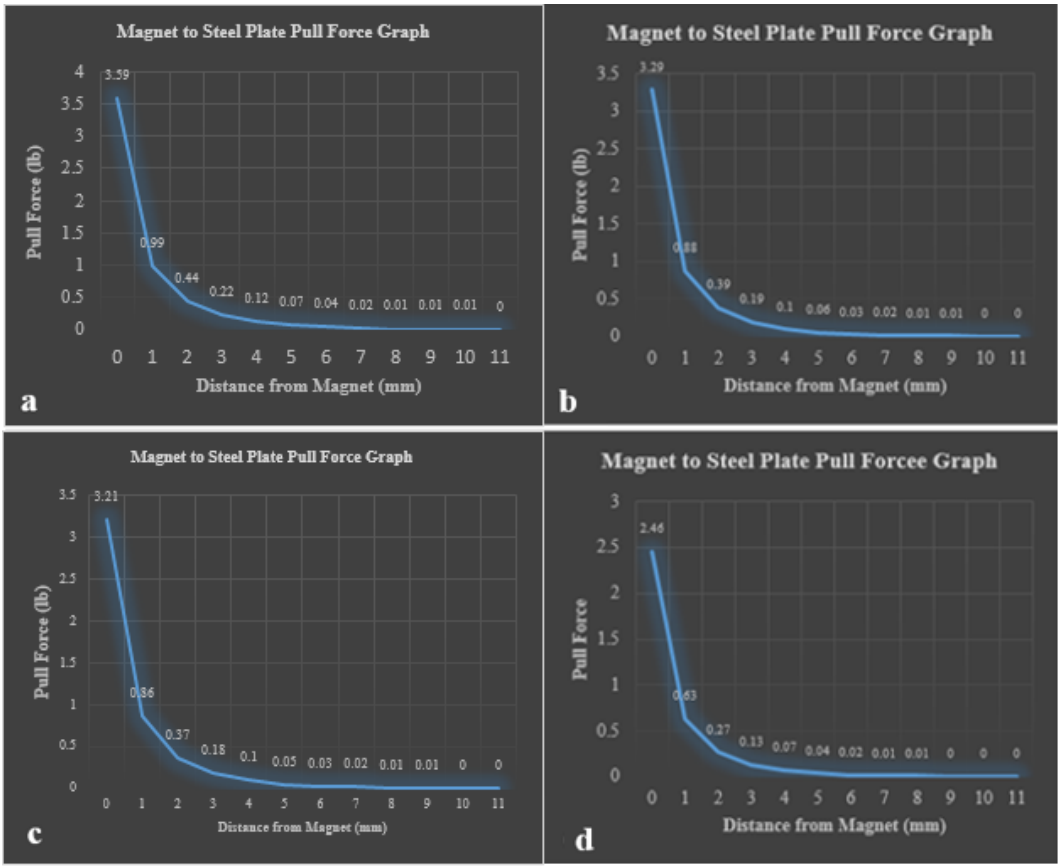

Fig. 3. 9 - Magnet to steel plate pull force graph (a) plot of a 0.25” x 0.25” magnet; (b) plot of a 0.25” x 0.20” magnet; (c) plot of a 0.25” x 0.1875” magnet; (d) plot of a 0.25” x 0.125” magnet.

The choice of sizes in this experiment was based purely on market availability. Other form factors could be explored in the future for optimized performance. Please, see **generator structure** for an understanding of the importance of the pull force simulation.

The magnets were placed at distances varying from 0.0 mm to 10.0 mm from a steel plate and the amount of forces required to separate them were evaluated. It was then observed that at approximately 5 mm from the magnet, the pull forces from each of the magnet profile were identical; in order words, there was no significant difference in using one magnet over another at this distance in terms of the pull forces. However, from this point on, the pull forces increase or decrease exponentially as you move nearer or farther from the magnets, respectively.

Now, since the generator is intended to be in an energy harvesting system that could be worn on the hip, lower thigh or the knee, and driven by the action of the leg motion, it must be designed such that it will have the least amount of impact on the normal gait of the person wearing it.

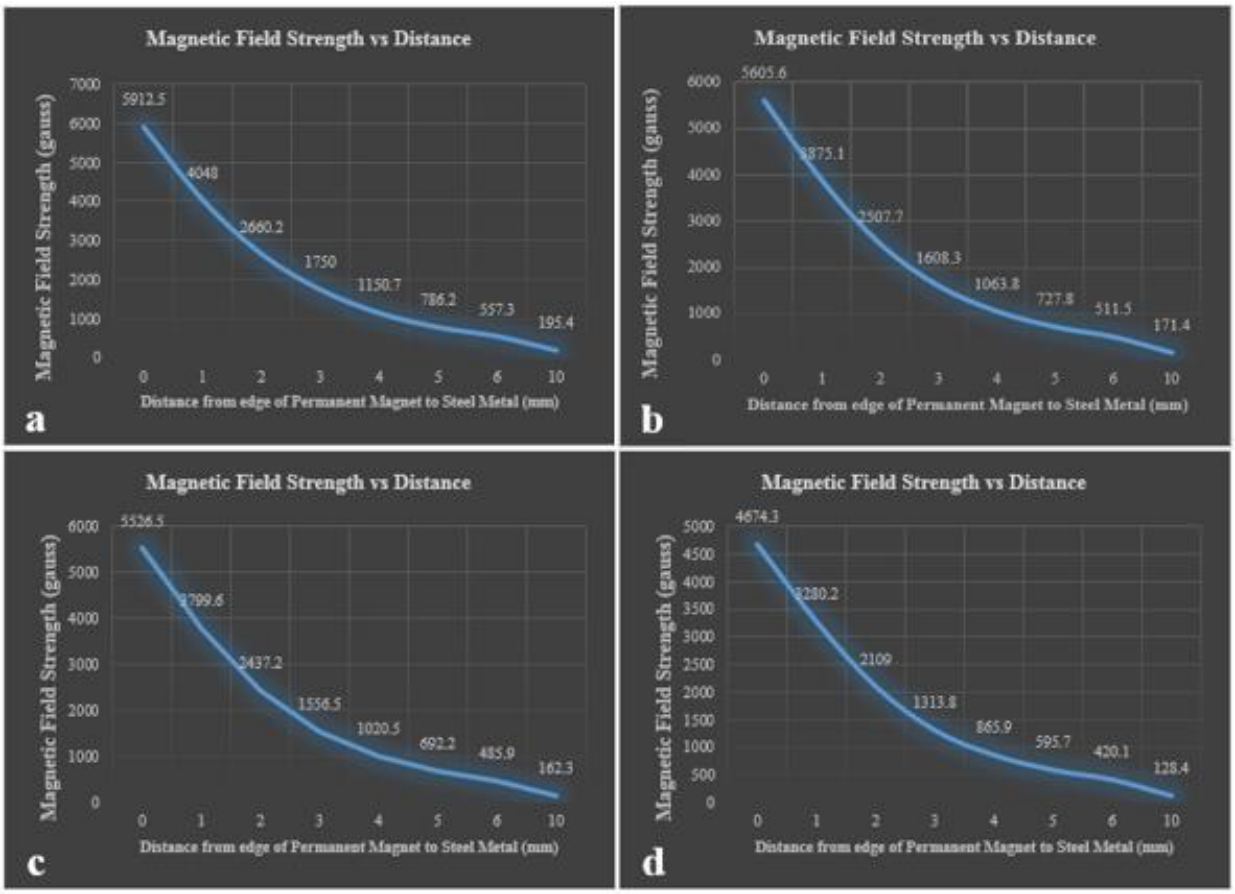

Fig. 3.10 - Magnetic Field Strength vs Distance (a) plot of a 0.25” x 0.25” magnet; (b) plot of a 0.25” x 0.20” magnet; (c) plot of a 0.25” x 0.1875” magnet; (d) plot of a 0.25” x 0.125” magnet

For the above reason, a decision was made to use a magnet that has the highest amount of magnetic flux density while at the same time maintaining the least amount of pull force from the same distance (it has already been determined empirically that at a distance of 5 mm, there was no significant difference in the pull forces between the four magnet profiles considered.

Therefore, the magnet of choice must be the magnet with the most magnetic field strength at the said distance of 5 mm – this allows for the adjustment of the air gap between 1 and 5 mm [17]). Fig. 3.10 shows the plot of all the magnetic field strengths versus distance for the four magnets considered.

Table 3. 3 – Magnetic Field Strength vs. Distance

Horizontal distance from center of magnet x (mm)	Vertical distance from edge of magnet y (mm)	0.25 x 0.25 (in)	0.25 x 0.2 (in)	0.25 x 0.1875(in)	0.25 x 0.125 (in)
		Magnetic Field Strength (gauss)	Magnetic Field Strength (gauss)	Magnetic Field Strength (gauss)	Magnetic Field Strength (gauss)
0	0	5912.5	5605.6	5526.5	4674.3
0	1	4048	3875.1	3799.6	3280.2
0	2	2660.2	2507.7	2437.2	2109
0	3	1750	1608.3	1556.5	1313.8
0	4	1150.7	1063.8	1020.5	865.9
0	5	786.2	727.8	692.2	595.7
0	6	557.3	511.5	485.9	420.1
0	10	195.4	171.4	162.3	128.4

Table 3.3 - Magnetic Field Strength vs. Distance for the 4 magnet profiles used in this simulation each evaluation for distances ranging from 0 to 10mm

From the above graphs and table, it was observed that the magnets with dimensions of 0.25” by 0.25” (sample [**a**]) have the highest value of magnetic field strength of all the other magnets at any distance from the magnet. But since the design is intended to have a minimal impact on the gait of the subject, a separation distance of 5 mm was chosen and hence this was magnet selected.

It was noted during the experiment, however, that the closer the magnet is to the core, the higher the magnitude of the induced voltage. This comes at a cost because extra work is needed to overcome the pull force (see Fig. 3. 9above). The information on Fig. 3.10 is also presented in Table 3. 3 as well.

The chosen air-gap of 5 mm is only the upper limit to allow the generator to be adjustable post fabrication, however, a lower air gap of 1 mm will be preferred for a higher amount of induced voltage. But as seen from the tables and figures above, this lower air gap makes it harder to drive the generator without some special adaptations.

This special adaptation comes in the form of the proposed ‘mechanical up-conversion’ motion translation gear box. This gear box has a lever arm at the front end connected to a roller clutch. The level arm, called the crank handle, helps to amplify the applied force and enables the generator to be moved much easier through the gear trains.

Note that using the roller-clutch gear box enables one to drive the generator more efficiently, thus, the gap between the magnet and the stator could further be reduced from 5 mm down to 1 mm. This point yields the highest amount of generated voltage and is used for post-fabrication adjustments.

3.3.3 Stator Core Material Selection

There are two types of magnetic materials that were could be used for the generator stator core. They are the magnetically soft materials and the magnetically strong materials. Magnetically soft materials exhibit strong magnetization in the presence of an external magnetic field but loses them when the external magnetic field is removed, while magnetically strong materials, on the other hand, retain their magnetism even when the external magnetic field has been removed.

It is important in this design that the stator core material does not retain its magnetism but could be easily magnetized in the presence of an external magnet and subsequently lose them as soon as the external magnetic field has been removed. This will ensure that as the magnet hovers and revolves over the stator core flanges, there is a constant change in magnetic flux as the stator segment is constantly magnetized and demagnetized – without the core retaining its magnetism.

For small motors and generators, it is recommended to use the 1008 steel (10% carbon content) for the core materials especially when they are used infrequently and for short periods of time [43]. Although many lower grades could be used, lower grades lead to lower electrical efficiency which could lead to a degraded overall performance. For this reason, the material selected was the 1010 steel (8% to 10% carbon content). This is akin to the conventional materials used in the design of conventional small generators and motors.

3.4 The Generator Structure

The most important requirement for this generator design is its long term reliability. In a sense, this is an on-demand AC voltage generator. Electrical power should always be available while the source of motion is present. For this reason, the generator must be able to function reliably under various frequency modes. The structure should be such that every movement of the rotor will produce a corresponding change in the magnetic flux linking the generator coils, which in turn enables energy harvesting.

The structure chosen as shown in Fig. 3.5 and Fig. 3.8 above provides such possibility. The Neodymium magnets are arranged with alternating magnetic polarities within a rotor assembly above the stator core and pointing downwards towards the stator flanges with the core setup in such a way that every complete revolution of the rotor causes 8 complete changes in flux polarity'/direction through the core – and consequently through the generator coil (see Fig. 3.8 above).

The term 'change in flux polarity' as used in this context is the magnetic flux created by a magnetic pole, say north pole pointing towards the top flanges, and then changing quickly to the one created by the opposite pole, say this time the south pole pointing towards the top flanges. So, in a sense, if the flux created when the North pole of the magnet is pointing towards the top flanges is assumed positive, the one created when the South pole of the same magnet is pointing towards the top flanges will be negative.

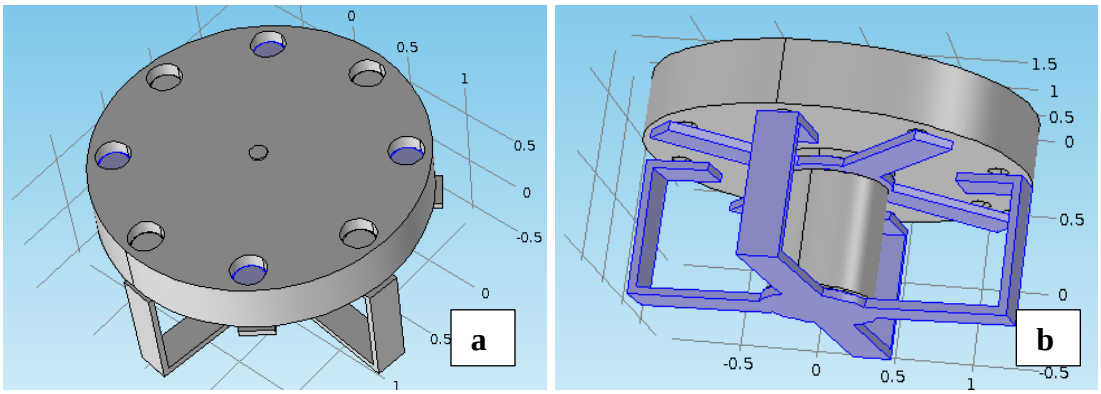

Fig. 3.11 – (a) Three-quarter view of the proposed generator design top side (left); (b) bottom side (right)

The proposed design simplifies the armature and coil winding design (Fig. 3.11), requiring only a single coil at the core of the generator. The placement of the magnet and core are essential in determining the amount of force required to move the rotor. The closer the magnets are to the core flanges, the more the harvested voltage but this will require additional force to overcome the pull force at this closer distance. As will be seen later, this will be leveraged in completing the adjustable generator design.

Conventional Electromagnetic generators have fixed air gaps between the stator and the rotor (Fig. 3.12 shows the geometry of conventional generators for illustration purposes only), while the air gap for the proposed novel concept (Fig. 3.13), is adjustable after fabrication. This will have a direct and predictable impact on the generated voltage. Refer to Table 3. 3 for the results showing how this adjustment will help in predicting any increment or decrement in harvested electrical energy as the rotor assembly is adjusted either closer to or farther from the stator core from 0.0 mm to 10.0 mm.

Since this generator design was intended to be a wearable energy harvester, the subjects can adjust the energy harvesting potential to meet their personal comfort level with respect to the amount of work done to overcome the pull force and generate the desired amount of output voltages. This makes the generator highly field customizable – implying the subject can customize the product freely while in use.

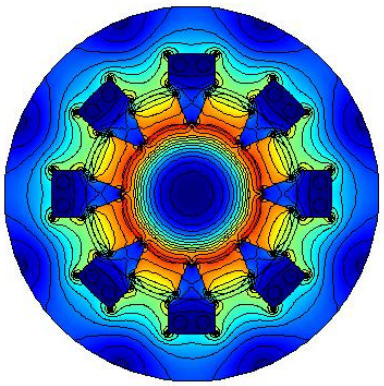
Fig. 3.12 – Geometry of Conventional Electromagnetic generator with fixed air gap between the Rotor and the Stator

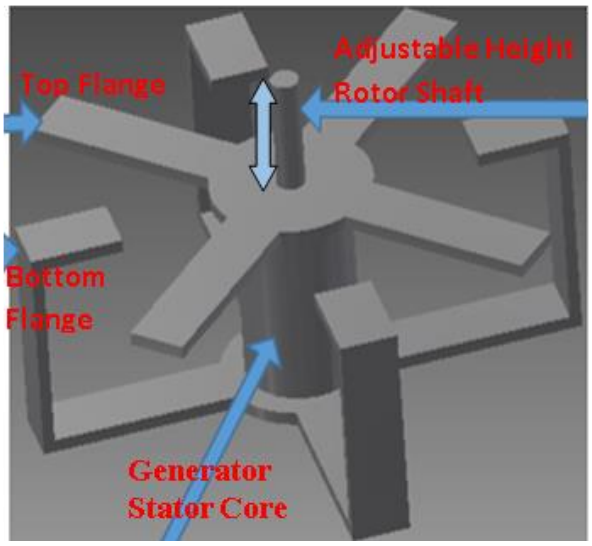

Fig. 3.13 - Three-quarter view of the proposed generator design showing the core sections: flanges – top & bottom, core and adjustable shaft for the rotor

3.5 Generator Simulation

Up until this time, the focus has been on the theories around the proposed new design and attempts to come up with a working model for the new generator concept. Now, having determined the core design layout, a simulation of the complete intended design was run to predict its performance before prototyping.

The AC/DC module of the COMSOL Multi-physics software was used to simulate the proposed Electromagnetic Energy Generator. During the simulations, two magnets with different magnetic remanences were used to establish a baseline – one with 1.2 T and the other with 0.8 T (higher and lower remanence, respectively). The generator speed was set as 100 RPM; the size of the generator was 45 mm, while the coil had 100 turns.

The performance of a higher and lower magnetic remanences were compared and their results presented, respectively, in Fig. 3.14 and Fig. 3.15.

The results as shown in those plots confirm the theory that higher magnetic remanences correspond with higher induced voltage and hence obviate any need to run further simulations using magnets with lower magnetic remanences. It was determined that lower weight and higher magnetic remanence magnets are ideal for this type of design to meet both the weight and performance requirement of a human-wearable generator.

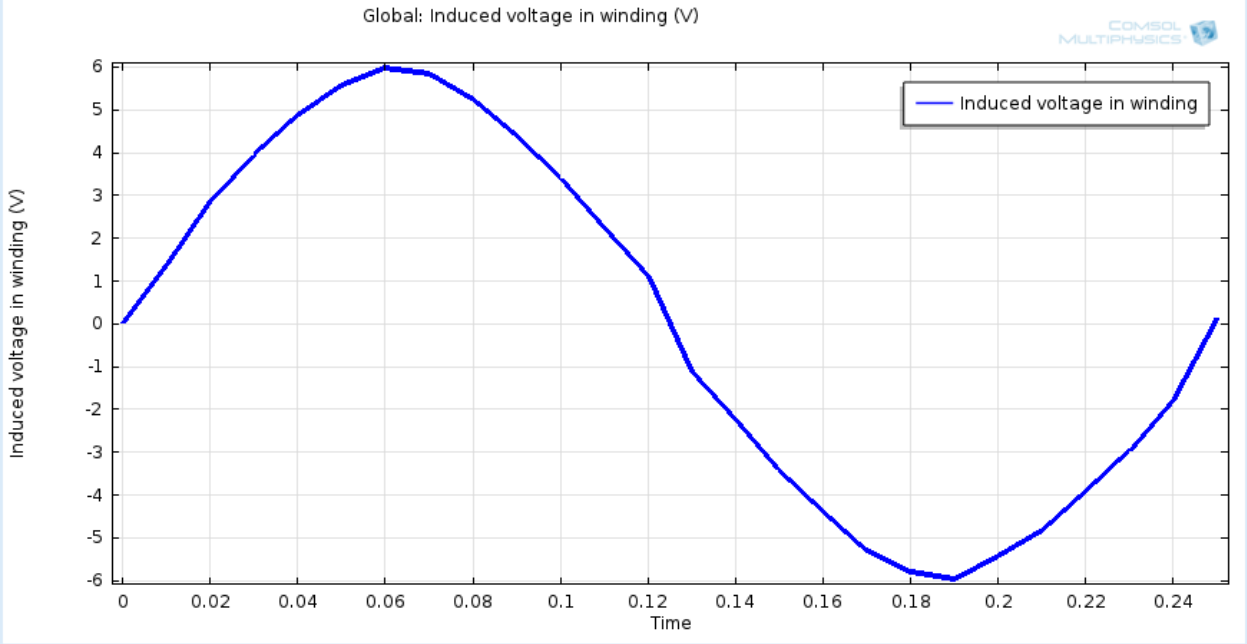

Fig. 3.14 - Simulation result: 12 V peak-to-peak (with Magnetic flux density of 1.2 T)

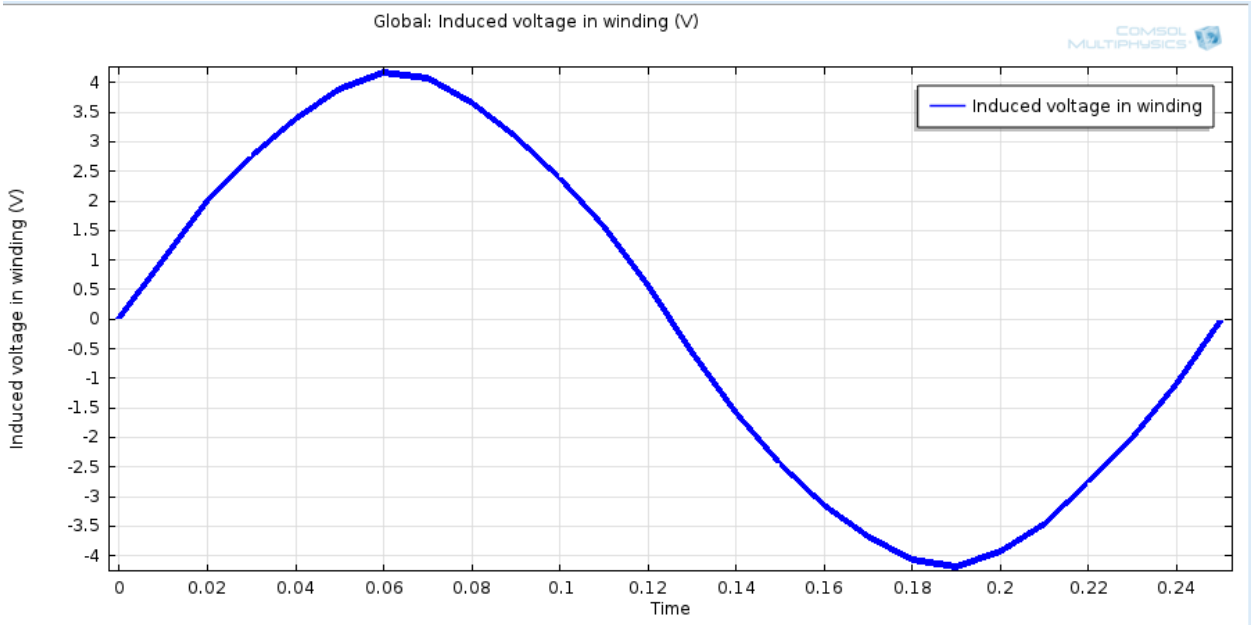

Fig. 3.15 - Simulation result: 8 V peak-to-peak (with Magnetic flux density of 0.8 T)

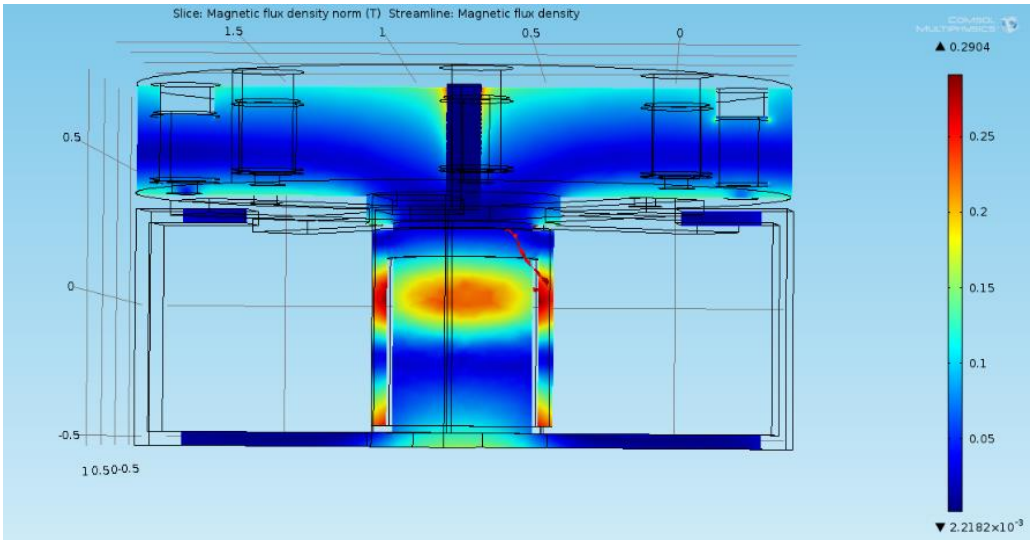

Fig. 3. 16 - Magnetic flux density distribution within the generator core during rotor motion

Fig. 3. 16 shows the magnetic flux changes within the core of the generator during the simulation. The problem solved by COMSOL is a typical time-dependent model problem in which the motion of the rotor and magnets are accounted for by the boundary condition between the rotor and stator geometries. Hence, there is no Lorentz term in the equation (equation 5), resulting in the following partial differential equation

$$\sigma \frac{\partial A}{\partial t} + \nabla x \left[\frac{1}{\mu} \nabla x A\right] = 0 \quad \text{.....Equation 5}$$

A simplified layout of this new concept is shown in Fig. 3. 17 while the corresponding COMSOL simulation of the magnetic flux density due to this arrangement is shown in Fig. 3.18. This simplified version is represented with a single magnet over the stator core. It was used to illustrate the flux linkage between the rotor and the stator core and the effect of the air gap on the magnetic flux linkages.

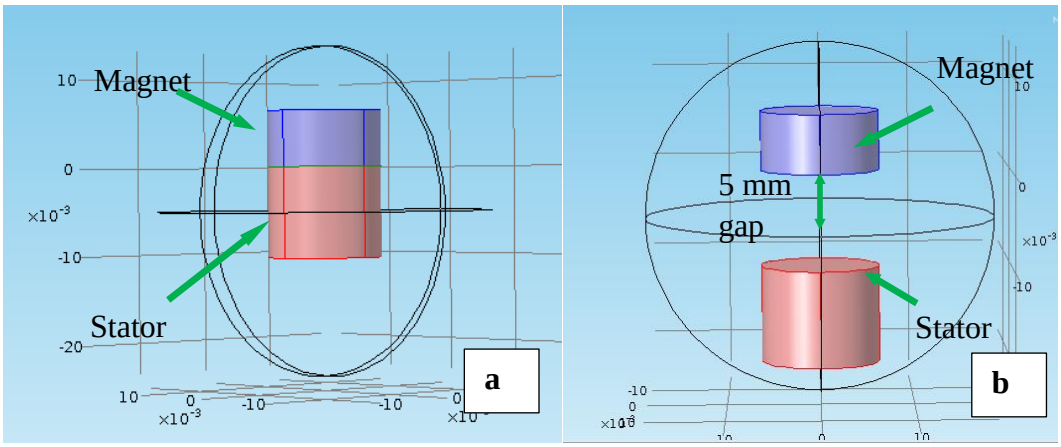

Fig. 3. 17 - Simplified layout of the new generator concept: (a) magnet directly on the flange at 0 mm from flange (left); and (b) magnet at 5 mm from flange (right).

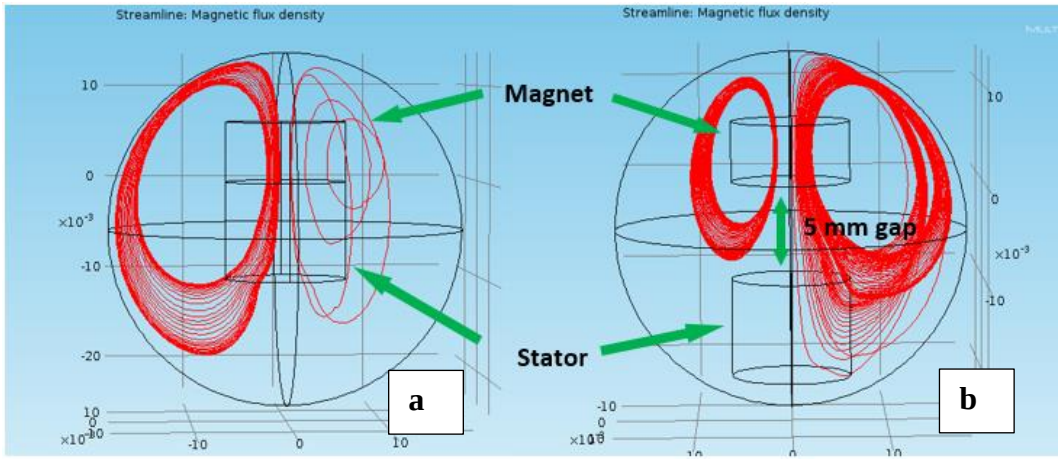

Fig. 3.18 - Magnetic flux density plot of the Simplified layout of the new generator concept. (a) Magnet directly on the flange or at 0 mm from flange (left) and (b) magnet at 5 mm from flange (right).

Notice that in Fig. 3.18 most of the magnetic flux lines cut across the entire coil cross-section on the left image representing the setup with the magnet at 0 mm from the stator core coil while the image to the right, representing the setup with the magnet at 5 mm from the core, has only a few magnetic flux lines cutting across the core coil area.

Having already stated that electromagnetic induction is proportional to the change in magnetic flux linkage, this simulation further proves that point that the closer the magnet is to the coil, the more the induced EMF and vice-versa. In other words, different distances between the stator core and rotor magnet assembly will represent different amounts of induced voltages by the generator (for the same rotor speed and the same number of turns of conductor wires).

An alternate way of looking at the simplified layout is shown in Fig. 3.19. The direction of the black arrows show the direction of magnetic flux for each magnet. Following the direction of the arrow makes the entire stator core behave like a single bar magnet when the rotor speed is theoritcally zero relative to a flange pair – this is the point at which the magnets are directly over corresponding flange pairs. The big piece in the middle represents the iron core in the center of the generator upon which the generator coil was wound – referred to as the stator core.

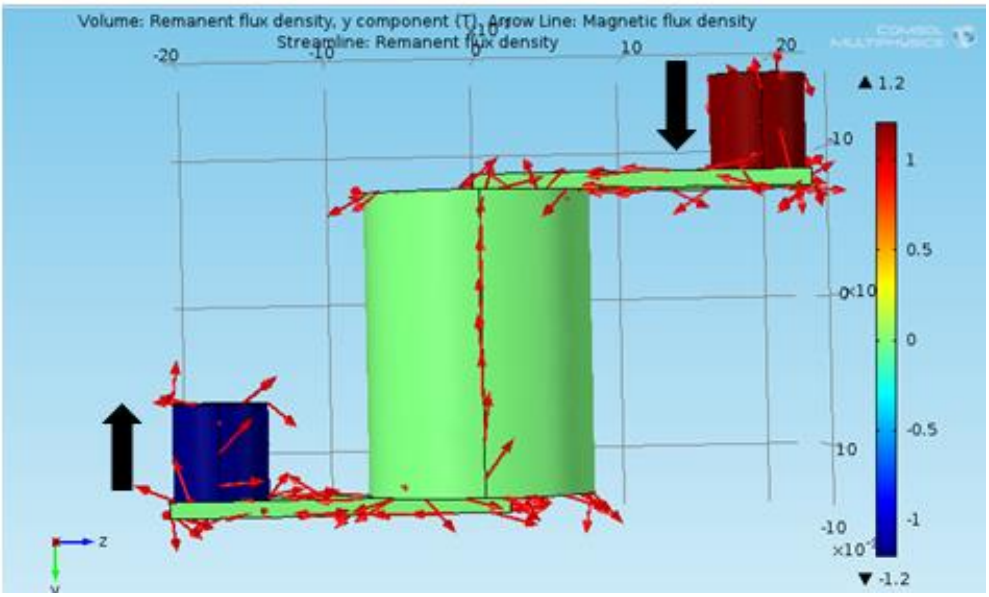

Fig. 3.19 - Alternate view of the Simplified Generator Simulation

Fig. 3. 20 below shows two stand-alone magnets with the lines of flux showing the direct of the north and south poles. The magnets in the rotor assembly and the above alternate representation of Fig. 3.19 are arranged in this fashion (alternate arrangement).

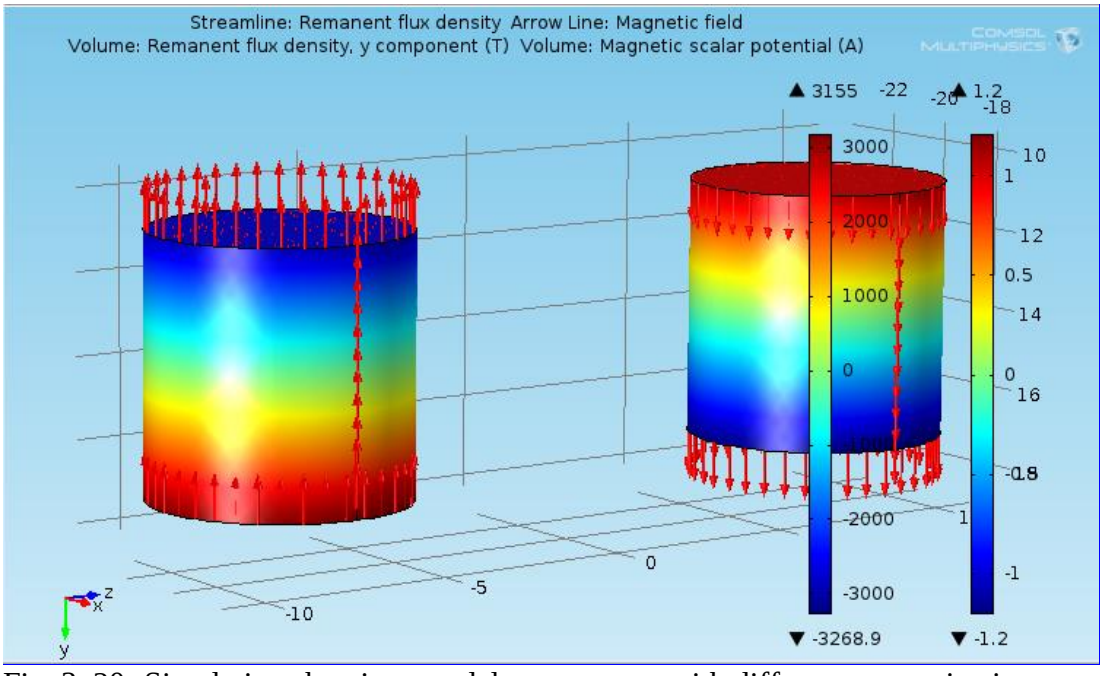

Fig. 3. 20- Simulation showing standalone magnets with different magnetization.

3.6 Design of the Motion Translation Gear-Box

3.6.1 Initial Concept

For this type of energy harvester, it was intended that energy is harvested only during a specific phase of motion. If it is worn by human subjects, their walk phase is used. If installed on doors or windows, opening or closing phases are used.

For wearable applications, this phase is what has been described as the swing phase or the negative work/energy cycle (in the case of hip or knee installation). To make this possible, a gear box was designed that engages the energy harvester only during the intended walk phase.

Previous work by other researchers [11] used a potentiometer and specific algorithms to determine the point at which energy harvesting phase would start. However, work was done all the time in moving the gear system in the gear-box.

The design presented in this thesis overcomes that shortfall by utilizing a one-directional roller clutch at the input stage or 'front end' of the motion translation gear-box (see Fig. 3. 21 below). The roller clutch engages only during the 'negative energy' cycle and ensures that only the motion of the swing phase is responsible for energy harvesting.

There is no wasted energy in moving the gears in the gear-box system when energy is not being harvested. The approach implies that anytime the machine gears move correspond to when energy is being harvested and thus the design is setup to correspond to the negative energy cycles only.

The motion translation gear-box consists of a lever arm called the crank handle in conjunction with a set of multi-stage gears. The crank handle connects to a combination of the roller clutch and a 100 toothed gear in the front end, while the mid-section contains a combination of a (20) toothed smaller gear and a 100 toothed bigger gear. A larger gear at the front end drives the smaller gear in the mid-section for a mechanical advantage of 5.

The front end could not make a complete revolution during regular walk phase since it could be connected to the leg, door or window and neither of these make a motion of 360^{o} angle during regular use. However, this mechanical advantage of five (5) means that a one-fifth revolution of the front end will result in one complete revolution of the mid-section 100 toothed gear. The front end is designed to accommodate up to 180^{o} rotation of the crank handle. Now, the mid-section 100-toothed gear is further connected to another 20-toothed smaller gear that drives the generator rotor directly. This helps maintain the intended mechanical advantage of 5.

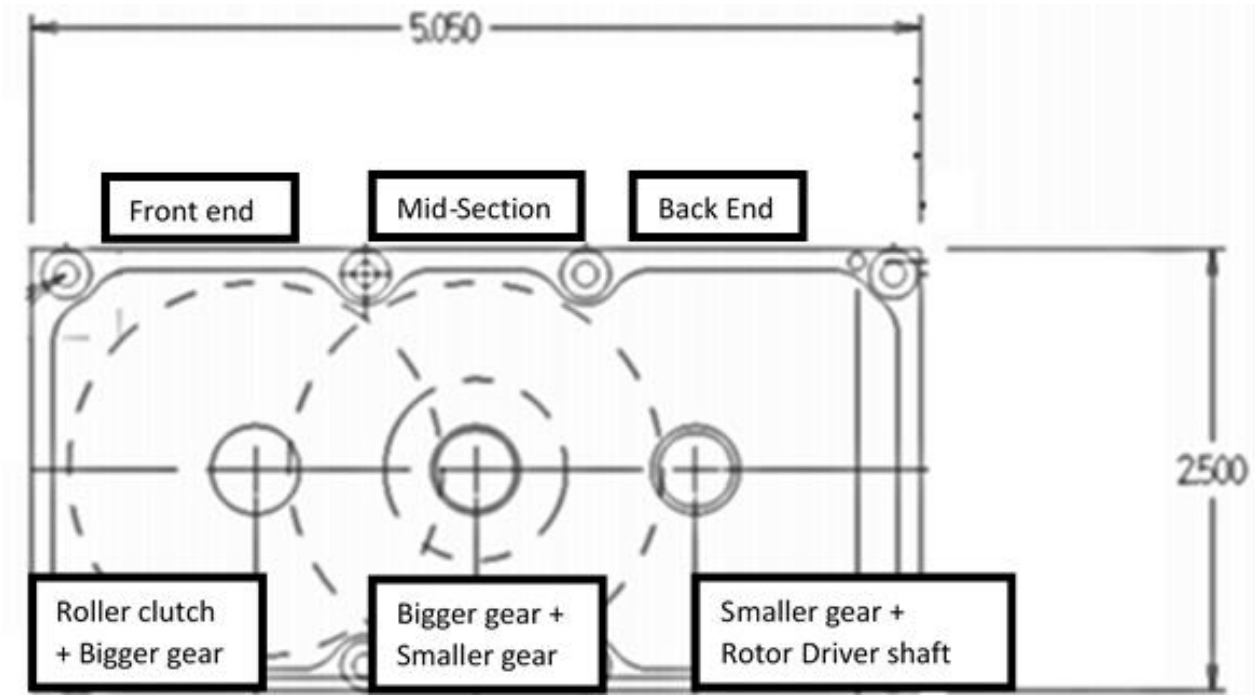

Fig. 3. 21 - Motion Translation Gear-box

When the crank handle is moved between 0^o and 180^o, the generator rotor continues to move in the same direction for up to 5 or more complete revolutions even when the motion source, for example the leg, has reversed direction. The motion continues with each subsequent swing phase and is neither affected by the stance phase nor by the positive work phase because of the one-directional clutch.

The speed of the rotor could go faster and could also complete more than five (5) revolutions if the leg was swung fast enough as in the case of a fast-paced walk, jog or run. At the speed of one step per second, the generator would rotate for at least five times and has been recorded to complete more than 10 revolutions due to the rotor which creates a flywheel effect. The faster the crank handle, the greater the flywheel effect; and the greater the flywheel effect, the higher the generated voltage.

Fig. 3. 22 below shows the inside view of the motion translation gear-box revealing the gear systems. The bigger gears are in red colors while the smaller gears are in grey colors. The housing of the motion translation gear box was made of aluminum while the gears and shafts are made of steel. There was a constraint on the mechanical advantage of the initial proof of concept design due to the availability of parts. Additional research work was done in this area for better mechanical advantage at less metabolic work. The result will be presented in the advancements and progress section.

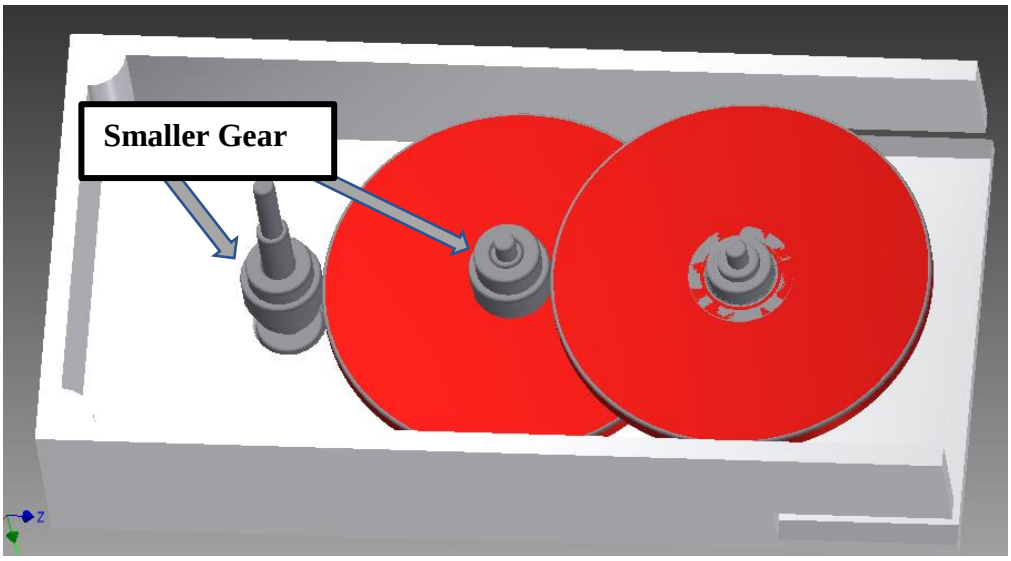

Fig. 3. 22 - Inside view of the motion translation gear-box showing the gear systems and rotor shaft

Fig. 3.23 below shows the cut-out/cross-sectional view of the machine revealing the roller clutch underneath the first big gear at the machine's front end. The crank handle (not shown) attaches firmly around the roller clutch and the motion source (e.g., hip/knee-harness/doors or windows harnesses (not shown)). The harness is mainly for mechanical attachment to the subject and has no impact on harvested voltage although the weight will affect the metabolic work rate.

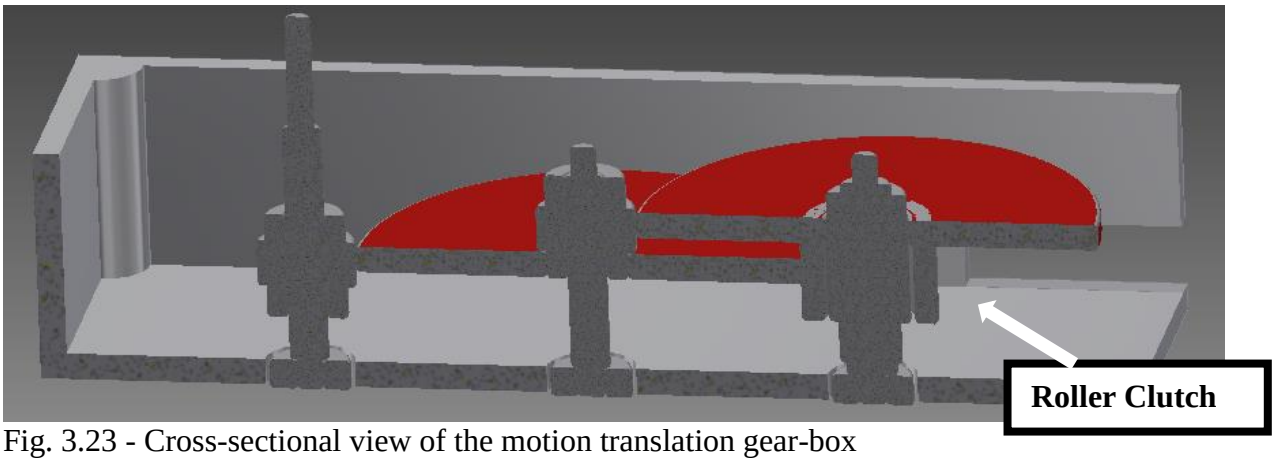

Fig. 3.23 - Cross-sectional view of the motion translation gear-box

The initial fabrication and testing were done with the current structure, however, additional work was done to improve the initial design of the motion translation gear-box. Some of the works include:

- Lightweight materials that are durable and reliable to improve the weight
- Expanded the size to integrate the generator and the motion-translation machine inside the same the unit
- Expanded the design to include a harness for attaching the complete machine to the harnesses.

3.7 Fabrication and Testing of the Initial Concept

After the simulation, the different parts were fabricated according to design and tested to prove the concept. During testing, the obtained result was comparable to the predicted outcome, with friction degrading the performance by limiting the rotor motion as the moving parts rub against each other. To counter this, a ball bearing was used between the generator stator shaft and the rotor.

The rotor magnets were placed at exactly 5 mm from the stator flanges to keep the pull force at its intended minimum. When placed closer (at say, 4mm, 3mm, 2mm or 1mm), it increases the initial force required to initiate a rotary motion but the induced voltage was correspondingly higher, but when placed a little farther away, the initial force required to initiate a rotary motion was reduced as expected, with a corresponding decrease in induced voltage. These behaviors agree with the predictions in Table 3.2 and Table 3. 3.

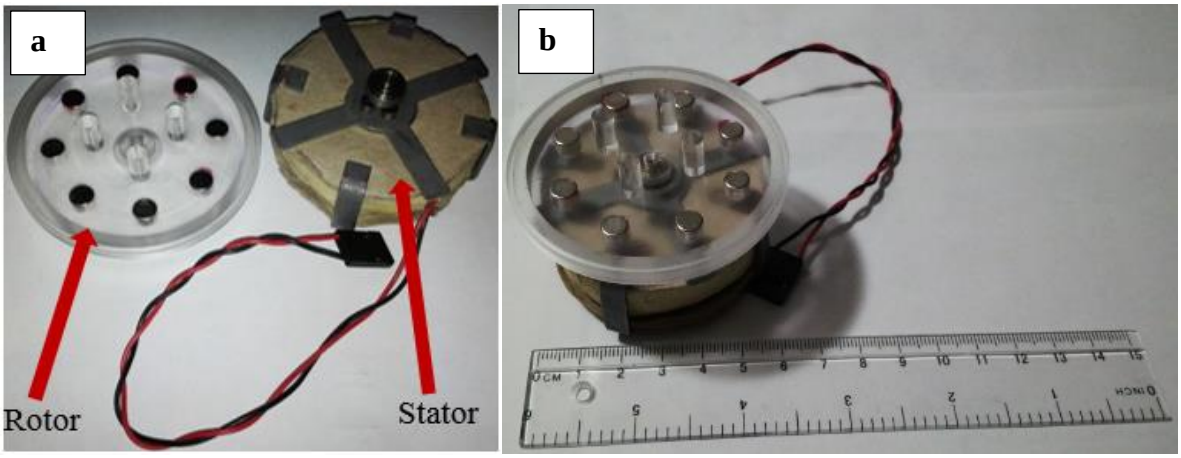

Fig. 3.24 - Fabricated generator design – (a) rotor and stator (left), (b) complete assembly (right)

The core material was made of magnetically soft materials as previously determined while the rotor was made of Plexiglas with 8 magnets in alternating pole arrangements around the top, positioned in such a way that when they are not in motion, they line up vertically and directly above each of the eight (8) stator flanges. The rotor assembly and the stator core and its winding are shown in Fig. 3.24. The image to the left shows the separate parts while the image to the right shows the complete generator assembly. The diameter of the generator, as indicated by the ruler is about 6 cm or about 2.36 inches, while the height is about 4 cm (although not indicated by a ruler). This was well within the design constraint.

To simulate a real-world type of use environment, the motion translation gear-box, discussed in section 0 was used to drive the generator. The generator output was connected to an oscilloscope and the voltage harvested shown in Fig. 3. 25. At a relatively low speed of one crank per second (approximately between 5 and 10 revolutions per second), the harvested voltage has a peak-to-peak value of 20 volts AC at no load.

Fig. 3. *25* shows the complete design cranked by hand and an oscilloscope view of the generated voltage. Channel one (1) of the oscilloscope was set at 10 volts per division.

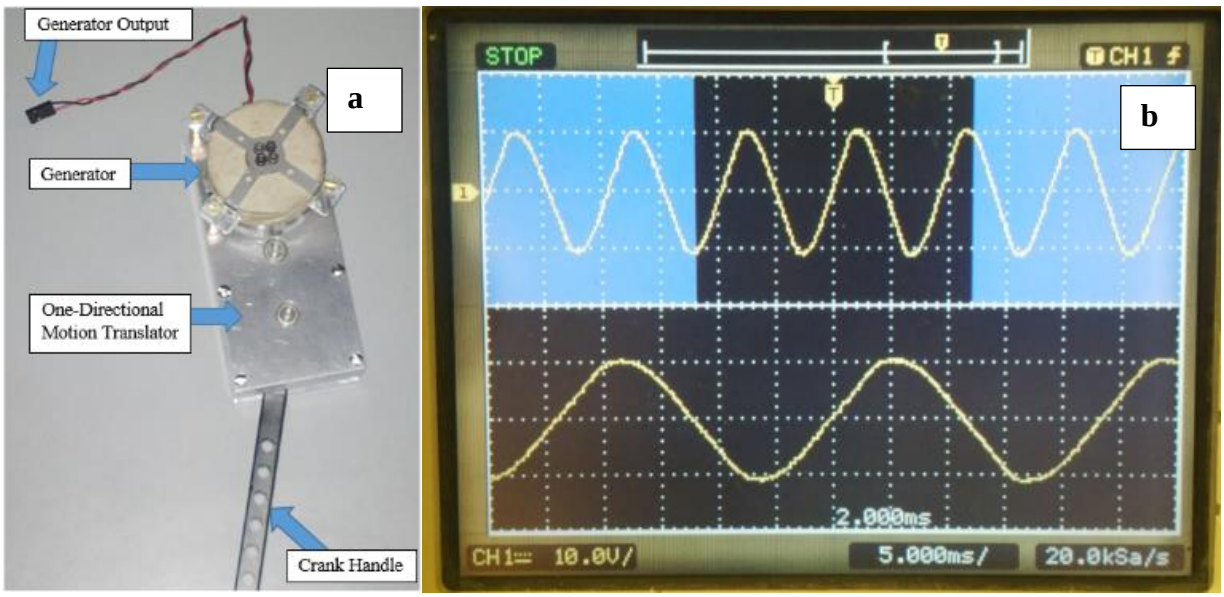

Fig. 3. 25 - Energy harvester – (a) the designed generator driven by crank handle (left), (b) Oscilloscope display showing a 20 volts AC peak-to-peak running at one crank cycle per second (right)

For an Electromagnetic generator, the number of poles is proportional to the generator frequency which is also proportional to the amount of harvested voltage. This will also result in an increased frequency of the generated voltage, however, the voltage must be rectified to be used in most electronic devices, hence higher frequency is a favorable factor.

The only limitation to the number of poles in this type of generator design is the minimum distance required between magnets to avoid any interference (flux leakages) between the magnetic flux lines of adjacent magnets. Otherwise, more poles are better for increased voltage generation.

In the current design, individual magnets are ‘open-circuited’ on the part facing away from the flanges. Further research and simulations were conducted to evaluate the impact of a closed versus an open magnetic circuit concept and to determine the corresponding impacts on the harvested voltage.

3.8 Test Setup

The new Electromagnetic energy generator was tested with the setup in Fig. 3. 26 below. Two different sets of windings were built and tested, one with 36 American Wire Gauge (AWG) (sample A) and another one with 26 AWG (sample B) wire sizes. Sample A has a DC impedance of 100 ohms and 3000 turns, while sample B has a DC impedance of 16 ohms and 800 turns.

The rotor speed was controlled to about 98 revolutions per minute (RPM) and was powered by a DC operated DC motor. The results obtained at different load conditions and at near same RPM are shown in tables 3.4 and 3.5 below.

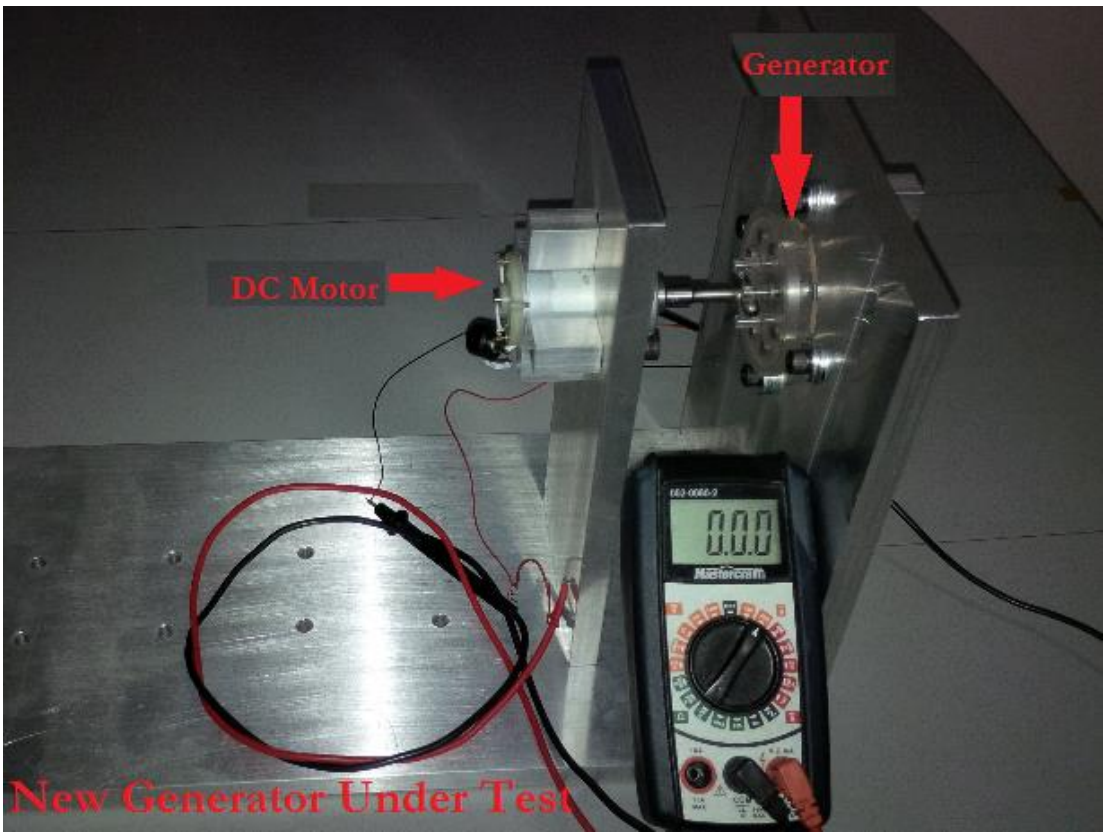

Fig. 3. 26 - Generator Design under Test

Table 3.4 shows the plot of the generator built with the 36 AWG gauge wire (which has a smaller cross-sectional area than the 26 AWG). The DC impedance of the wire is much higher than that of the 26 AWG gauge wire. This agrees with equation 3 in which the wire with a smaller cross-sectional area will have a higher DC impedance versus the same of wire with a bigger cross-sectional area.

The weight was much lower but so also was the generated power. The maximum power for this configuration was 0.3528 Watt, generated when the load impedance was 50 – ohms (a purely resistive load) – see corresponding values in red texts in Table 3.4.

Table 3. 4 – Generator with 36 AWG Wire Gauge Performance under various load conditions

S/N	Open Circuit Voltage (AC)	Generator Impedance	Load Impedance (purely resistive load) (Ω)	Output Voltage (AC)	Power (W)
1	**13 Volts**	**Rs = 100 Ω**	∞	13	0.0000
2			40	3.50	0.3063
3			**50**	**4.20**	**0.3528**
4			100	5.00	0.2500
5			150	6.00	0.2400
6			250	7.00	0.1960
7			500	8.80	0.1549
8			750	10.30	0.1415
9			1000	10.70	0.1145
10			1500	11.60	0.0897
11			2000	11.90	0.0708
12			2500	12.50	0.0625
13			4400	12.20	0.0349

The 26 AWG gauge coil (Larger cross-sectional area of coil) has lower DC impedance and as expected, was much heavier. However, it produced a higher amount of power for similar RPM as the 36 AWG gauge coil.

Table 3.5 shows the plot of the generated voltage and the corresponding power across a purely resistive load (for each tested load impedance). The maximum power for this configuration was 1.5340 Watts, generated over a load of 3.6 – ohms (in Fig. 3.28).

Table 3. 5 – Generator with 26 AWG Wire Gauge Performance under various load conditions

S/N	Open Circuit Voltage (AC)	Generator Impedance	Load Impedance (purely resistive load) (Ω)	Output Voltage (AC)	Power (W)
1	**13 Volts**	**Rs = 16 Ω**	∞	13	0.0000
2			**3.6**	**2.35**	**1.5340**
3			4.7	2.22	1.2460
4			10	2.90	0.8410
5			100	6.13	0.3758
6			150	7.25	0.3504
7			250	8.45	0.2856
8			500	9.92	0.1968
9			750	9.70	0.1255
10			1000	10.31	0.1063
11			1500	10.40	0.0721
12			2000	11.92	0.0710
13			2500	10.70	0.0458

Graphical representations of the above tables are shown below in Fig. 3. 27 and Fig. 3. 28 below for the 36 AWG and the 26 AWG wire gauge configurations, respectively.

Using the coil made with the 26 AWG or sample B at about 800 turns gives rise to 16 ohms for the coil impedance (see table 3.5). The reactive portion of the impedance then needs to be matched using the corresponding value of a capacitor.

These preliminary results show output power ranging from 35 mW to 1.5 Watts. Note that given the relatively low frequency of the generator, eddy current losses will not have a significant impact on the generated voltage and also the inductive reactance was ignored for the same reason since both are frequency dependent.

The generator was driven at a controlled RPM of about 100 RPM in this initial design. The results obtained from these informed the increase in the RPM from 98 to 2900. An almost thirty times increase in RPM to increase the frequency from about 6.5 Hz to about 193 Hz (from equation 6 below) and as a result increase the generated voltage as predicted by equations 1 and 4.

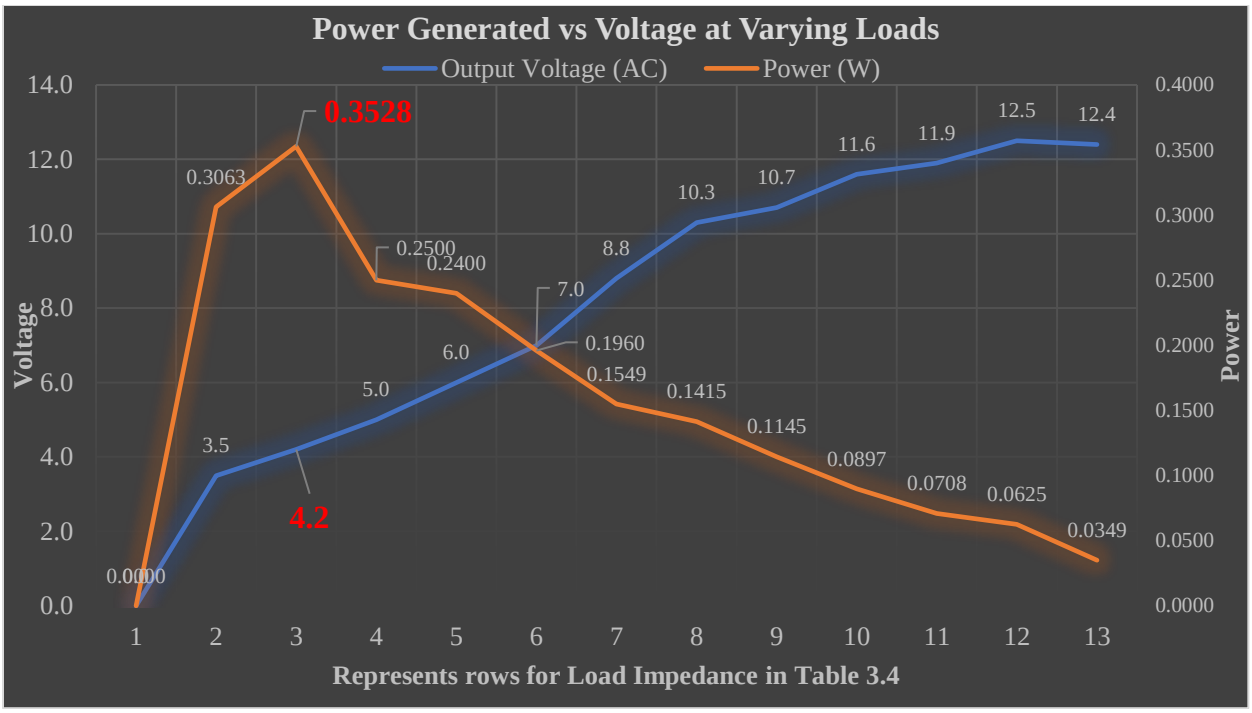

Fig. 3. 27 – Plot of the 36 AWG Generator Output Characteristics under various load conditions

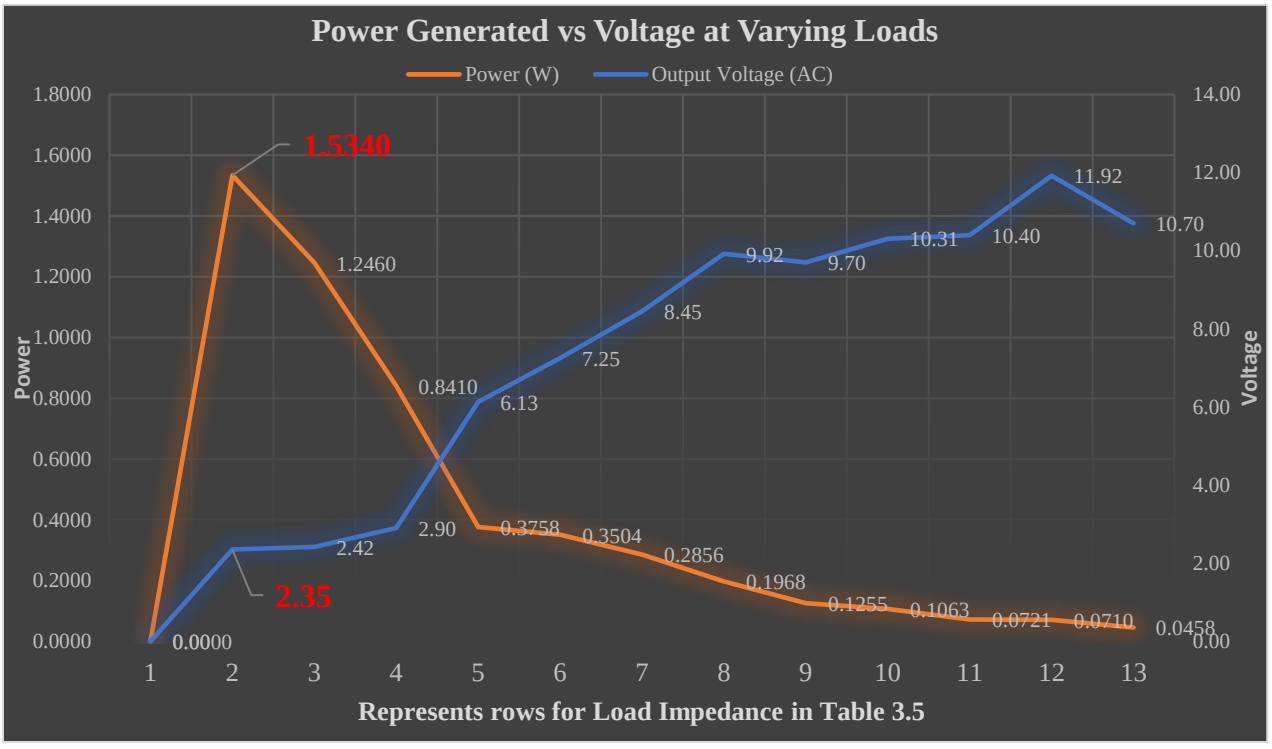

Fig. 3. 28 – Plot of the 26 AWG Generator Output Characteristics under various load conditions

3.9 Summary of Preliminary Result

The results obtained so far from the initial testing of the new concept could be used to power some low power electronic devices as shown in Table 3.4 and Table 3.5. However, optimizations were needed to fine-tune and improve the efficiency of the device. The stage it was tested was independent of the intended human interface, but the obtained voltages agree closely matched with the predicted outcome based on the simulated results.

Now, when the rotor was turned with the fingers at a relatively low spin speed, the output voltage was between 5 and 15 volts after rectification. However, when driven with the hand-cranked motion translation gear-box at about 100 RPM, the generated output voltage was around 20 Volts peak-to-peak before rectification.

Different coil sizes were tested with comparable results. Lower coil wire gauge (bigger cross-sectional area) yielded same voltage if wound with same number of turns but the coil DC impedance was much lower and the current carrying capacity was correspondingly higher.

The tested coils were both made of 1000 turns wound around a hollow plastic former. The core of the generator was then inserted through this hollow former. Both coil sizes were taken from the American Wire Gauges (AWG) chart. The first coil was from a 26 AWG wire and it has a DC impedance of 15.4 ohms while the second coil was from a 36 AWG wire with a DC impedance of 105.5 Ohms.

The coils have current carrying capacities of 360 mA and 35 mA, respectively. The weight of the first coil was about 130 grams while that of the second coil was about 13 grams – excluding the weight of the stator core and the rotor arrangement which were 47 grams and 38 grams respectively.

The combined weight of the generator is 216 grams with the larger coil and 98 grams with the smaller coil. The motion translation gear-box was responsible for an additional weight of 454 grams for the entire setup. This motion translation gear-box converts the leg motion, during only the negative work cycles, into a rotary motion used to drive the electromagnetic energy harvester.

The low DC resistance of both coils make them suitable for use with many off-the-shelf AC-to-DC rectifiers. Any of the coils could be used with an off-the-shelf rectifier without the need for any expensive power conditioning circuitry to achieve a maximum power transfer to the load. One such power conditioning circuit was adopted which detects the presence of an external load and powers it directly or recharged an internal storage battery for later use.

At the combined weight of 98 grams with maximum output power of 0.3528 Watt, the figure of merit for the 36 AWG generator is 3.6 Watts/kilogram, while that of the 26 AWG generator with maximum power of 1.534 Watts, and a combined weight of 216 grams is 7.1 Watts/kilogram.

Table 3. 6 - Inductance Table: Measured using Impedance, Inductance, Resistance & Capacitance (ZLRC) meter.

Medium	26 AWG Coil				36 AWG Coil			
	Solid Core		Laminated Core		Solid Core		Laminated Core	
	Inductance (mH)	Reactance (X_L = Ω)	Inductance (mH)	Reactance (X_L = Ω)	Inductance (mH)	Reactance (X_L = Ω)	Inductance (mH)	Reactance (X_L = Ω)
Air	24.9	30.21	24.9	30.21	171	207.45	171	207.45
Core only	38.6	46.83	32.2	39.31	488	592.01	378	458.57
Full assembly	85.4	103.6	49.1	59.57	702	851.63	519	629.62

Table 3. 6 - Inductance Table: Measured using Impedance, Inductance, Resistance & Capacitance (ZLRC) meter.

Table 3.6 contains a combined result of the preliminary readings and the improved readings with the laminated core. This is combined to show both sets of results side by side. Although there is a reduction in inductances for the laminated core, the arrangement in the design fabrication has no impact on reducing eddy currents. The reduction noticed was merely due to the reduction in the size of the material within the core.

The inductive reactance is calculated using:

$X_L = 2\pi FL$

Where F = $\frac{[Number\ of\ poles\ (8)\ X\ RPM\ (2900)]}{120}$ = 193 Hertz. ……..... Equation 6

Chapter 4

Advancements and progress

4.1 Advancements and Progress

The proof of concept presented in the previous chapter demonstrated a device that could be used as is, however, as set out from the beginning, once the key parameters have been identified, they will be optimized for a better function.

4.1.1 Optimizations Over Initial Concept

1. Throughout the course of this research work, continuous improvement efforts were dedicated towards finding the optimum materials and material sizes including coils, magnets, motion translation gear-box and overall housing for the system level product. More simulations and experiments were conducted on the magnet configuration with and without a 'magnetic closed circuit'. In the end, improvements over the initial concept and results were made.

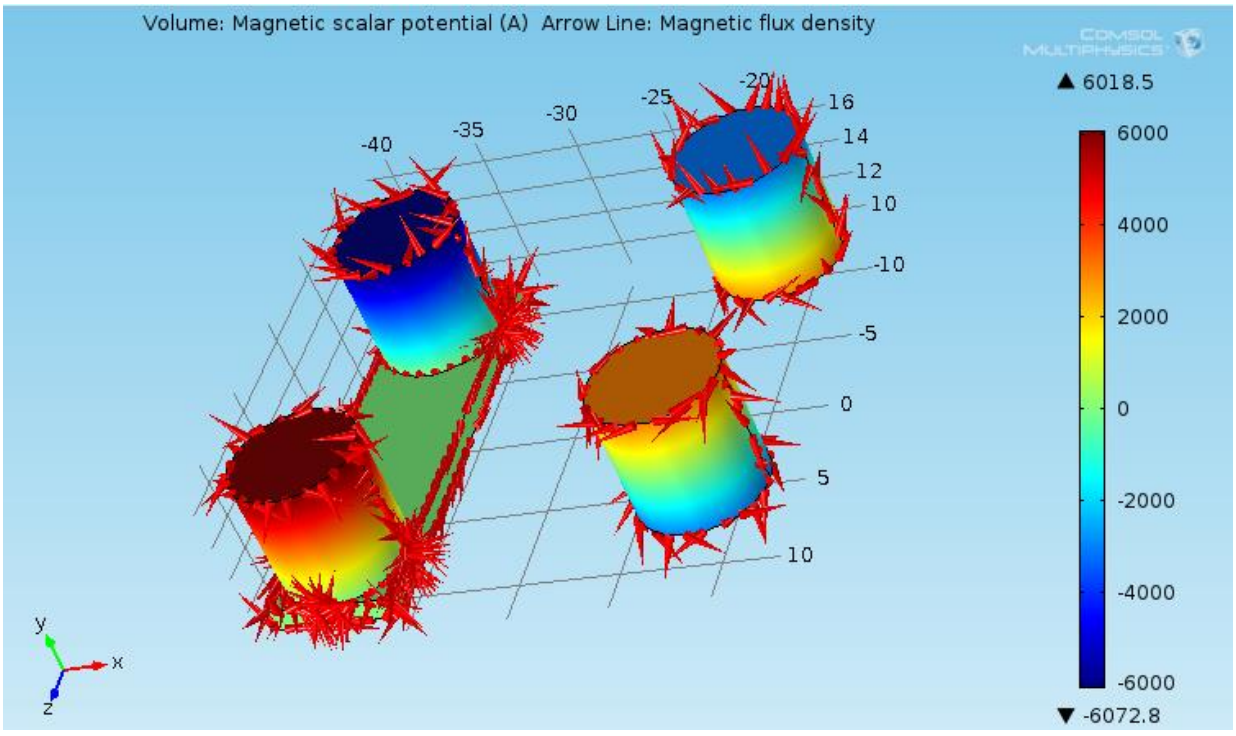

Fig. 4.1 - three-quarter top view of open- and closed-circuit configurations of magnets

Preliminary simulation results showed that there were more potential for harvesting higher amount of energy with a magnetically closed-circuit configuration over the magnetically open-

circuit configuration as shown in the top view and the bottom view of the magnetic flux density plot in Fig. 4.1 and Fig. 4.2 respectively.

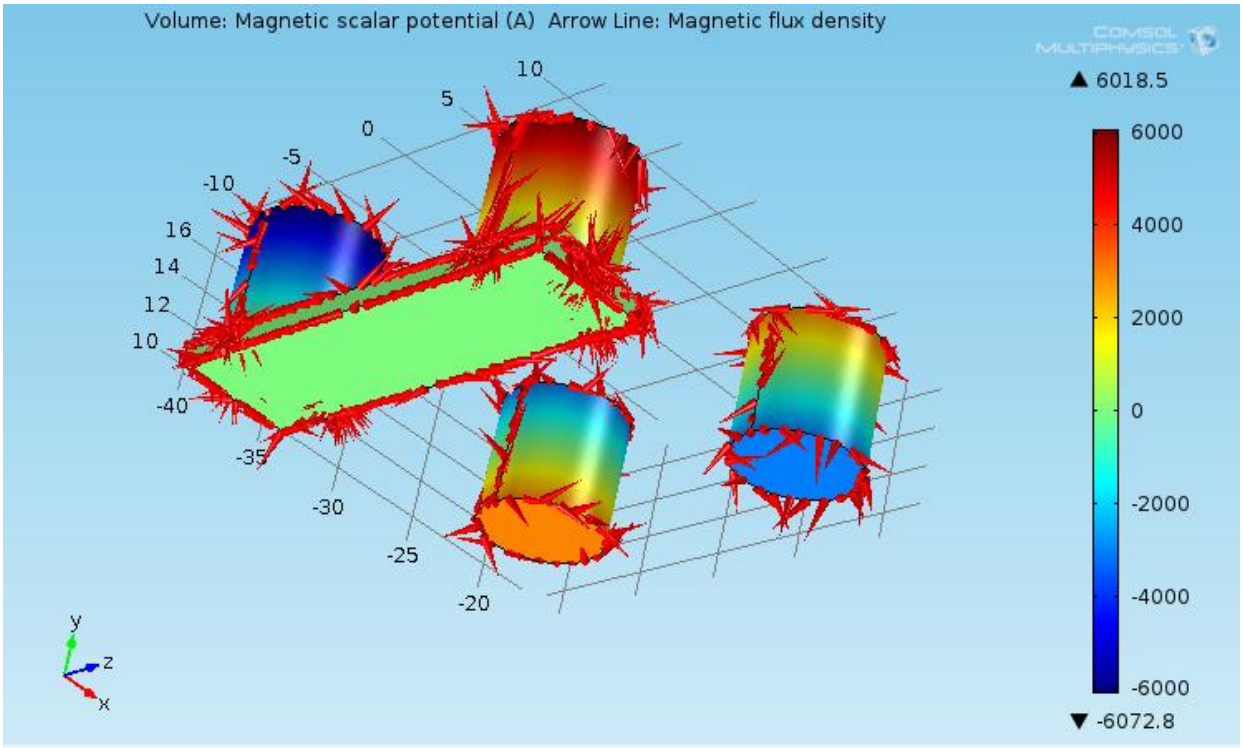

Fig. 4.2 - Three-Quarter Bottom view of Open and Closed-Circuit Configurations of magnets.

2. Plastic materials were used for the motion translation gear-box and overall housing instead of metals. The reason for this change was to improve the overall weight coefficient.

3. Optimized the generator design for best performance by modifying the design of the adjustable height rotor shaft to allow easy and seamless adjustment of the rotor height.

4. Optimized the mechanical advantage of the motion translation gear-box to increase speed and hence the generated voltage per step while maintaining an overall low weight and profile.

4.1.2 Improved Generator Structure

In this section, the proposed architecture of the generator is presented. The structure of the proposed new generator is different from most conventional AC generators in the sense that while most synchronous generator structures are such that the rotor and stator are radially

concentric - one inside the other, this new structure proposes a stacked rotor-stator arrangement approach. Fig. 4.3 below shows the proposed new structure.

This type of arrangement allows room for adjusting the amount of air gap between the rotor and stator post fabrication. The final configuration, as will be seen later, has a completely detachable rotor assembly making it easy to independently use the same rotor on multiple stators or vice versa.

Now, there is hardly any hard and fast rule about air gaps in electric machine designs, but it is understood that smaller air gaps lead to higher electrical efficiency but, of course, increased cogging torque which invariably leads to an increased air noise [11], [41].

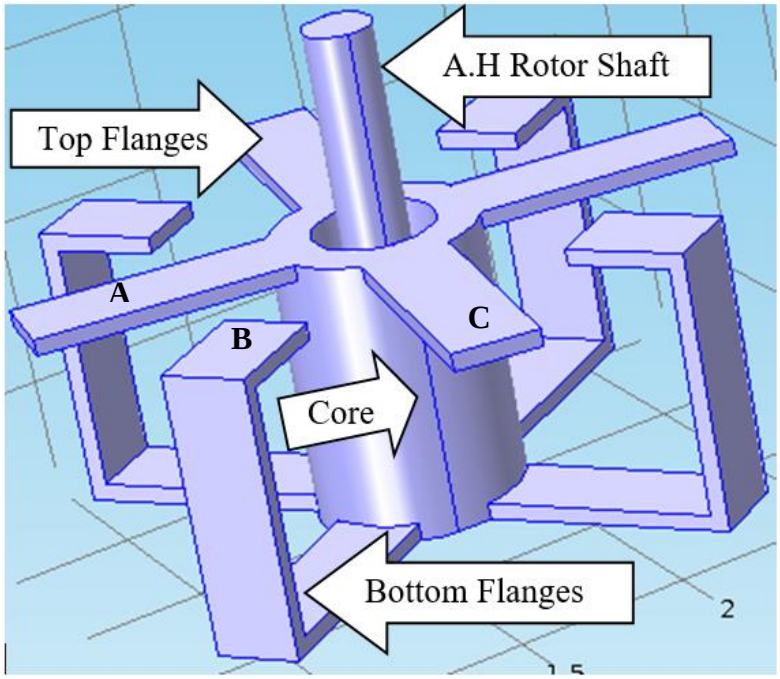

Fig. 4.3 – New generator structure: The new configuration showing the top and bottom flanges, the adjustable height shaft, and the A-B and B-C notation of how the magnets on the rotor interface with the stator flanges.

On the other hand, bigger air gaps lead to lower electrical efficiency and reduced cogging torque and correspondingly reduced air noise. Although a lower air gap is preferred for electrical efficiency, extremely low air gap could lead to stalled operation due to excessive cogging - the extreme magnetization force between the strong magnets and the stator core.

This leads to an inevitable trade-off in electric machine design which needs to be addressed carefully. To provide the most optimal air gap, one should analyze the generator specifications for any set of operational conditions – meeting the torque and output power requirements while maintaining enough room for manufacturing tolerances.

To accommodate variations in manufacturing tolerances [44], [45], a minimum air gap length of 1.0 mm will be adopted for this new concept.

Currently, the air gaps in most generators are hardly adjustable post fabrication, but the new generator structure based on this research work solves that problem. There would be two adjusting slots on opposite sides of the rotor housing that will allow a user to adjust the rotor to predetermined air gap size depending on the application of the generator. During testing, it was observed that when operating at a fixed RPM, the output voltages from the generator at the various air gap levels correspond with theoretical predictions and simulation results as demonstrated in the tables in sections 4.2 and 4.4. The equivalent circuit of the Electromagnetic generator is shown in Fig. 3.4 above. The coil impedance determines the amount of voltage drop from the generated voltage which depends, in part, on the load impedance.

During the test of the proof of concept, the measured results show that the output voltages were higher when the direct current (DC) load impedances are equal or higher than the coil DC impedances. This behavior is expected to maximum power transfer and the complex portions of the generator coil were deemed to have little or an insignificant impact.

By design, each stator flange is positioned directly under a strong Neodymium rare earth magnet on the rotor. The arrangement is such that all the top flanges are under similar magnetic polarities while the bottom flanges are directly under the opposite polarities of the other magnets. At the same time, adjacent magnets are linked on the ‘free ends’ with a soft magnetic material to close the magnetic circuit forming the back core. This arrangement mimics a single bar magnet made up of two separate magnets linked together at one of their opposite poles or more appropriately, a horse-shoe magnet.

Fig. 4. 4 shows an FEMM simulation of the simplified version of the new generator arrangement. This simplified structure draws from the path traced by the arrows in Fig. 3.8 above. It is, therefore, a representation of such a path using a pair of opposite pole magnets as a sample set. As previously indicated the magnets are closed on the opposite sides (and opposite poles) with a magnetically soft material to create a magnetically closed-circuit.

The ‘big orange arrows’ in the structures of Fig. 3.8 correspond with the ‘stator core’ in Fig. 4. 4 below. While the ‘magnetic pair pieces [labeled A, B, C, and D]’ in Fig. 3.8 correspond with the ‘back core’ of Fig. 4. 4.

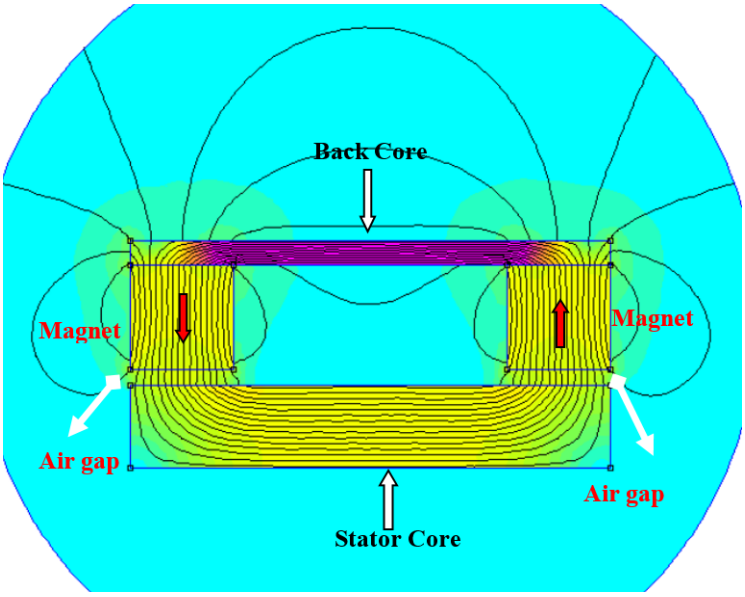

Fig. 4. 4 – FEMM simulation of the simplified concept: The simulated magnetic flux density lines connecting the rotor and stator show that all flux lines going through the stator core with a few flux lines above the rotor (back core).

The FEMM simulation of the simplified Generator structure shows two magnets that are alternately polarized, and one pair of their opposite poles linked together with a magnetically soft material with predetermined thickness (see Section 4.2). From the simulation results, all available flux lines emanating from the two remaining opposite poles of the permanent magnets are linked through the core material (also a magnetically soft material) via the air gap. In the simulation, the air gap was adjustable from 1 mm up to 5 mm on each end of the magnet pair.

During normal operation, the magnet pairs will revolve over the top and bottom flanges resulting in the magnetic flux (ϕ) changing direction by 180 degrees within the core – going from say $+\phi$ to $-\phi$ by the time a pair completely moves over from one top and bottom flange pair to the next. Say two consecutive top flanges are labeled 'A' and 'C', and the bottom flange between them is labeled 'B', then, a magnet pair going from A and B to B and C (see Fig. 4.3 above) will result in the magnetic flux density changing direction by 180 degrees within that core. The coil on the core will experience this change leading to an Electromagnetic induction on the coil. The rate of this change being directly proportional to the induced EMF.

4.1.3 The Coil Design and Construction

The stator core does not have slots like conventional generators, hence the coil design was a single continuous coil on a spool or former worn over the core. To make the design swappable, the coils were not placed directly on the stator core rather they were wound on a plastic former or spool which would later be worn as a sleeve on the stator core. As in the original proof of concept, two separate coil sizes were made for the improved proof of concept. One from a 26 AWG and the other from a 36 AWG gauge insulated copper wires respectively. Each consisting

of between 800 and 3000 turns of continuous winding on the plastic (non-magnetic) former or spool. The length of the former or spool corresponds with that of the stator core.

These coils would later be used in testing the 'swappable' rotor design. For each coil design, each end was soldered to one side of a pair of flexible wires and covered with insulating tapes. These wire pair pieces were then used to connect the coils to external loads. The weights of the windings and the spools are 92 and 32 grams, respectively. The coil assembly were then worn around the stator core before the bottom flanges were screwed on to complete the stator assembly. The measured DC impedances of the coils are 11 and 311 Ohms, respectively.

4.1.4 The Rotor and Stator Design and Construction

The rotor was designed with strong consideration for a light weight construction. It was made from a transparent Plexiglas with 'magnet pockets' arranged equidistant from each other in a circular pattern. Cylindrical magnets are seated in these pockets with adjacent magnets having alternating polarities in the vertical orientation. The alternate poles of nearby magnets facing away from the stator are linked in pairs using a magnetically soft material to close the magnetic circuit. This creates a back-core effectively improving the efficiency and concentration of the magnetic flux density towards to stator core (as determined by the simulations shown in Fig. 4.1 and Fig. 4.2).

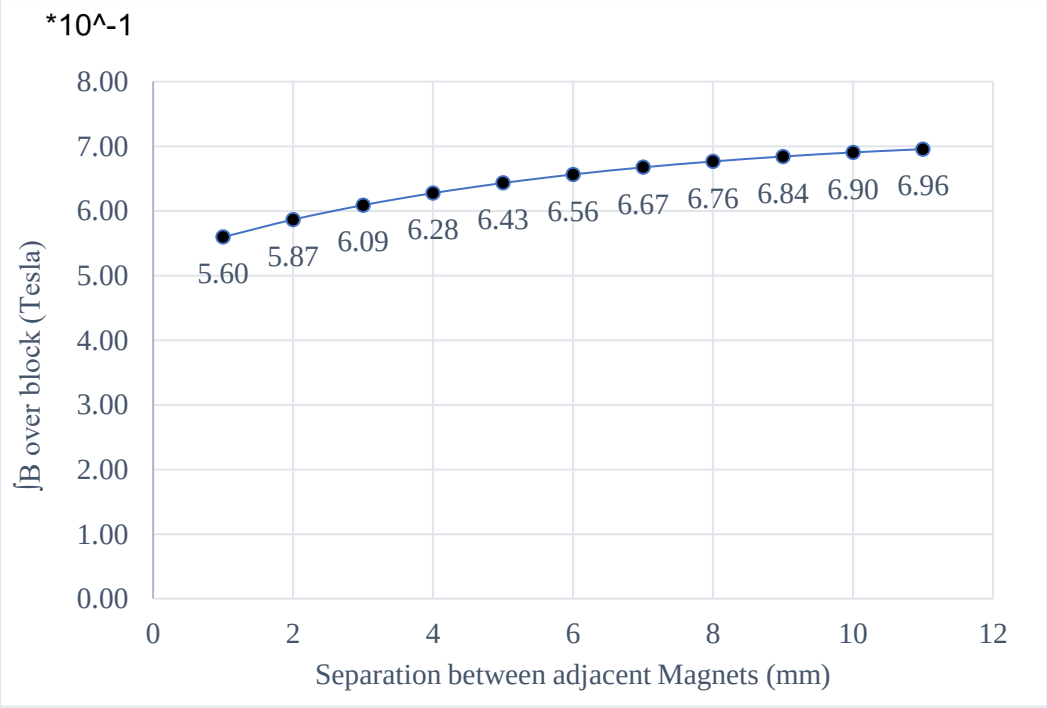

Fig. 4. 5 – Simulation of the separation between adjacent magnets – from 1.0 mm to 11.0 mm separation.

To determine the distance each magnet is placed from the next, an FEMM simulation was run considering several possible separation distances. Fig. 4. 5 shows the plot of the separation distance versus the integral of B over the stator core – this value (the integral of B) is the numerical equivalent of the average of the summation of the absolute values of 'B' across the stator core block as used in the simulation.

It could be observed that as the distance decreases, the absolute value of the integral of B decreases correspondingly but the integral increases as the distance increases. The plot also shows that after a finite length, the integral of B peaks and any further increase in separation distance will not contribute to any significant improvement.

From the plot, a minimum separation distance of 8 mm between adjoining corner edges was chosen. For the size of magnets used, this distance ensures that a magnet has completely moved away from the top of one flange before going over the next flange – this will guarantee that the stator core maintains a bar magnet-like characteristic whose polarity changes with the rotor motion – refer to Fig. 3.8 following the direction of the arrows on the stator core as the rotor revolves.

The size of generator chosen for the proof of concept is a 50 mm by 45 mm design. Based on this, the number of magnets permitted with this design approach is eight, resulting in four pairs of linked magnets [labeled A, B, C, and D in Fig. 3.8 above]. This then means that the number of magnets correspond to the total number of flanges, where each magnet is directly and vertically above a corresponding flange.

Apart from the magnet arrangement, another very important aspect of the rotor design is the air gap adjustment construction. This design uses the so-called ball-plungers to control the size of the air gaps by keeping the rotor at a predetermined height above the stator.

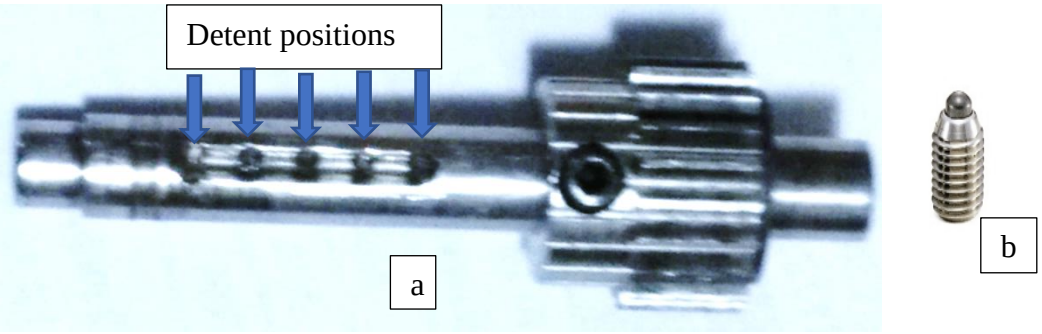

Fig. 4. 6 – (a) Rotor shaft showing 5 detent positions and (b) a ball-plunger

In this improved proof of concept, a spring-loaded ball (in the end of the plunger body) runs in a shallow vee-groove that is parallel to the center-line of the shaft (Fig. 4. 6). This prevents the rotor body from spinning on the shaft during normal operation. Furthermore, at about 1.25 mm intervals, there are a series of five conically-shaped indents machined along the groove center-line that are about 0.25 mm deeper than the groove itself. These act as "detents" since the ball-end will drop into them when the rotor body is slid along the shaft. It takes a fair amount of extra axial force to push the rotor past the indents, giving rise to the detent action.

The stator design uses the same material type and thickness for the flanges as the ones used for the back core. The final stator core dimension of the generator prototype is a summation of all the core dimensions of the linked magnet pairs, resulting in four times the sizes used in the simulation.

4.2 Simulation and Optimization

In this section, a comprehensive simulation and analysis is done for all the materials used in the new generator design. This is done to determine and optimize the core parameters. First, a simulation was run to determine the minimum thickness of the magnetic material that will be used to close the magnetic circuit in the proposed structure as well as the minimum thickness of the core flanges. This exercise is essential because too small a thickness would lead to high magnetic saturation. On the other hand, excessively thick material only adds to the overall weight of the generator without any significant electrical advantage. It was indicated in [46] that high saturation is responsible for higher flux leakages in electrical machines.

This simulation to determine material thickness was run with a fixed air gap length of 1.0 mm. The stator core dimension was also fixed at 6.35 x 5 x 20.7 (D x H x L) mm corresponding to the Depth (which corresponds with the Magnet diameter), Height/Thickness and Length, respectively. Note that the length is a sum of the diameter of the two magnets and the minimum separation distance (6.35 + 8 + 6.35) mm.

Fig. 4. 7 shows the simulation of material thicknesses from 0.5 mm to 5.0 mm. It is observed that the magnetic flux density lines tend to all but escape through the 0.5 mm thick plate but are gradually and predictably constrained within the material as the plate thickness increases. One important observation in this scenario was that any additional increase in the plate material beyond 3 mm yielded no significant effect on the apparent direction of the magnetic flux lines and hence no impact on the induced voltages for the generator built with such material. The optimum thickness was thus found to lie between 2.5 mm and 3.0 mm.

When a generator is designed with the said optimum plate thickness, it will perform at a similar electrical efficiency as a thicker plate. It was therefore recommended to use a plate of this thickness to ensure that no unnecessary weights were added.

Simulation results showing the magnetic flux lines for 0.5 mm and 1.0 mm plate thicknesses.

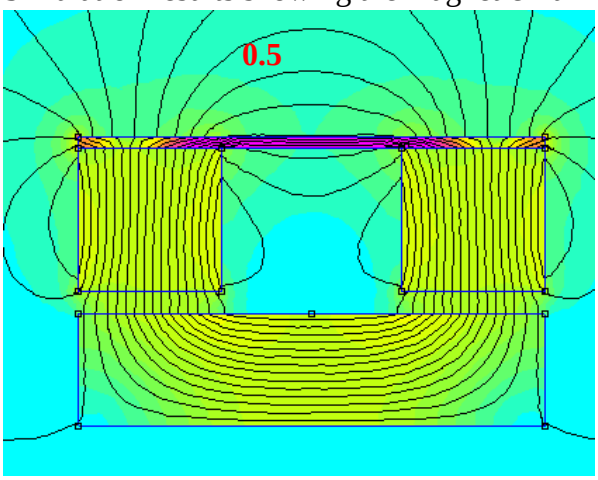

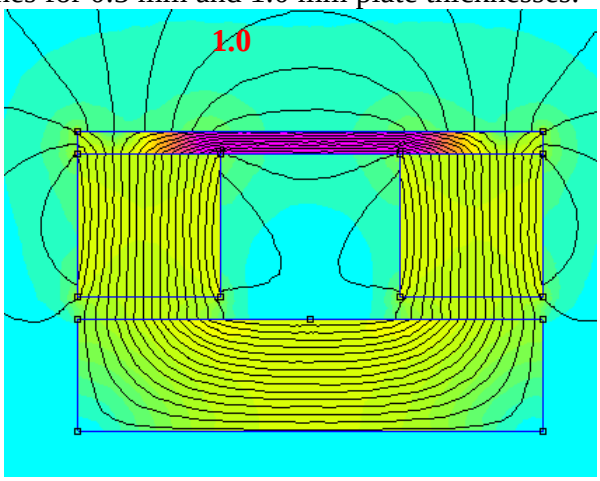

Simulation results showing the magnetic flux lines for 1.5 mm and 2.0 mm plate thicknesses.

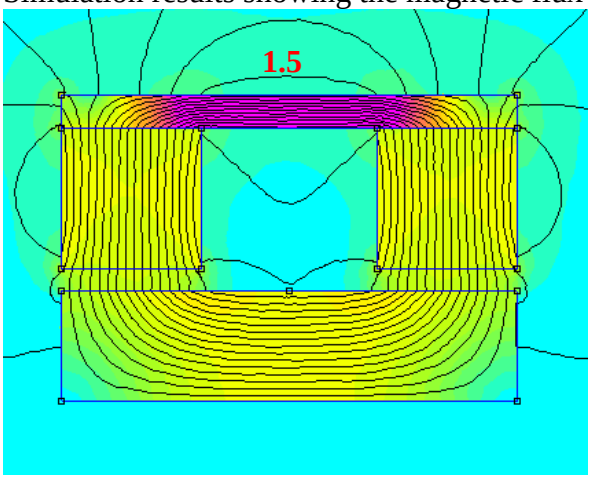

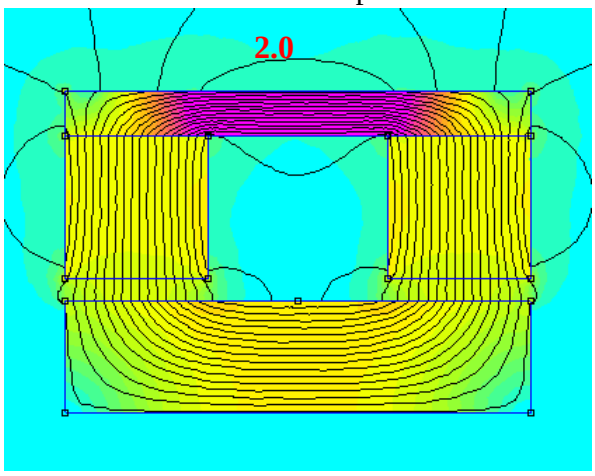

Simulation results showing the magnetic flux lines for 2.5 mm and 3.0 mm plate thicknesses.

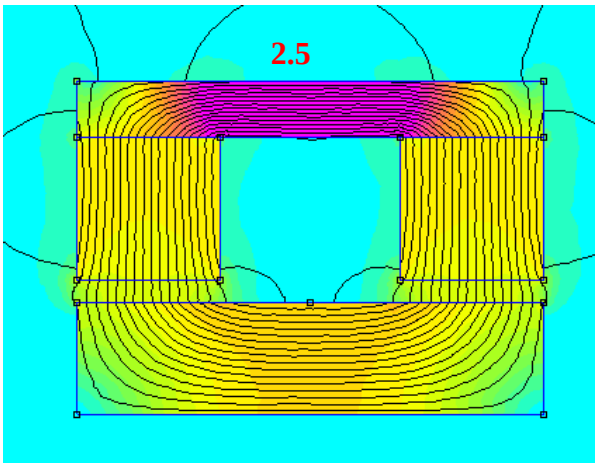

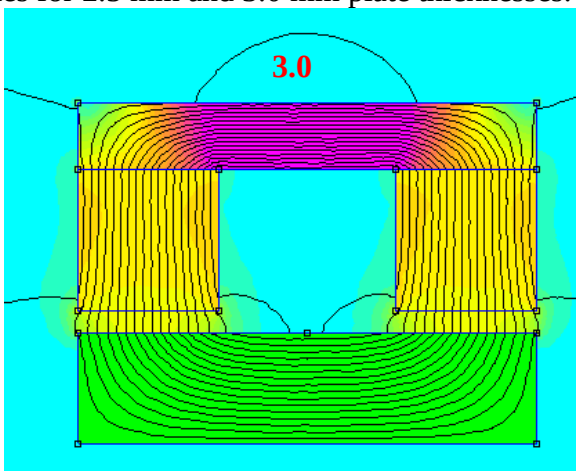

Simulation results showing the magnetic flux lines for 3.5 mm and 4.0 mm plate thicknesses.

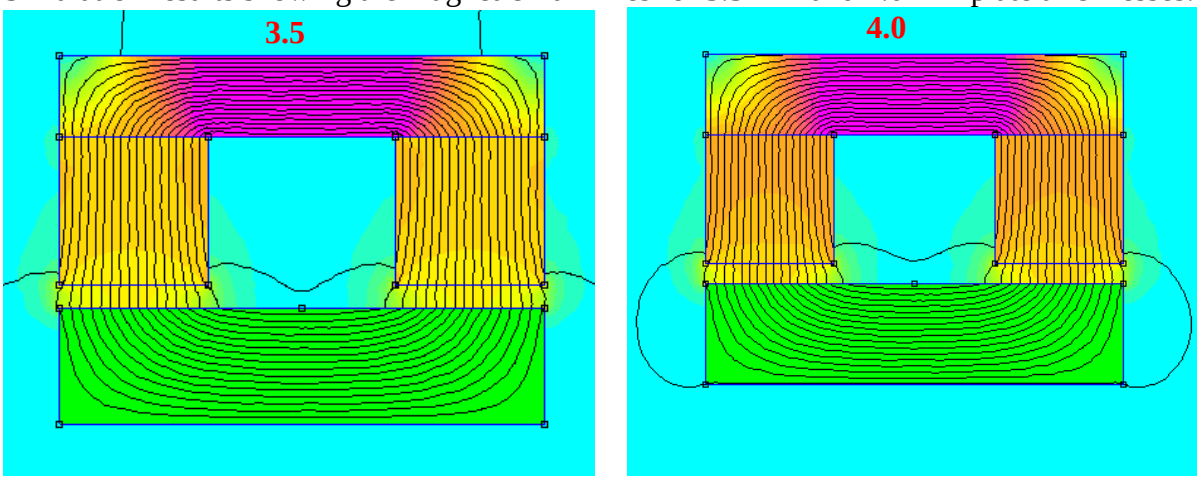

Simulation results showing the magnetic flux lines for 4.5 mm and 5.0 mm plate thicknesses.

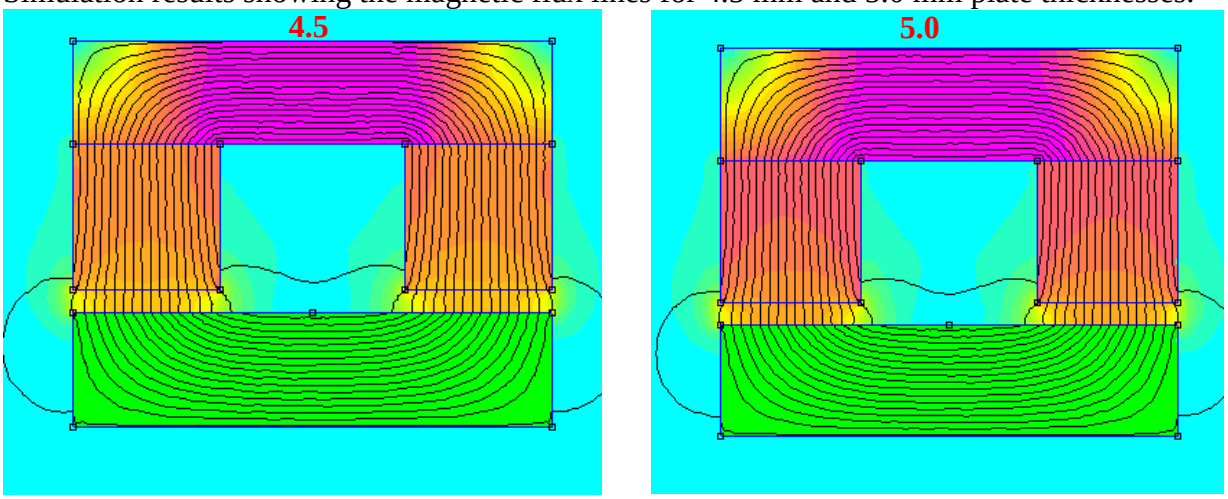

Fig. 4. 7 – Material thickness determination: The above show the simulation results for thickness ranging from 0.5 mm to 5.0 mm. Optimum thickness was achieved at around 2.5 to 3.00 mm.

The plate thickness is a function of the size and the magnetic properties of the plate itself and that of the permanent magnets used in the design. The type and size of the magnet chosen for this simulation is the 6.35 mm by 6.35 mm cylindrical neodymium rare earth magnet (NdFeB 40 MGOe) and the plate is a 1018 soft iron steel. The plate width was chosen to correspond with the diameter of the magnet, while the thickness was determined by the simulation.

The value of integral of **B** over the stator core increases as the air gap decreases. The results are summarized in Table 4. 1. As the rotor revolves, the actual values change in polarity. This change in polarity is directly linked to the induced EMF.

It was also observed that for the back core, as the plate thickness increases, the absolute value of the integral of **B** over the back core increases correspondingly. This result is summarized in Table 4.2.

Table 4. 1 – Integral of B over the stator core

Air Gap (mm)	X-Component (Tesla m^3)	Y-Component (Tesla m^3)	Core Dimension (m^3)	X-Component |B| (Tesla)	Y-Component |B| (Tesla)
1	-4.45E-07	7.13E-12	6.57E-07	0.68	1.08E-05
2	-3.79E-07	5.19E-12	6.57E-07	0.58	7.90E-06
3	-3.26E-07	-2.90E-14	6.57E-07	0.50	4.42E-08
4	-2.82E-07	1.31E-11	6.57E-07	0.43	1.99E-05
5	-2.25E-07	-7.51E-12	6.57E-07	0.37	1.14E-05

Table 4. 1 - The absolute values of the integral of B over the stator core.

Table 4.2 – Determining optimum plate thickness for back core

Plate Thickness (mm)	X-comp (Tesla m^3)	Y-comp (Tesla m^3)	Core Dimension (m^3)	X-comp |B| (Tesla)	Y-comp |B| (Tesla)
0.5	-3.83E-07	4.66E-12	6.57E-07	0.58	7.09E-06
1.0	-4.25E-07	5.21E-12	6.57E-07	0.65	7.92E-06
1.5	-4.64E-07	1.54E-11	6.57E-07	0.71	2.35E-05
2.0	-5.00E-07	1.47E-11	6.57E-07	0.76	2.24E-05
2.5	-5.34E-07	4.01E-12	6.57E-07	0.81	6.11E-06
3.0	-5.63E-07	-1.07E-11	6.57E-07	0.86	1.63E-05
3.5	-5.84E-07	-1.89E-11	6.57E-07	0.89	2.88E-05
4.0	-5.93E-07	-2.79E-11	6.57E-07	0.90	4.25E-05
4.5	-5.97E-07	-2.18E-11	6.57E-07	0.91	3.32E-05
5.0	-5.99E-07	-1.97E-11	6.57E-07	0.91	2.99E-05

Table 4.2 - Simulated field lines and intensity to determine the optimum plate thickness for the back core and stator flanges.

4.3 Prototype Fabrication and Assembly

During the prototype fabrication, a soft iron steel plate or disc was machined into the desired shapes for all metal pieces (the magnets back core, the top and bottom stator flanges), while a steel rod was machined and used for the stator core.

Some changes were made to overcome some practical challenges. For instance, the original design of the adjustable rotor shaft was changed from a pinch-drag to a push-pull design. To maintain the modular rotor design, a new way was devised to have the complete assembly in a fast and seamless manner. To do this, a ball bearing was inserted on the stator core with a bore the right size for the adjustable rotor shaft (see Fig. 4. *8*). This structure allows the shaft to rotate alongside the rotor as a complete rotor assembly. The generator is shown without a final housing to reveal the unique design. The rotor could be driven by a belt or a teeth and gear assembly.

Another important aspect is the adjustable rotor height mechanism. The shaft was made from a steel material with a centerline groove on one side. A ball plunger was used through one side of the rotor disc at about the centerline groove. On the opposite of the ball plunger is an ordinary set-screw that was added only to counter-balance the effect of the ball plunger - to keep the rotor balanced when in motion. This added set-screw was not meant to touch the shaft as this would impede the sliding of the rotor along the shaft.

When inserting the shaft into the rotor disc, the ball plunger was backed-off so that the tip will just touch the shaft's outer diameter (OD) with a little bit of resistance. The shaft was then twisted in the rotor bore until the plunger tip found (located) the longitudinal vee-groove. Afterwards, the pressure on the ball plunger was gently increased (by turning it clockwise) so that the shaft can slide in the rotor bore with some reasonable level of resistance such that the shaft will not easily turn in the bore.

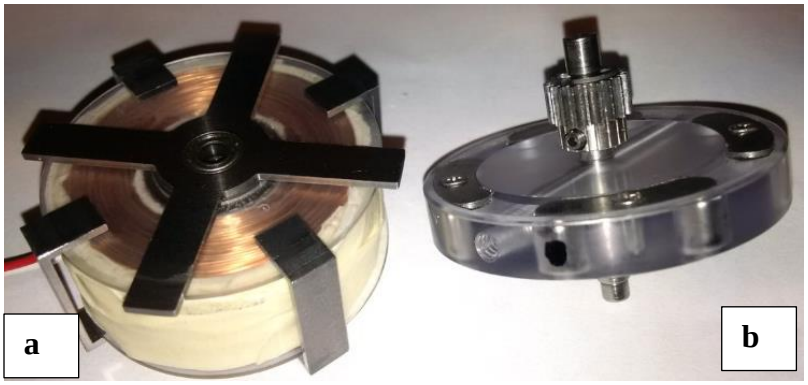

Fig. 4. 8 - Complete generator assembly: (a) The stator assembly with the top and bottom flanges, core and coil assembly fully installed. (b) The rotor assembly is shown to the right of the figure.

Once satisfied that the shaft will not easily turn in the bore, the detent positions were located and checked that the ball plunger "clicks" into position without introducing excessive angular play. Any excess angular play was removed by tightening the ball plunger a little bit more to reduce this movement. Fig. 4. 8 shows the complete stator assembly with the top and bottom flanges, core and coil assembly fully installed, while Fig. 4.8 shows the complete assembly with the rotor installed on the stator via the shaft and ball bearing.

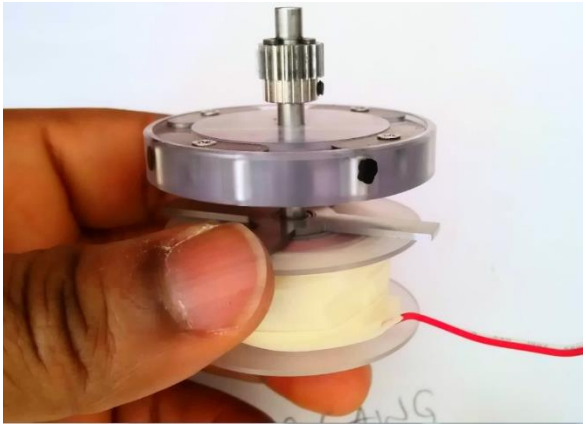

Fig. 4. 9 - Complete generator assembly: The Complete assembly showing the rotor, stator and a gear on the rotor shaft for connecting to other gears or a pulley.

If the plunger is fastened too tight it will be more difficult to slide the rotor along the shaft to the next detent position and can cause excessive wear. Ideally, the plunger should be used in conjunction with a hardened shaft to minimize the risk of burrs that could be created if the plunger slips.

The coil spool was machined from a single cylindrical plastic into the shape of the spool. The wall thickness of the spool, including that of the top and bottom parts, were 1.25 mm. Being a non-magnetic material, it has no impact on the flow of the magnetic flux lines, but it was important that the thickness is at a minimum to ensure the coils are as close to the stator core as possible (since magnetic flux density decrease exponentially as distance from source increases).

4.4 Experimental Results

To test the new generator, it was important to run it at a constant revolution per minute (RPM) for each air gap level. Tables showing the open circuit voltages for respective air gaps are shown below for each of the stator coils. Tables 4.3 and 4.4 show the unloaded voltage conditions while tables 4.5 and 4.6 show the output voltages when the rectified generated voltages were each connected to a 100-Ohm load.

The speed of the rotor was kept constant at 2900 RPM using a constant speed motor. This eliminates variability and ensures each coil-air gap combination is test run at same speed as others. To baseline the new generator concept, a similarly sized off-the-shelf DC motor was run at same RPM and the open circuit DC voltage and the DC voltage on a 100-Ohm load were 5.4 VDC and 0.47 VDC, respectively.

Table 4. 3 – 26 AWG coil (800 Turns)

RPM	Air Gap	Open Circuit AC Voltage
2900	1 mm	33.1
2900	2 mm	19.50
2900	3 mm	10.02
2900	4 mm	4.00
2900	5 mm	1.30

This table shows the open circuit output voltages of the generator with 26 AWG coil at different air gaps.

Table 4. 4 – 36 AWG coil 3000 turns

RPM	Air Gap	Open Circuit AC Voltage
2900	1 mm	60.5
2900	2 mm	44.9
2900	3 mm	18.6
2900	4 mm	7.12
2900	5 mm	2.84

This table shows the open circuit output voltages of the generator with 36 AWG coil at different air gaps.

Note that the open circuit output voltages drop significantly for every 1 mm increase in the air gap which agrees closely with the value of the magnetic flux density indicated in the FEMM simulation for the corresponding distances (see Table 4.1 above). Remember that the generated voltage is directly proportional to the change in the Magnetic flux density linking the conductors.

Comparing tables 4.3 and 4.4 above reveals that the induced voltage is not exactly proportional to the number of turns. The reason could be attributed to the distance of the coil to the core of the generator. The further away from the core, the less the influence of the magnetic flux linking the coil.

Notice also that these windings were done with different wire gauge sizes. This means that the same core area could contain varying numbers of coil turns. In the proof of concept, the 26 AWG wire occupied the entire core area for only 800 turns while the 36 AWG wire occupied a fraction of the same core area.

Table 4. 5 – 26 AWG coil

RPM	Air Gap	DC Voltage on 100 Ω load
2900	1 mm	10.20
2900	2 mm	6.31
2900	3 mm	3.03
2900	4 mm	1.12
2900	5 mm	0.20

This table shows the DC output voltages of the generator with the 26 AWG coil on a 100-Ohm load at various air gaps.

Table 4. 6 – 36 AWG coil

RPM	Air Gap	DC Voltage on 100 Ω load
2900	1 mm	3.20
2900	2 mm	1.60
2900	3 mm	0.82
2900	4 mm	0.37
2900	5 mm	0.14

This table shows the DC output voltages of the generator with the 36 AWG coil on a 100-Ohm load at different air gaps.

The generated AC voltages were then rectified using a full wave bridge rectifier and used to drive a low impedance load of 100 Ohms. For this load level, a maximum of 1.04 W could be delivered by the generator with coil made from the 26 AWG coil, while a maximum of 102.2 mW was delivered with the 36 AWG coil.

This demonstrates clearly the need for a better power management system to maximize the output power. The OKI-78SR buck-boost converter was used to improve the harvested power. See section 4.6.2.

Fig. 4.7 shows each unit construction as well as their modular (plug-and-play-like) design. To run the generator, the rotor will be plugged into the ball bearing on the stator and the shaft of the rotor driven by any motion source. Further to that, Fig. 4.8. shows the complete generator and the removable rotor system as a unit ready for test. The new system is shown without an enclosure to reveal the complete design stack-up.

4.5 Discussion

For low voltage, low power generator design, a slightly thinner plate could also be used. Observe that from tables Table 4. 1 and Table 4.2, the absolute values of the integral of the magnetic flux density generated on the X-Components are several orders of magnitude higher than those generated for the corresponding Y-Component. This was based on the orientation of the polarities of the permanent magnets and that of the stator core in the simulation (see also Fig. 4.3). Therefore, the values used in these analyses were only those corresponding to the X-Components which simplifies the analysis (for the same reason, the values of the Y-Components were not used as they will not affect the overall behavior or performance in a significant manner).

The generator design used different coil wire gauges and number of turns to determine the optimal performance of the proof of concept. In section 4.4, two tables showing the voltages measured across two coils were shown. Voltages from a 26 AWG wire gauge coil were shown on Table 4. 3, while Table 4. 4 shows the results from the 36 AWG wire gauge coil.

The number of turns for the coils were 800 and 3000, respectively. The coil ratio is about 1:3.75, however, the voltages measured across the coils were not related by that same ratio. This is because of the size differences between the coils. This meant that the coils with the larger cross sectional area wire is relatively farther from the core of the generator, and hence interact more with the magnetic flux linkages, compared to that of the smaller wire gauge coil.

To verify that this is indeed an anomaly (the non-ratio relationship), a new coil designed from the same wire gauge made with different turns tapped at 500, 1000, 1500, 2000, 2500 and 3000 respectively, see Fig. 4. 10. The generator was assembled with an air gap of about 2 mm and the generated voltages at the same RPM presented in Table 4. 7.

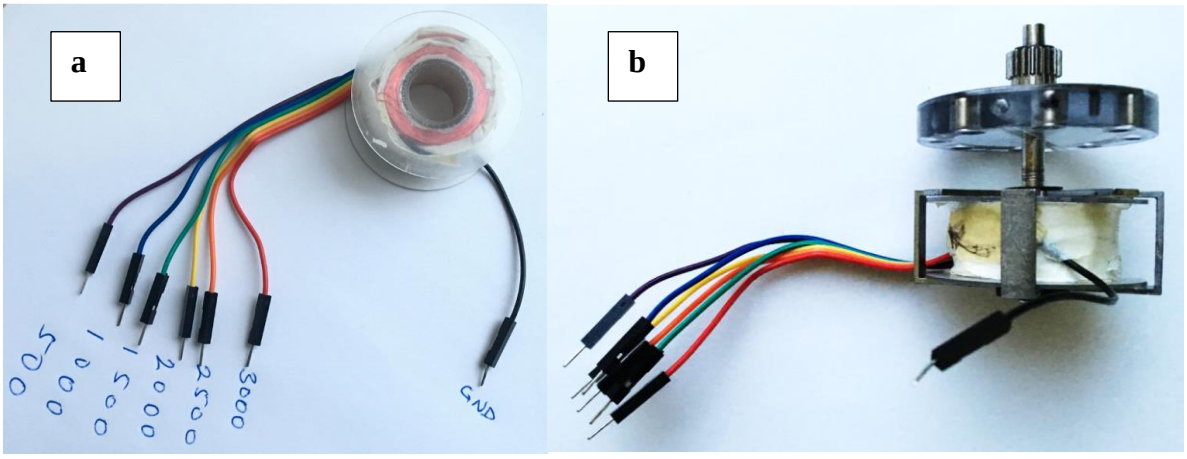

Fig. 4. 10 – New coil design tapped at 500, 1000, 1500, 2000, 2500 and 3000 respectively. (a) the coil design (b) showing the full setup – coil, rotor shaft and rotor-magnet assembly

Notice that as the number of turns increased, the amount of generated voltages increased predictably, satisfying section 3.1.1, and equations 1 and 2. The DC impedance of the coil increased as well with the increase in the number of turns. This agrees with the formula for calculating the impedance of conducting wires which relates the resistance of a conductor directly to its length and inversely proportional to its cross sectional area, the resistivity of the conductor being a constant, see equation 3.

Table 4. 7– Solid Stator Core Generator

	Number of Turns	Coil Impedance	Output Voltage
1	500	45.80	5.1
2	1000	94.70	16.1
3	1500	147.10	24.1
4	2000	203.00	31.6
5	2500	262.00	39.2
6	3000	325.00	46.1

The above results were from the original concept with a solid stator core. To investigate the impact of eddy current losses due to the solid core, a laminated core was used. The new stator core was made up of circular rings of 1010 grade steel that are laminated and stacked together within the core of the stator. The top and bottom flanges were attached by specially fabricated 3-D printed parts to complete the new core (See appendix). Table 4. 8 shows the results obtained from the new stator core. The coil and rotor were the same for both – used in a modular fashion.

While analyzing the new laminated structure and its potential impact on reducing eddy current losses, it was observed that the construction of Fig. A.2.2 (see the appendix) was not able to significantly impact the effect of eddy current losses, however, owing to the relatively low operating speed and frequency of the generator, it was determined that the effect of eddy currents might not have a measurable effect on this energy harvester. The observed reduction in inductance and induced voltages with respect to the laminated core, could then only be linked to the reduction and/or difference in the effective area of the stator core.

Table 4. 8 – Laminated Stator Core Generator

	Number of Turns	Coil Impedance	Output Voltage
1	500	45.80	5.8
2	1000	94.70	11.4
3	1500	147.10	18.2
4	2000	203.00	24.7
5	2500	262.00	30.0
6	3000	325.00	37.4

Various variable speed motors were used to drive the generator ranging from a couple of hundreds of RPMs to a couple of thousands of RPMs. The generated voltages increased, predictably as the RPM increased. The maximum speed of the available motor was 2900 RPM.

A gear box was designed and developed. It was demonstrated that the theoretical optimum RPM for the new concept is about 5000 RPM. The design and construction of the gearbox are discussed in section 4.6.1.1.

4.6 System Integration

4.6.1 Mechanical subsystem

The energy harvesting technology used in this research is the electromagnetic energy generator. This generator is a brushless AC generator described in the previous sections. For this energy harvesting system to function, a source of motion is required for the generator. In this section, the sources considered include human motion as well as other mechanical sources such as swinging doors and windows.

Now, the above-mentioned sources are low speed sources and would require an up-conversion technique to increase the speed applied to the rotor. In this section, the discussion will be focused on the design of the mechanical up-conversion method employed both for the multi-purpose energy harvesting system as well as the methods adopted for wearable applications.

4.6.1.1 The Roller Clutch design

For this multi-purpose energy harvester, a mechanical up-conversion gear box was designed to increase the speed of the generator with respect to the speed of the original source of motion. Now, since there is also a wearable aspect to this energy harvesting system, it was designed to harvest energy only during one motion cycle. In this design, some of the negative energy generated during the different walk phases were harvested. Negative energy corresponds to the swing phase of the walk cycle which in turn corresponds to the work done in braking of the knee. It helps in deceleration and in maintaining stability [9]. This approach is analogous to the regenerative systems used by electric vehicles in recharging their batteries [10].

It was discussed in section 4.5 above that the Electromagnetic energy generator was tested at a fixed rate of 2900 RPM with an optimum RPM projected to be greater than or equal to 5000 RPM. For this reason, and assuming a speed of one step per second, a mechanical up-conversion gearbox was designed to produce a speed in the desired range.

The gear-ratio for each of the stages, as shown in Fig. 4.9 is 5:1. The gearbox comprise of a three-stage spur gear and a fourth stage being the generator rotor gear.

Equation for Speed [in RPM]:

$$[1 \times 5 \times 5 \times 5] = 125$$

$$125 \times 60 = 7500 \text{ RPM}$$

Note that when moved at a relatively fast pace, at say, one step per second, a flywheel effect is created which causes the first stage to complete a full revolution from about one-fifth revolution of the first gear from the crank handle about the roller clutch (approximately about 72-degree rotation).

Fig. 4.9 shows the design of the mechanical up-conversion gear system. It contains a crank handle to be affixed to the motion source on one side – swinging legs, doors, windows or any other motion source(s). The other side of the crank handle connects to a combination of the roller clutch and the complete gear system that make up the mechanical up-conversion system. The roller clutch transmits the motion to its shaft in one direction but is free-running in the reverse direction making it possible to selectively transmit the motion to the gears as desired. It is possible to change the direction of the motion of the roller clutch by simply inverting its orientation within the gear box.

The mechanical up-conversion is achieved by multiplying the number of steps per second by the system gear ratio multiplied by 60. It was previously determined from experimental methods that an RPM of 5000 is the optimum speed for the energy harvesting generator. Therefore, a three-stage spur-gear box was designed with a total mechanical advantage of between 62 and 125. When the input shaft moves once per second, the output shaft revolves at an RPM of between 3750 and 7500.

A two-level planetary gear system with a gain of 10 for each level would produce similar RPM for the same input speed and would be more compact than the spur gear system. However, its construction would require a face or bevel gear at the frontend for attaching the input shaft and the roller clutch in much the same way as the current spur gear system.

A planetary gear, which derives its name from its similarity in design and construction to the planets in our solar system, is a gear system that consists of outer gears called planet gears, revolving around a central gear called the sun gear. It is mounted on a movable carrier which rotates relative to the sun gear. The sun gear itself is self-balancing on the planet gears and distributes its torque on them.

4.6.1.2 Gear Box Packaging

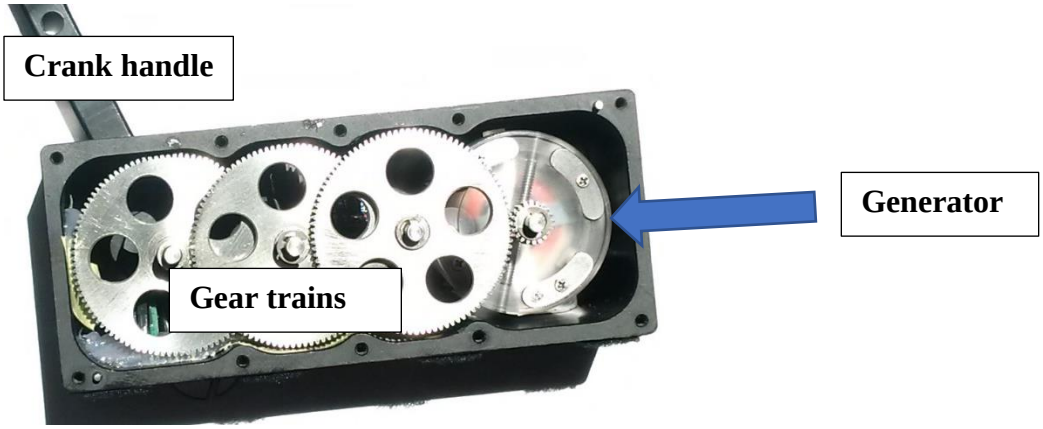

Fig. 4. 11 - Gear box and the energy harvesting generator.

To the right of the gearbox enclosure is the electromagnetic generator. While the three-stage gears are to the left. The crank handle is to the left-most and is used to link the gearbox enclosure to the swinging ‘arm’ of the motion source.

Note that the spur gears have five equally distributed holes where materials have been removed to improve the weight of the system while maintaining balance while revolving.

4.6.2 Electrical Subsystem

The electrical subsystem consists of the energy harvesting generator, a bridge rectifier, a DC-DC converter, and a Power management circuit comprising the internal battery charging system, and a USB charger for the external loads.

The energy harvester is adjustable and adaptable for different energy harvesting applications. However, the output voltage is subjected to energy modification before many applications. This modification is what is popularly called voltage rectification.

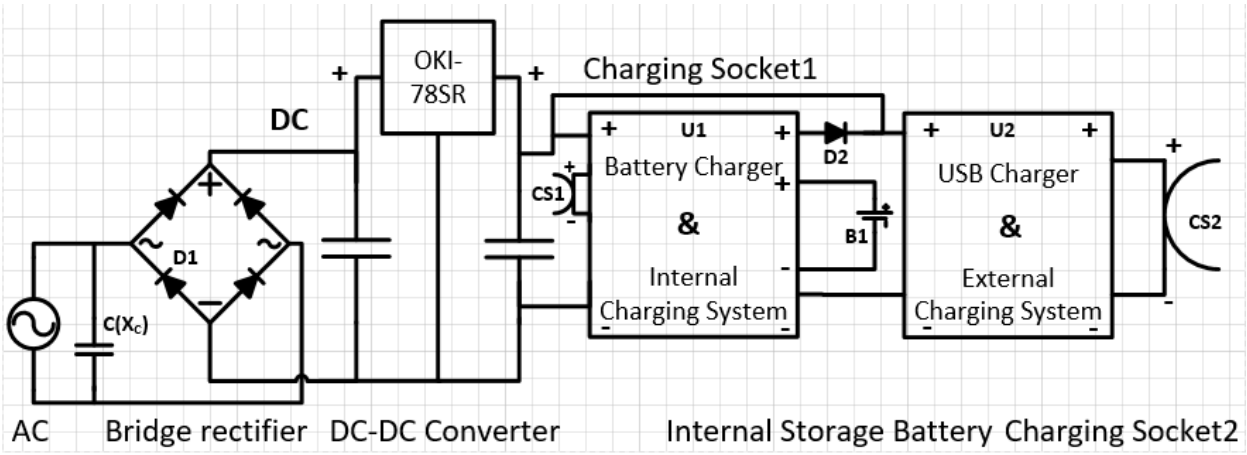

Fig. 4.12 - Diagram of the electrical subsystem.

4.6.2.1 Rectifier:

The bridge rectifier (D1 in Fig. 4.12 above), is a full wave bridge rectifier designed with 4 diodes (preferably with Schottky diodes). Schottky diodes have lower forward drop voltage compared to silicon diodes. Silicon diodes typically have forward voltage drop ranging between 600 and 700 mV while the Schottky diode forward voltage drop is merely between 150 mV and 450 mV which makes for a higher speed and better system efficiency. The overall impact is that most of the harvested energy reaches the DC-DC converter circuit. In the proof of concept, a DP-M packaged full-wave bridge rectifier with a maximum forward voltage drop of 1.1 volts was used.

4.6.2.2 DC-DC Converter:

To increase the amount of harvested power, a DC-DC converter was used to convert a high voltage - low current input into a low voltage - high current output. This was achieved using the OKI-78SR DC-DC switching regulator (Fig. 4.13) from Murata power solutions [35]. This converter has a single output that offers tight regulation and high efficiency directly to the connected load. Being a direct replacement for the T0-220 package 78xx series linear regulators, it typically requires no extra external components. The configuration chosen for this work offers a 5 volts output with a maximum output current of 1.5 Amps.

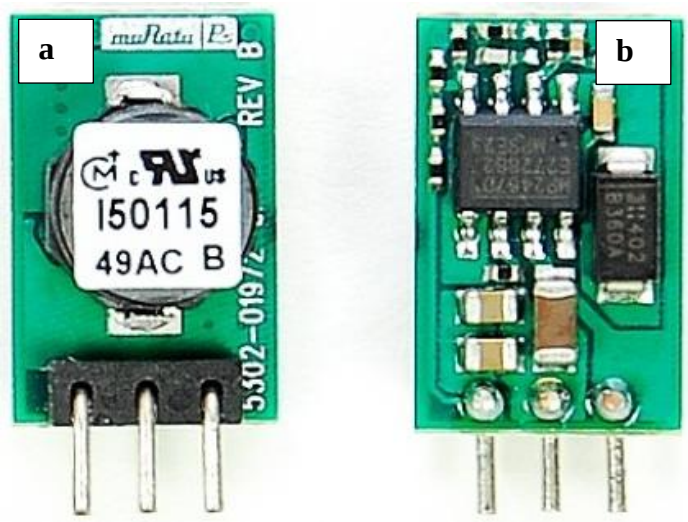

Fig. 4.13 – OKI-78SR DC-DC converter (a) front side (b) opposite side

The decision to use this converter was made because it offers an ultra-wide input range of 7 to 36 Volts DC at rated efficiency of 90.5% which is suitable for variable output energy harvesters. Based on component choices, it is expected that the output power of the generator would be up to 7.5 Watts.

Theoretical Output power = IV = 5 x 1.5 = 7.5 Watts

4.6.2.3 Impedance Matching

In chapter one, the concept of impedance matching was mentioned as an advantage of this type of system. However, impedance matching will only deliver fifty percent of generated power at best. Now, since the system contains inductances and potentially stray capacitances, impedance matching requires that the system operate at a fixed frequency. The fixed frequency will correspond to the rated frequency of the motion translation gear box.

In the section on preliminary results (section 3.9), this frequency was calculated to be around 193 Hz. Impedance matching will then only apply at this frequency. To achieve this, a capacitor whose value will make the capacitive reactance equal in magnitude but opposite in sign to that of the inductive reactance of the generator coil must be used across the connected load – which in this case is the bridge rectifier. The resistance of the bridge rectifier then only need to equal the real portion of the of the series impedances – Section 5.1.1 and 5.1.2.

But this energy harvesting system in this research work is designed to work across several frequencies and not just a fixed frequency. This then implies that impedance matching will only be optimal at the said rated frequency, meaning that power generated outside this ‘optimal frequency’ will not be optimally transferred to the load.

While this is achievable and desirable in many applications, and as set out at the onset of this thesis, it was determined that a system that allows at least parts of all generated power to be transferred to the load while also favoring maximum power transfer, when operating at optimum RPM, will be adopted for this energy harvester.

4.6.3 Charging Systems:

4.6.3.1 Charger for Internal Storage Battery

For a multi-purpose energy harvesting system, it is possible that an external load may not be connected all the time while energy is being harvested, hence, it is important to include an internal energy storage system that would hold the harvested power temporarily and supply such power on demand to an external load. For this purpose, an ultra-capacitor or a rechargeable battery could be used. In the proof of concept, a lithium-ion 3.7 Volts rechargeable battery was used.

This requires a separate battery charger for the internal battery storage system. Now, it is also possible that power is taken from the system at the same time, when this is the situation, the system automatically routes most of the harvested power to the external charging system while the internal battery receives only trickle charges.

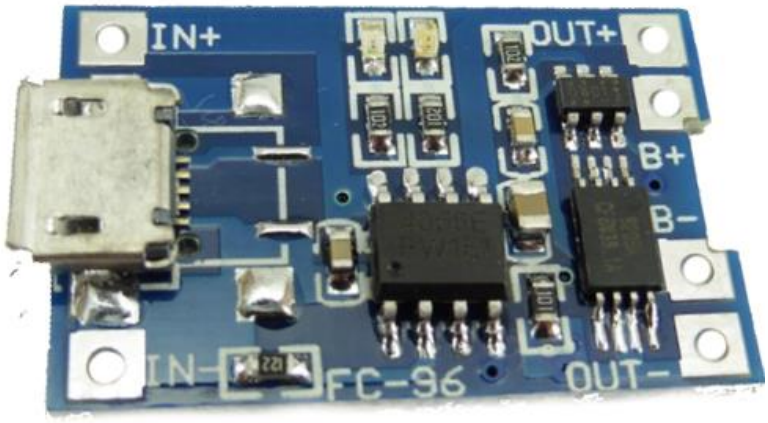

Fig. 4.14 – internal charger with multiple input & output ports

This design approach was made possible by the TP4056-based constant-current/constant-voltage linear charger for single cells lithium-ion batteries, see Fig. 4.14. This chip works perfectly well with USB and wall adapters and other DC voltage sources, hence a system was incorporated that makes it possible for users, when desired, to charge the multi-purpose energy harvester from external sources, which could include charging through a USB/wall charger via the CS1 port while retaining the ability to charge the system separately from the harvested voltage.

This chip protects the internal storage battery from over-charging by automatically terminating the charging cycle when the charge current drops to one-tenth of the programmed value after the final float voltage has been reached.

The manufacturer data indicated that there are other important features of the TP4056 chip which include current monitor, under voltage lockout and automatic recharge, two status pins used to indicate charge termination and the presence of an input voltage. These features combine to make this chip ideal for an energy harvesting power management circuit.

4.6.3.2 Charger for Externally Connected Loads

As the design goal of the energy harvester is to supply power to, or charge a load that is external to the energy harvesting enclosure, a pulse frequency modulation (PFM) USB charger based on the TP8350 charging circuit was employed, see Fig. 4.15. This charger takes power from either the internal storage battery or directly from the energy harvester to supply power to and/or charge an externally connected load.

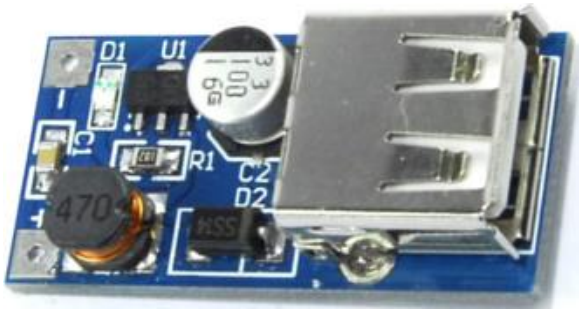

Fig. 4.15 - External charging circuit for external loads.

This charger, which is a boost charger, takes an input of between 0.9 and 5 Volts and produces a regulated 5 Volts output at 1 Amp output which could then be used to supply power to or used to charge a connected load. A USB port (labeled CS2 in Fig. 4.12 above) gives access to this circuit via the side of the multi-purpose energy harvesting enclosure/housing. This charger detects the presence of an external load and starts charging/supplying power to it automatically.

The USB port used here is the standard 2.0 USB port which accepts all compatible USB chargers. The boost converter produces a regulated output voltage of 5 volts, which is equivalent to what many smart device chargers produce. This then means that the connected device must be rated to handle the generated power. As stated above, the TP8350 chip circuitry provides both over-voltage and over-current protection by providing a stabilized and regulated output.

4.7 Complete System

4.7.1 Contents of the System

The complete multi-purpose energy harvesting system includes the generator, the gearbox and gear train for mechanical up-conversion, the full-wave rectifier circuit, the DC-to-DC converter, the battery charging circuit for the internal storage system and finally the external charging system for the externally connected load(s), each of which have been described in details in the preceding sections.

In this section, their inter-connections will be discussed. The core of this energy harvesting system remains the Electromagnetic energy generator. However, this generator alone is not sufficient for an energy harvesting system that is efficient and multi-purpose in nature. Mechanical up-conversion was required to increase the generators RPM so that the generated voltage will mirror the predicted output.

Now, since the source of motion are intermittent and perhaps unpredictable at times, the amplitude of the generated voltages varies widely. The use of the OKI-78SR series DC-DC converter ensures that the wide range of generated voltages are regulated and channeled to the required charging circuit.

4.7.2 Charging the Charger

This system is designed to be rechargeable from various sources, namely, the energy harvester, wall outlets and other suitable sources of energy. When used partly indoors and partly outdoors, the internal storage battery of the energy harvesting system could be charged whenever a suitable source of power is available through the micro-USB port. The energy stored by this means would then be used in charging and/or supplying power to externally connected load(s) when the need arises. This also ensures that the storage battery does not get drained completely if unused for an extended period. Now, while in the field, the internal storage battery or an externally connected load is constantly receiving power from the system, a toggle switch could be connected in the system in place of D2 (in Fig. 4.12 above) and used to override the automatic selection of where the harvested power is directed – either to the internal storage battery (when an external load is not available) or to an externally connected load when available.

4.8 Interface Methods and Mechanisms

There are many ways to interface the multi-purpose energy harvesting system to the ‘host’. A few of those will be discussed in this section. Due to the form factor of the improved proof of concept, it is capable of being installed on any object that has a hinge and swivel interface, namely – the door, the window, the elbow, the hip or the knee. Each of these has a stationary part, a joint, and a moving part about the joint relative to the stationary part. The design harvests

energy only in one cycle of the motion. In human motion, this cycle corresponds to the stopping and stability phase – this is the so-called negative energy phase referred to in the previous sections. This ensures that there is a minimal impact on the regular motion of the moving part while performing the required task (for the doors and windows – opening and closing, for the human motion – moving and stopping).

Fig. 4.16 shows the installation on a hinged device – which could be a door or a window. The installation is made up of two parts - a stationary and a moving part. The stationary part consists of the gearbox enclosure, the energy harvesting generator, and the power conditioning circuitry. While the moving part consist of the crank handle and a slotted base.

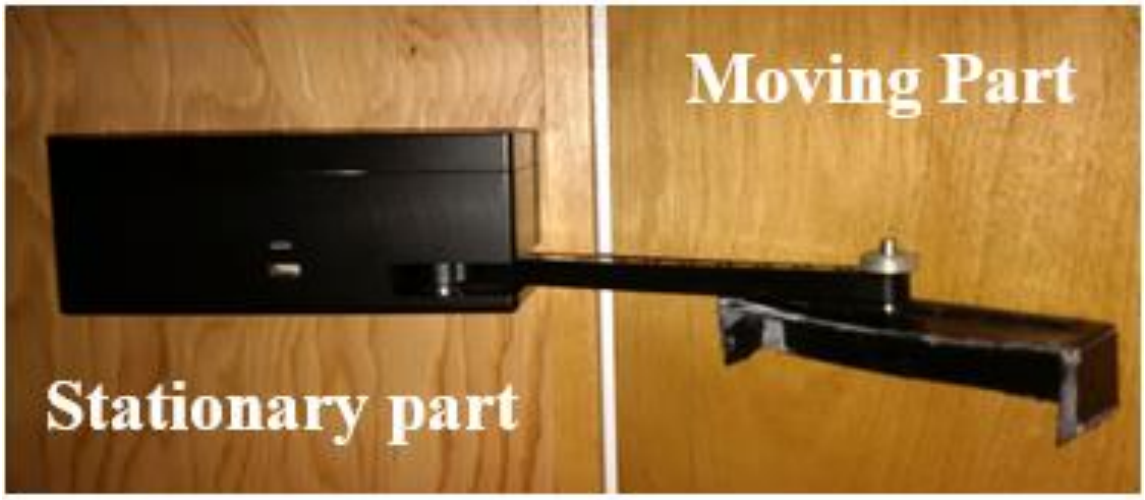

Fig. 4.16 - The installation on a hinged surface with moving and stationary parts clearly shown.

The crank handle is connected to the slotted base via a bolt and nut interface. The bolt and nut assembly slides within the slotted base as the hinged device is being opened and/or closed. This action drives the crank handle which in turn drives the gearbox to create the mechanical up-conversion that is required by the electromagnetic generator to harvest a significant amount of electromagnetic energy.

In Fig. 4.15 below, the image to the left shows the installation on the hip via the belt. This choice was made bearing in mind that most soldiers carry water canisters and other appliances in the upper part of the lower limbs. This energy harvesting system will simply replace one of such carry-ons while providing electrical power for their other gadgets. In this proof of concept, a thigh-wrap made from fabric with a slotted whole for the crank handle was used to affix the crank handle about the knee. As the knee moves, the crank handle moves in sync creating a mechanical up-conversion causing the generator rotor to move accordingly.

The complete harness for the human interface is a pouch made from fabric with belt-like hooks that is held in place by the belt. For proper fit, a wider belt works better. The energy harvesting system can be easily inserted into or removed from the pouch just like a water canister from the soldier’s pouch.

The image to the right shows the installation on the knee with a special adaptation of a fabric-based knee brace.

Fig. 4.17 - Typical Human Interface – (a) Hip-mounted installation on the left and (b) Knee-mounted installation on the right.

4.9 Experimental Results

The projected power for the energy harvester is between 2.5 and 7.5 watts. When compared to the generated power, it was estimated that the output power ranges from 4.25 Watts and 5 Watts. This estimate was based on the fact that the system generates 5 Volts output when measured with a digital multi-meter. This voltage is then fed into a smart phone requiring a minimum of 850 mA to initiate a charge and the device started charging. This is in line with the specs of the TP8350 which delivers 5 volts at 1 Amp.

4.10 System Efficiency

4.10.1 The Efficiency of the Mechanical Subsystem

The overall system efficiency is down to the cumulative efficiencies of the subsystems – the mechanical and the electrical subsystems. For instance, the mechanical up conversion machine converts linear mechanical motion into rotary mechanical motion. To do this, a force meter was attached to the crank handle and force was gradually applied until the crank handle moved. The maximum recorded force it took to move the crank handle by 45 degrees was about 57.4 gram-force. This is particularly important because of the arrangement of magnets on the rotor and the arrangement of the stator flanges.

It appears this force was particularly required to overcome the magnetic force of attraction between the magnets and the stator flanges. Once this initial force was overcome, the crank handle moves with less force than the peak recorded force. This peak force alternates between stator flange and rotor magnet pairs.

Fig. 4.18 below is a representation of the foregoing; where F is the applied force, r (the length of the crank handle) is the radius from the axis of rotation to the point of the application of the force, while rSinϴ is the Lever arm – this is the perpendicular distance from the point of the application of the force to the line parallel to that of the application of force.

The input mechanical power is calculated as:

Power = Torque * Angular Speed (Rad/sec); where Torque = rFSinϴ.

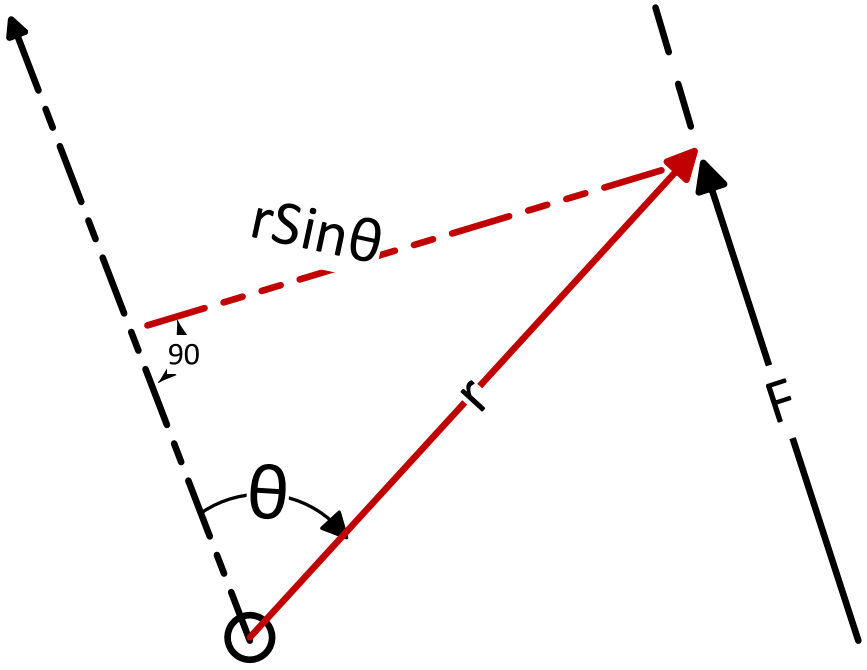

Fig. 4.18- Calculation on input mechanical power.

In the design concept presented in this thesis, r is 75 mm, and F = 57.4 gram-force.
Converting force to Newton at 1 g-f = 0.00980665 N; 57.4 g-f = 0.5629017 N.

$$\text{Torque} = 0.075 \times 0.5629017 \times \text{Sin}45 = 0.02985.$$

And power = Torque × Angular Speed.
Angular speed is calculated by: $\omega = (2\Pi \times \text{RPM})/60$ at RPM of 2900,

$$\omega = (2\Pi \times 2900)/60 = 303.8095$$

Therefore:

$$\text{Power} = 0.02985 \times 303.8095 = 9.068713575 \text{ W}$$

The input mechanical Power is approximately 9.07 Watts. Factoring in the efficiency of the mechanical up-conversion of the gearbox made up of three-stage spur gear system. It is a well-known fact that the efficiency of Spur gears lies somewhere between 94% and 98%.

Taking the above into consideration, the average efficiency of the three-stage system will lie somewhere between 83% and 94%. Hence the power available at the input of the generator is expected to be between 7.5 Watts and 8.5 Watts from the mechanical input of about 9.07 Watts.

4.10.2 The Efficiency of the Electrical Subsystem

The efficiency of the electrical subsystem could be analyzed in two parts. First, the generator takes a mechanical input power and coverts it into an electrical output power. The generated voltage was found to be as high as 60.5 volts [43], with a forward voltage drop of 1.1 volts for the rectifier used, this would result in an efficiency of about 98% (ignoring internal losses in the generator especially since we are analyzing the efficiency of the system after generation). This voltage is then fed into the OKI-78SR series with a manufacturer-rated efficiency of 90.5%. This brings the efficiency of the electrical subsystem to about 88.69%.

Combining the Mechanical and Electrical efficiencies gives an **overall efficiency** of the entire energy harvesting system to between 73.6% and 84.26%.

4.11 Summary

To summarize these sections, a new brushless electromagnetic AC voltage generator with a detachable and an adjustable height rotor has been presented. The net weight of the full assembly measuring 50 mm by 45 mm is 170 grams with the coil made from a 26 AWG gauge wire and 110 grams with the coil made from a 36 AWG gauge wire. The voltage and power output from the new generator concept can be used to power custom-made energy harvesting devices. The maximum open circuit voltage for the coils used was more than 60 VAC while the maximum rectified voltage over a load of 100 Ohms was over 10 VDC. This means an average power of 1 Watt could be generated by directly driving the load from a full wave rectifier circuit.

To increase the efficiency of the harvested power in energy harvesting applications, a buck-boost power supply would be used for voltage conditioning. Note that the generator reactance was not addressed in initial test. So the 100-Ohm load did not take into consideration any form of impedance matching. This was further discussed in section 4.6.3.3 above.

The generator will be used in an energy harvesting design to verify and confirm its suitability. A quick test with a buck converted generated up to 2.5 Watts which was used to charge a BlackBerry Z30 Smart phone.

After some further design iterations, an improved proof of concept was presented from section 4.6 above as a multi-purpose energy harvesting system with the final output power falling between 2.5 and 5.0 Watts, although the generated power could potentially reach up to 7.5 Watts at rated speed of 2900 RPM. The final output power was determined by the TP8350 charging system at the output whose output is 5.0 Volts at 1.0 Amp.

This output power, however, is big enough to power many electronic devices and was successfully used to start and continue charging the BlackBerry Z30 Smartphone working at an average pace of one (1) step per second. The original equipment manufacturers'(OEM) charging adapter for his Smartphone was rated at 5.0 Volts/850 mA and its battery rated at 2880 mAh.

The final prototype weighs about 700 grams, which is lighter than the previously published works [9] by up to 250 grams. This is especially important when used as a wearable system.

Although there is significant reduction in weight and size, there are still other improvement opportunities. These include the use of the Planetary gear system in place of the spur gear system used in the proof of concept for this Thesis. The planetary gear system will make the design more compact and lighter at the same time with fewer stages [39].

Moreover, the energy harvesting system is not only wearable but could also find application in other energy harvesting applications. This thesis demonstrated how this could be used in remote sensing applications. Here, either a door or a window or any other swinging/hinged barrier opens or closes to actuate the energy harvester. The energy so generated will be used by the sensor to send the required information to a remote monitoring center. Because of the amount of power that could be harvested by the current design, it is possible to use it to offer full power solution to autonomous wireless monitoring systems.

In summary, the multi-purpose energy harvesting system met the set target of up to 5 watts and the complete system packaging could be further optimized and miniaturized to make it more portable.

Chapter 5

Summary and contributions

5.1 Summary

The research presented a new way to design an electromagnetic energy generator suitable for multipurpose wearable energy harvesting systems. One of the unique features of the generator is its adjustable nature – the ability to easily and seamlessly customize the generator for different energy harvesting applications and different output power levels.

The customization is done by simply pulling or pushing the rotor shaft to the next detent location. Installing the generator, in the current enclosure, to any host environment is modular in nature. The energy Harvester can be worn around the elbow, hip, and knee joints while the structure also allows it to be installed in kitchen cabinets, door and window openings.

5.2 Contributions and future work

5.2.1 Contributions

This thesis presented a new form of electromagnetic energy harvesting system with multipurpose functionality. The generator can be used for different levels of energy harvesting projects whose input power requirements could range from as low as milli watts all the way up to a few watts. Here are some of the main contributions:

1. **Design of a new customizable electromagnetic energy generator:** This Thesis demonstrated a customizable electromagnetic energy generator suitable for various applications. The main design demonstrates a new way to develop electromagnetic energy generators for energy harvesting purposes. This includes simplified stator and rotor arrangements as well as a winding arrangement on a single spoon. The variable air gap between the stator and the core makes for a post-fabrication customizable energy harvesting system. The system generated between 2.5 watts and 7.5 watts of electrical power at an overall system efficiency of up to 84%.

2. **Improved Power Management System:** Another important contribution is an improved power management system that automatically detects the presence of an external load and

routes generated power to it utilizing the technique of impedance matching to maximize the transfer of generated voltage to the load, and reroutes the generated energy to charge an internal storage battery when no external load was detected. It also uses power from other sources, including wall outlets, to power an internal charging system to protect the internal storage battery from completely draining when the energy harvester has not been in use for an extended period.

3. **Adaptable Multi-Use Enclosure:** Yet another equally important contribution is a modular multipurpose energy harvesting system enclosure that can be used on both human and other non-human hosts. This enclosure is driven by the same 'crank handle' on any surface whereupon it was installed with minimal adaptation.

4. **Adaptive Voltage Generation for Electric Vehicles:** And last but not the least, the design presented in this thesis could be used as an adaptive voltage generator for electric vehicles allowing the adjustable nature of the generator to be used in electric cars and motor-cycles in the **regenerative charging system**. In this way, the generator can be engaged selectively to help maintain the car/motor-cycle speed or used as part of the braking system to reduce the car speed while generating the required energy used to recharge its internal batteries. Used in this configuration, the adjustable height rotor will be selectively engaged depending on the actual speed versus the required speed. The lowest air gap will be engaged when the braking system is engaged. The adjustable air gap engaged in an inverse proportion with the applied speed. This could be the next level or the future of energy harvesting through regenerative braking.

5.2.2 Suggested Future Work

While the energy harvester presented in this thesis was capable of generating enough electrical power for powering some low power electronic devices, the generator could still be improved to optimize its overall performance and minimize losses. For instance:

1. **Automatic/dynamic impedance tracking rectifiers:** A study dedicated to a rectifier with a dynamic input impedance that will be capable of adjusting automatically to the source impedance with respect to the operating frequency. This rectifier should be able to dynamically match both the real and complex portions of the source impedance automatically. This will improve the harvested power across all frequencies (RPM) than just at the rated/optimum RPM.

2. **Custom designed rectifiers:** An improvement of the power management system to use custom designed rectifiers could improve the overall system efficiency. It is understood that using MOSFETs as rectifiers offer greater potentials and efficiency in energy harvesting systems, as they have lower forward voltage drops as compared to their diode counterparts (Silicon, Germanium, Schottky). It is therefore, highly recommended to carry out further research here to determine and compare the overall efficiency improvement.

3. **Optimum wire size on the core:** The results presented in tables 4.3 and 4.4 showed that the ratio of the increase in the number of turns of the generator wires does not directly correspond one for one to an increase in the induced voltage. Although, tables 3.4 and 3.5 show a relatively close relationship, work still needs to be done to determine the optimum distance from the core at which induced voltage climaxes for the same flux linkage and RPM. This should be done using the same wire gauge size.

4. **Alternate gear box materials:** The weight of the final proof of concept was slightly under 700 grams, however, the target was to get a product within 500 grams. Further research should be done on other forms of materials for the gearbox enclosures. The use of fiberglass, for instance, should be explored. Also, 3D printed housing, to deliver the exact shape and size of the intended devices, could be a desirable alternative path to pursue.

5. **Thinner Spur Gears:** The spur gear system used in motion translation gear box of the proof of concept presented in this thesis could be thinner and with more materials removed from the face of the gear material. This will reduce the overall weight of the device and get one closer to the desired final product weight.

6. **Planetary Gear System:** Use of a planetary gear system instead of the spur gear system in the motion translation gear box might help reduce the overall product size and weight. This concept should be explored to determine how suitable they could be. The adaption of the face gear might be tricky and challenging but worth researching. Plastic gears might be preferred over metal gears and this will reduce the weight of the material even further for the same material size but before making this determination, an extended research – simulations and experimentations – have to be done to determine their practicality and durability.

References

[1] N. Gurusamy, I. Elamvazuthi, N. Yahya, S. Parasuraman, and M. K. A. A. Khan, "Biomechanical energy harvesting from human lower extremity gait: A comparative analysis," *2017 IEEE 3rd Int. Symp. Robot. Manuf. Autom. ROMA 2017*, vol. 2017-Decem, pp. 1–5, 2017.

[2] L. C. Rome, L. Flynn, E. M. Goldman, and T. D. Yoo, "Generating Electricity While Walking with Loads," *Science (80-.).*, vol. 309, no. 5741, pp. 1725 LP – 1728, Sep. 2005.

[3] R. Riemer and A. Shapiro, "Biomechanical energy harvesting from human motion: theory, state of the art, design guidelines, and future directions," *J. Neuroeng. Rehabil.*, vol. 8, p. 22, Apr. 2011.

[4] P. Niu and P. Chapman, "Evaluation of Motions and Actuation Methods for," *Electronics*, pp. 2100–2106, 2004.

[5] K. R. Williams and P. R. Cavanagh, "A model for the calculation of mechanical power during distance running," *J. Biomech.*, vol. 16, no. 2, pp. 115–128, 1983.

[6] C. Chen and W. H. Liao, "A self-sensing magnetorheological damper with power generation," *Smart Mater. Struct.*, vol. 21, no. 2, 2012.

[7] J. M. Donelan, Q. Li, V. Naing, J. A. Hoffer, D. J. Weber, and A. D. Kuo, "Biomechanical energy harvesting: Generating electricity during walking with minimal user effort," *Science (80-.).*, vol. 319, no. 5864, pp. 807–810, 2008.

[8] P. DeVita, J. Helseth, and T. Hortobagyi, "Muscles do more positive than negative work in human locomotion," *J. Exp. Biol.*, vol. 210, pp. 3361–3373, Oct. 2007.

[9] P. Niu, P. Chapman, L. DiBerardino, and E. Hsiao-Wecksler, "Design and optimization of a biomechanical energy harvesting device," in *2008 IEEE Power Electronics Specialists Conference*, 2008, pp. 4062–4069.

[10] P. Niu, P. Chapman, R. Riemer, and X. Zhang, "Evaluation of motions and actuation methods for biomechanical energy harvesting," in *2004 IEEE 35th Annual Power Electronics Specialists Conference (IEEE Cat. No.04CH37551)*, 2004, vol. 3, pp. 2100-2106 Vol.3.

[11] M. Donelan, Q. Li, V. Naing, J. Hoffer, D. Weber, and A. D. Kuo, "Biomechanical Energy Harvesting: Generating Electricity During Walking with Minimal User Effort," *Science*, vol. 319, pp. 807–810, Mar. 2008.

[12] M. Pozzi and M. Zhu, "Pizzicato excitation for wearable energy harvesters," *SPIE Newsroom*, Jun. 2011.

[13] PowerActive, "Disposal of Lead Acid Batteries." [Online]. Available: http://d2leais691vm21.cloudfront.net/wp-content/uploads/2014/09/WP104-Disposal-of-Lead-Acid-Batteries.pdf. [Accessed: 26-Jul-2019].

[14] L. Chao, C. Tsui, and W. Ki, "A Batteryless Vibration-based Energy Harvesting System for Ultra Low Power Ubiquitous Applications," in *2007 IEEE International Symposium on Circuits and Systems*, 2007, pp. 1349–1352.

[15] F. Yildiz, "Potential Ambient Energy-Harvesting Sources and Techniques" *Energy*, pp. 40–48, 2007.

[16] G. Bassani, A. Filippeschi, and E. Ruffaldi, “Nonresonant Kinetic Energy Harvesting Using Macrofiber Composite Patch,” *IEEE Sens. J.*, vol. 18, no. 5, pp. 2068–2076, 2018.
[17] J. O. Ugwuogo and S. Safavi-Naeini, “A New Brushless AC Electromagnetic Generator Design Using an Experimental and Design Optimization Approach,” *IEEE Trans. Magn.*, vol. 54, no. 8, pp. 1–7, 2018.
[18] J. M. Donelan, V. Naing, and Q. Li, “Biomechanical energy harvesting,” *RWS 2009 IEEE Radio Wirel. Symp. Proc.*, pp. 1–4, 2009.
[19] P. L. Chapman, “Power management for energy harvesting devices,” *RWS 2009 IEEE Radio Wirel. Symp. Proc.*, pp. 9–12, 2009.
[20] S. Almouahed, M. Gouriou, C. Hamitouche, E. Stindel, and C. Roux, “The use of piezoceramics as electrical energy harvesters within instrumented knee implant during walking,” *IEEE/ASME Trans. Mechatronics*, vol. 16, no. 5, pp. 799–807, 2011.
[21] J. Granstrom, J. Feenstra, H. A. Sodano, and K. Farinholt, “Energy harvesting from a backpack instrumented with piezoelectric shoulder straps,” *Smart Mater. Struct.*, vol. 16, no. 5, pp. 1810–1820, 2007.
[22] J. Y. Hayashida, “Unobtrusive Integration of Magnetic Generator Systems into Common Footwear by,” *, BS thesis, Dept. Electr. Eng. MIT Media Lab. Massachusetts Inst. Technol.*, 2000.
[23] N. S. Shenck, J. A. Paradiso, and R. Environments, “Energy Scavenging with shoe-mounted Piezoelectrics,” *Media*, pp. 30–42, 2001.
[24] R. D. Kornbluh *et al.*, “Electroelastomers: applications of dielectric elastomer transducers for actuation, generation, and smart structures,” in *Proc.SPIE*, 2002, vol. 4698.
[25] L. Xie and M. Cai, “Increased piezoelectric energy harvesting from human footstep motion by using an amplification mechanism,” *Appl. Phys. Lett.*, vol. 105, no. 14, pp. 10–14, 2014.
[26] Q. Li, V. Naing, and J. M. Donelan, “Development of a biomechanical energy harvester,” *J. Neuroeng. Rehabil.*, vol. 6, no. 1, p. 22, 2009.
[27] Q. Li, V. Naing, J. A. Hoffer, D. J. Weber, A. D. Kuo, and J. M. Donelan, “Biomechanical energy harvesting: Apparatus and method,” *Proc. - IEEE Int. Conf. Robot. Autom.*, vol. 48109, pp. 3672–3677, 2008.
[28] F. Heremans and R. Ronsse, “Design of an energy efficient transfemoral prosthesis using lockable parallel springs and electrical energy transfer,” *IEEE Int. Conf. Rehabil. Robot.*, pp. 1305–1312, 2017.
[29] M. Gorlatova, P. Kinget, I. Kymissis, D. Rubenstein, X. Wang, and G. Zussman, “Energy harvesting active networked tags (EnHANTs) for ubiquitous object networking,” *IEEE Wirel. Commun.*, vol. 17, no. 6, pp. 18–25, 2010.
[30] P. Peumans, A. Yakimov, and S. R. Forrest, “Small molecular weight organic thin-film photodetectors and solar cells,” *J. Appl. Phys.*, vol. 93, no. 7, pp. 3693–3723, 2003.
[31] S. P. Subbarao, M. E. Bahlke, and I. Kymissis, “Laboratory Thin-Film Encapsulation of Air-Sensitive Organic Semiconductor Devices,” *IEEE Trans. Electron Devices*, vol. 57, no. 1, pp. 153–156, 2010.
[32] S. Sherrit, “The physical acoustics of energy harvesting,” pp. 1046–1055, 2009.
[33] Wikipedia, “Energy harvesting,” 2015. [Online]. Available: http://en.wikipedia.org/wiki/Energy_harvesting#Thermoelectrics. [Accessed: 13-Jul-2015].
[34] J. O. Ugwuogo, “On-Demand Energy Harvesting Techniques - A System Level

Perspective," University of Waterloo, 2012.
[35] M. Electronics, "Thermal Energy Harvesting - Infinite Clean Power for Wireless Sensor Networks." [Online]. Available: https://www.mouser.ca/thermal_energy_harvesting/. [Accessed: 28-Jul-2019].
[36] A. Khaligh, P. Zeng, and C. Zheng, "Kinetic energy harvesting using piezoelectric and electromagnetic technologiesstate of the art," *IEEE Trans. Ind. Electron.*, vol. 57, no. 3, pp. 850–860, 2010.
[37] Y. Huang, R. Doraiswami, M. Osterman, and M. Pecht, "Energy harvesting using RF MEMS," *Proc. - Electron. Components Technol. Conf.*, pp. 1353–1358, 2010.
[38] A. Sample and J. R. Smith, "Experimental results with two wireless power transfer systems," *RWS 2009 IEEE Radio Wirel. Symp. Proc.*, pp. 16–18, 2009.
[39] Georgia Tech Research, "Ambient Electromagnetic Energy Harnessed for Small Electronic Devices," 2011. [Online]. Available: http://www.rh.gatech.edu/news/68714/ambient-Electromagnetic-energy-harnessed-small-electronic-devices. [Accessed: 26-Jul-2019].
[40] "epdf.pub_inductance-loop-and-partial.pdf." .
[41] National Imports LLC, "Permanent Magnet Selection and Design Handbook." [Online]. Available: https://cdn2.magcraft.com/pdf/Permanent-Magnet-Selection-and-Design-Handbook.pdf. [Accessed: 28-Jul-2019].
[42] ELECTRICAL TECHNOLOGY, "EMF Equation of an Alternator and AC Generator." [Online]. Available: https://www.electricaltechnology.org/2012/11/emf-equation-of-alternator-or-ac.html. [Accessed: 28-Jul-2019].
[43] M. H. Committee, *Metals Handbook; Volume 1, Properties and Selection of Metals*, Eight Edit. Metals Park, Ohio: American society for metals, 1961.
[44] G. W. Cho *et al.*, "The stabilization of cogging torque variation by manufacturing tolerances," *IEEE CEFC 2016 - 17th Bienn. Conf. Electromagn. F. Comput.*, pp. 0–5, 2017.
[45] D. Palani, Z. Azar, A. Thomas, Z. Q. Zhu, and D. Gladwin, *Modeling technique for large permanent magnet generators accounting for manufacturing tolerances and limitations*. 2016.
[46] T. Gundogdu, Z. Q. Zhu, J. C. Mipo, and P. Farah, "Influence of magnetic saturation on rotor bar current waveform and performance in induction machines," *Proc. - 2016 22nd Int. Conf. Electr. Mach. ICEM 2016*, pp. 391–397, 2016.

Appendices

A.1 Energy Conversion Calculations by walk phases

Table A. 1 shows a summary of the work done [10] at different walk phases by select parts of the body – Ankle, Knee and Hip. The values will be used in determining the respective energy calculations in the sections that follow.

Phases of work that are performed in the ankle joint are represented by A1-4, phases for work done at the knee are represented by K1-4, while H1-3 represent phases of work done at the hip joint. Work represents the net summation of work at the joint muscles and negative values represent negative work [10].

Table A. 1 - Work performed at the leg joints during a walking step normalized by subject's mass

Work during the phase (J/kg)	average (J/kg)	standard deviation (J/kg)
A-1 work (Ankle)	-0.0074	0.0072
A-2 work (Ankle)	0.0036	0.0046
A-3 work (Ankle)	-0.111	0.042
A-4 work (Ankle)	0.296	0.051
K-1 work (Knee)	-0.048	0.032
K-2 work (Knee)	0.0186	0.026
K-3 work (Knee)	-0.047	0.015
K-4 work (Knee)	-0.114	0.015
H-1 work (Hip)	0.103	0.047
H-2 work (Hip)	-0.044	0.029
H-3 work (Hip)	0.090	0.027

The joint work calculation for an 80-kg person walking at normal speed is based on this equation:

$$\frac{work}{step} = weight\ x\ [|phase_1| + |phase_2| + \cdots + |phase_n|]$$

The phases for this calculation are based on the work in [10] with units of J/step.

A.1.1 Work phase definitions

Here, the letters and numbers used in Table A. 1 will be described. A1 is the energy absorption by the dorsiflexors after heel contact; A2 is the energy generation by the dorsiflexors to pull the leg forward over foot; A3 is the absorption by the plantar flexors as leg rotates forward over foot; while the generation of energy by the plantar flexors at push-off is represented by A4.

The energy absorbed at the knee by quadriceps femoris muscle during weight acceptance is represented by K1; K2 is the energy generated by the quadriceps femoris muscle as knee extends during mid-stance; the energy absorbed by the quadriceps femoris muscle as knee flexes during late stance and early swing is K3; and K4 is the energy absorbed by the knee flexors (hamstring muscles) as the knee extends late in swing.

Hip extensors generate energy represented by H1 as the hip extends (hip flexion reduces) during weight acceptance; H2 is the energy absorbed by the hip flexors in mid-stance as backward-rotating thigh is decelerated; while H3 is the energy generated by the hip during late stance and early swing to accelerate the lower limb upward and forward" [10].

These are the phases experienced by the lower limbs during normal gaits that are used to determine the work done by each limb segment.

A.1.2 Energy calculation for the ankle

Using the values corresponding to the ankle joint on Table A. 1, one can determine the amount of total work versus negative work using the corresponding phases.

$$W_{total} = weight\ x\ [|phase_1| + |phase_2| + \cdots + |phase_n|]$$

$$W_{total} = 80\ x\ [|-0.0074| + |0.0036| + |-0.111| + |0.296|]$$

$$= 33.45\ \frac{J}{step}$$

$$W_{negative} = 80\ x\ [-0.0074 - 0.111] = -9.47\ \frac{J}{step}$$

$$\frac{W_{negative}}{W_{total}} = \frac{9.47}{33.45} = 28.3\%$$

Thus, the total energy is 33.45 J, and the negative portion is 9.47 J.

A.1.3 Energy calculation for the knee

Using the values corresponding to the knee joint on Table A. 1 above, one can also determine the amount of total work versus negative work utilizing the corresponding phases.

$$E_{total} = 80\ x\ [|-0.048| + |0.0186| + |-0.047| + |-0.114|]$$

$$= 18.2\ \frac{J}{step}$$

$$E_{negative} = 80\ x\ [-0.048 - 0.047 - 0.114]$$

$$= -16.72\ \frac{J}{step}$$

$$\frac{E_{negative}}{E_{total}} = \frac{16.72}{18.2} = 91.9\%$$

Thus, the total energy is 18.2 J, and the negative portion is 16.72 J.

A.1.4 Energy calculation for the hip

Using the values corresponding to the hip joint on Table A. 1 above, the amount of total work versus negative work using the corresponding phases is determined as follows:

$$E_{total} = 80\ x\ [|0.103| + |-0.044| + |0.090|]$$

$$= 18.96\ \frac{J}{step}$$

$$E_{negative} = 80\ x\ [-0.044]$$

$$= -3.52\ \frac{J}{step}$$

$$\frac{E_{negative}}{E_{total}} = \frac{3.52}{18.96} = 18.56\ \%$$

Thus, the total energy is 18.96 J, while its negative portion is 3.52 J.

A.2 Reducing Power Losses by Using a Laminated Core

**Please note that fig. A.2 does not accurately represent an effective way to reduce eddy current losses. The figure was used due to the limitation placed by the original generator design and the difficulty in adapting a suitable and better layout. The orientation of the circular rings within the stator core will not have a significant impact in reducing eddy current losses. This section, therefore, discusses the general approach to reducing eddy current losses, not necessarily the impact of the layout represented in fig. A.2*

To improve on the reactance of the generator coil, it is important to analyze the impact of the magnetic circuit. Fig. A.1 is a solenoid-like coil used to explain the impact of the length and the area of the magnetic circuit. Here 'l' is the length of the generator core while 'r' is the radius.

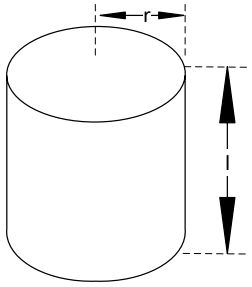

Fig. A.2.1 – Illustration used for explaining the inductance of a coil.

$L = \frac{N^2 \mu A}{l}$

$\mu = \mu_r \mu_0$

Where:

L = Inductance of the coil in Henrys

N = Number of turns in wire coil (straight wire = 1)

μ = Permeability of core material (absolute, not relative)

μ_r = Relative permeability, dimensionless (μ_0 = 1 for air)

μ_0 = 1.26 x 10^{-6} T-m/At permeability of free space

A = Area of coil in square meters = πr^2

l = Average length of coil in meters

From the above equation, four factors can be identified that affect the inductance of an inductor – namely, the coil Area; the Number of turns; the Length of magnetic circuit and the Permeability of the intervening medium.

As the area of the coil increases, if other factors are kept constant, the inductance increases. Same goes for the number of turns and the permeability of the intervening medium. On the other hand, when the length of the magnetic circuit increases, the inductance decrease.

For the research in focus, the coil, the area, and the number of turns were kept constant and the permeability of the intervening medium changed to a lesser value in order to reduce the inductance of the generator coil.

This is why the choice of a ring-like core was made. These were laminated and stacked on a 3-D printed non-magnetic material to hold the core in place – fig. A.2. The results of the new inductances for different coil sizes and number of turns are shown in table 3.6.

Notice, from table 3.6, the differences in inductances and corresponding impedances between using a solid core versus a laminated core in the generator stator core design. This is evident in all coil sizes used – whether with the 26 AWG gauge wire or the 36 AWG gauge wire.

Predictably, the inductance of the larger gauge wire (26 AWG) is lower as compared to that of the smaller gauge wire (36 AWG).

Please, note that these observable differences will not significantly change the effect of eddy current effects in any measurable way due to the current design layout but could affect the value of the inductive reactance. A bottom-up design will benefit especially from this kind of situation since the designer can select the right materials and design parameters to produce the desired outcome.

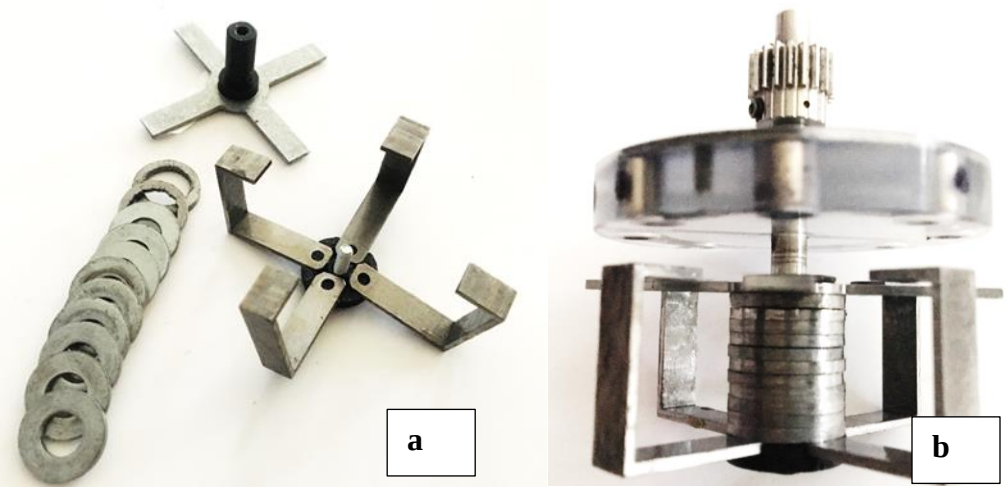

Fig. A.2.2 – Stator materials for the improved generator design with laminated core. (a) Laminated core and top and bottom flanges (b) generator stack-up without the coil

On the left hand side of fig. A.2 is the exploded view while the stack up is shown on the right hand side without the coil, of course, to reveal the laminated material stack up. The rotor is installed to give a view of the complete assembly when finished.

Using a laminated core with the properly layout/orientation (vertical rather than the radial orientation shown in fig. A.2 above) will effectively reduce eddy current losses in the core. This is because the effective area is the area of a single laminated sheet. And applying the formula for resistance (see Equation 3), the resistance of the core increases with reduced cross-sectional area.

Now, if the induced voltage in the core is fixed, an increased core resistance effectively reduces the current flowing through the core – from the formula V = IR.

This then implies that the power loss due to the eddy current (P_{loss}: which is the power lost to heat) will decrease:

$$P_{loss} = I^2R.$$

This is moreso since:

$$P_e = K_e \times B_{max}^2 \times f^2 \times t^2 \times V$$

Where:

P_e = Eddy Current loss (W)

K_e = Eddy current Constant

B = Flux Density (wb/m^2)

F = frequency of magnetic reversals (Hz)

T = thickness (m) and

V = Volume (m^3)

From the above formula, and all other factors being equal, eddy current loss varies with the square of the core material thickness.

To further investigate the impact of eddy current on the generated voltages on the single core performance versus the laminated core, a uniform air gap was chosen (between 1 mm and 2 mm) for both the solid core and the laminated core for the same number of turns (3000). Then the generator was also run at a constant RPM of 2900 while the open circuit and loaded voltages were measured for each core type.

The results so obtained were then applied in the below formula to determine the losses associated with each core type.

The open circuit and loaded circuit voltages were 49.1 and 45.7 respectively for the solid core and 37.4 and 35.0 for the laminated core. Applying the formula:

$Z_S = R_L\left(\frac{V_G}{V_L} - 1\right)$

V_G is the Generator open circuit voltage, and V_L is the measured voltage across a load, while a load (R_L) of 10 Kilo-Ohms was connected across the load. Rs = 325 (which is the measured dc impedance of the generator coil).

Remembering from Fig. 3.4 and assigning $Z_S^2 = R_s^2 + X_L^2$ || where $X_L = \omega L = 2\Pi FL$

A.2.1 Series Impedance with Respect to The Solid Core

Applying $Z_S = R_L\left(\frac{V_G}{V_L} - 1\right)$, Z_S = 743.98 (while X_L = **669.24**)

A.2.2 Series Impedance with Respect to The Laminated Core

Also applying $Z_S = R_L\left(\frac{V_G}{V_L} - 1\right)$, Z_S = 685.71 (while X_L = **603.79**)

The capacitor required to create enough reactance for each of the above (solid core and laminated core) will have to match **669.24** and **603.79** respectively.

A.2.3 Calculating The Value of the Parallel Capacitor

Applying the formula to calculate the Capacitive impedance:

$X_C = \frac{1}{\omega C} = \frac{1}{2\Pi FC}$ (where ω = 2ΠF, C = capacitance value, F =frequency).

$C = \frac{1}{2\Pi F X_C}$.

The capacitance of the capacitor obtained using this formula is the capacitor whose value will give an impedance equal in magnitude but opposite in sign with the inductive impedance of the series inductor.

Now, making $X_L = X_C$ and substituting the corresponding values in sections A.2.2 and A.2.3 above for the solid core and laminated core, respectively:

$C_{solid\ core} = \frac{1}{2\times\Pi\times193\times669.24}$ = 1.23 µF and

$C_{Laminated\ core} = \frac{1}{2\times\Pi\times193\times603.80}$ = 1.37 µF

This value needs to be connected across the bridge rectifier circuit to match the 'complex' portion of the generator impedance (this capacitor is referred to as **C(X$_C$)** in Fig. 4.12). The 'real' portion will be matched by the bridge rectifier using the impedance matching approach discussed in section 4.6.3.3.

A combination of capacitors can be used to achieve the equivalence of each of the calculated values for each core type. This will ensure that the complex portion of the series impedance is matched at rated RPM (frequency).

Alternatively, a standard value of 1.5 µF exists which could be used for both generator core type, however, this will predictably move the matching frequency (from currently rated RPM) to a new value.

Using the capacitor value of 1.5 µF in each of the capacitor value calculations and solving for F results in:

$F_{solid\ core}$ = 158.479 Hz

$F_{Laminated\ core}$ = 175.656 Hz

When these values are substituted in the formula for determining frequency from the RPM, the new rated matching RPMs are:

$RPM_{solid\ core}$ = 2377.19 and

$RPM_{Laminated\ core}$ = 2634.833.

A.3 American Wire Gauge (AWG)

The American Wire Gauge is a standardized system for Wire Gauges that is predominately used in North America for the diameters of rounded, solid, nonferrous, and electrically conducting wires. The cross-sectional area of each gauge determines its current carrying capacity. This standard has been in use in North America since 1857.

The dimensions are given in the ASTM standards B258.

Higher gauge numbers signify lower wire diameters and consequently, lower current-carrying capacity, and vice-versa. In other words, a bigger gauge number, for example, gauge 36, is smaller than and hence possesses lesser current-carrying capacity than a gauge 26 wire.

A.3.1 Wire Gauge Calculation for Wire Gauges from 36 to 0:

The diameter of a gauge [No. n AWG] wire is determined by the following formula:

$d_n = 0.005\ inch\ x\ 92^{\frac{36-n}{39}} = 0.127\ mm\ x\ 92^{\frac{36-n}{39}}$ ……. *Equation 7*

The gauge can be calculated from the diameter using:

$n = -39log_{92}\left(\frac{d_n}{0.005\ inch}\right) + 36 = -39log_{92}\left(\frac{d_n}{0.127\ mm}\right) + 36$ ……Equation 8

And the cross-sectional area determined using:

$A_n = \frac{\pi}{4} d_n^{\ 2} = 0.000019635\ inch^2\ x\ 92^{\frac{36-n}{19.5}} = 0.012668\ mm^2\ x\ 92^{\frac{36-n}{19.5}}$

……Equation 9